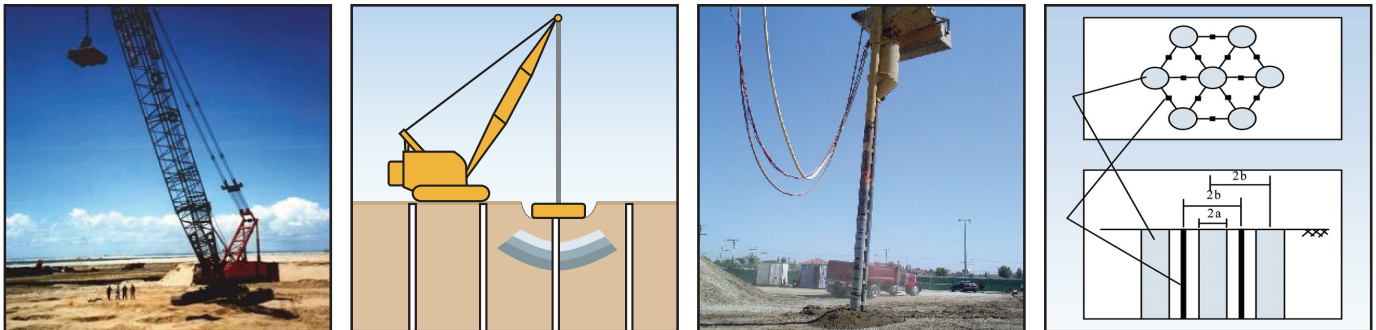# Liquefaction Remediation in Silty Soils Using Dynamic Compaction and Stone Columns

by

S. Thevanayagam, G.R. Martin, R. Nashed, T. Shenthan, T. Kanagalingam and N. Ecemis

NOTICE

Liquefaction Remediation in Silty Soils Using Dynamic Compaction and Stone Columns

by

S. Thevanayagam,[1] G.R. Martin,[2] R. Nashed,[3] T. Shenthan,[3] T. Kanagalingam[3] and N. Ecemis[4]

1   Associate Professor, Department of Civil, Structural and Environmental Engineering, University at Buffalo, The State University of New York
2   Professor, Department of Civil Engineering, University of Southern California
3   Post-Doctoral Research Assistant, Department of Civil, Structural and Environmental Engineering, University at Buffalo, The State University of New York
4   Ph.D. Candidate, Department of Civil, Structural and Environmental Engineering, University at Buffalo, The State University of New York

MCEER
University at Buffalo, The State University of New York
Red Jacket Quadrangle, Buffalo, NY 14261
Phone: (716) 645-3391; Fax (716) 645-3399
E-mail: *mceer@buffalo.edu*; WWW Site: *http://mceer.buffalo.edu*

Preface

The Multidisciplinary Center for Earthquake Engineering Research (MCEER) is a national center of excellence in advanced technology applications that is dedicated to the reduction of earthquake losses nationwide. Headquartered at the University at Buffalo, State University of New York, the Center was originally established by the National Science Foundation in 1986, as the National Center for Earthquake Engineering Research (NCEER).

Comprising a consortium of researchers from numerous disciplines and institutions throughout the United States, the Center's mission is to reduce earthquake losses through research and the application of advanced technologies that improve engineering, pre-earthquake planning and post-earthquake recovery strategies. Toward this end, the Center coordinates a nationwide program of multidisciplinary team research, education and outreach activities.

MCEER's research is conducted under the sponsorship of two major federal agencies, the National Science Foundation (NSF) and the Federal Highway Administration (FHWA), and the State of New York. Significant support is also derived from the Federal Emergency Management Agency (FEMA), other state governments, academic institutions, foreign governments and private industry.

The Center's Highway Project develops improved seismic design, evaluation, and retrofit methodologies and strategies for new and existing bridges and other highway structures, and for assessing the seismic performance of highway systems. The FHWA has sponsored three major contracts with MCEER under the Highway Project, two of which were initiated in 1992 and the third in 1998.

Of the two 1992 studies, one performed a series of tasks intended to improve seismic design practices for new highway bridges, tunnels, and retaining structures (MCEER Project 112). The other study focused on methodologies and approaches for assessing and improving the seismic performance of existing "typical" highway bridges and other highway system components including tunnels, retaining structures, slopes, culverts, and pavements (MCEER Project 106). These studies were conducted to:

- assess the seismic vulnerability of highway systems, structures, and components;
- develop concepts for retrofitting vulnerable highway structures and components;
- develop improved design and analysis methodologies for bridges, tunnels, and retaining structures, which include consideration of soil-structure interaction mechanisms and their influence on structural response; and
- develop, update, and recommend improved seismic design and performance criteria for new highway systems and structures.

The 1998 study, "Seismic Vulnerability of the Highway System" (FHWA Contract DTFH61-98-C-00094; known as MCEER Project 094), was initiated with the objective of performing studies to improve the seismic performance of bridge types not covered under Projects 106 or 112, and to provide extensions to system performance assessments for highway systems. Specific subjects covered under Project 094 include:

- development of formal loss estimation technologies and methodologies for highway systems;
- analysis, design, detailing, and retrofitting technologies for special bridges, including those with flexible superstructures (e.g., trusses), those supported by steel tower substructures, and cable-supported bridges (e.g., suspension and cable-stayed bridges);
- seismic response modification device technologies (e.g., hysteretic dampers, isolation bearings); and
- soil behavior, foundation behavior, and ground motion studies for large bridges.

In addition, Project 094 includes a series of special studies, addressing topics that range from non-destructive assessment of retrofitted bridge components to supporting studies intended to assist in educating the bridge engineering profession on the implementation of new seismic design and retrofitting strategies.

The objective of this report is to introduce a rational analysis procedure and design guidelines for liquefaction hazards mitigation in saturated sands and non-plastic silty sands using Dynamic Compaction (DC) and Vibro-Stone Columns (SC). A numerical model was developed to simulate the densification processes during both techniques through quantifying pore pressure generation due to vibrations caused by successive impacts on the ground surface or repeated insertions of a vibratory probe into the ground. The effects of site-specific conditions such as hydraulic conductivity, fines content, etc. were quantified for a range of energy contents delivered to the soil at specific spacing. In addition, the effects of field operational parameters such as energy per impact, number of impacts, time cycle between impacts, impact grid spacing, impact grid pattern, and wick drain spacing, in the case of DC, or area replacement ratio and wick drains spacing in the case of SC, on post-improvement resistance to liquefaction were included in the study. Based on the results, design charts and design guidelines for liquefaction mitigation in silty soils using DC and SC are provided. Design procedures and design examples are also provided.

SUMMARY

A number of different densification techniques have been developed to mitigate liquefaction in loose saturated granular soils. Dynamic compaction (DC) and vibro-stone column (SC) are among the most field proven and commonly used techniques. The DC technique involves high-energy impacts to the ground surface by systematically dropping heavy weights of 5 to 35 Mg from heights ranging from 10 to 40 m to compact the underlying ground using heavy crawler cranes. Vibro-stone column installation process involves insertion of a vibratory probe with rotating eccentric mass and power rating in the vicinity of 120 kW. The probe plunges into the ground due to its self-weight and vibratory energy, which facilitates penetration of the probe. Once the specified depth (depth of stone column) is reached, the probe is withdrawn in steps (lifts) of about 1m. During withdrawal of the probe, the hole is backfilled with gravel. During each lift, the probe is then reinserted expanding the stone column diameter. This process is repeated several times until a limiting condition is achieved. Sand deposits densified by DC and SC are more resistant to liquefaction, and have performed well during earthquakes. Silty sand deposits appear to perform well when improved by either technique supplemented with wick drains.

In both improvement techniques, during the ground improvement works, the repeated ground vibrations induced by the DC and vibratory probe cause a rise in pore water pressures and subsequent soil consolidation, resulting in a denser arrangement of particles. In highly permeable soils, these techniques also cause increases in the lateral confining stresses in the soil. Hence, the soil resistance to liquefaction increases.

Liquefaction in loose saturated soils is a process involving energy dissipation due to frictional loss along grain contacts during cyclic loading, leading to destabilization of the soil structure. The energy required to cause liquefaction depends on the density of packing of the grains and confining stress. If the energy dissipated in a saturated loose deposit by an earthquake exceeds the energy required to cause liquefaction on a per volume of soil basis, the soil liquefies. Similarly, if the energy dissipated due to vibrations caused by DC or vibratory probe exceed the energy required to cause liquefaction, pore pressure approaches 100 percent of confining stress. Therefore, it is possible to design ground improvements required to resist liquefaction on the basis of earthquake energy and energy delivered by DC and vibratory probes. It is also possible to determine the degree of improvement in density of the soil due to repeated applications of dynamic compaction and vibro-probe insertions during stone column installation, and design compaction or vibro-stone column installation parameters to increase the soil density to resist liquefaction due to a design earthquake.

Current practice for design, suitability assessment, and determination of optimum field operation parameters rely mainly on field pilot tests, past experience, and empirical equations. At present, there are no detailed analytical procedures available to determine the densification achievable or to analyze the effects of various operational parameters on the degree of improvement in both sands and non-plastic silty soil deposits. Advanced analytical techniques and computational tools need to be developed to aid these design analyses, taking into consideration site-specific soil conditions.

In this report, an analytical model for simulation of the performance of soil deposits during ground improvement projects, using energy principles governing soil liquefaction and soil densification by consolidation during dynamic compaction and stone column installation, has been developed. Effects of preinstalled wick drains on relieving the pore pressures and enhancing densification during DC and SC installation have been included in these numerical models for low permeable silty soils. Simple attenuation relationships were used to estimate the energy dissipated in the soil.

Experimental data based on energy principles coupled with relationships for spatial distribution of energy dissipation during DC and SC vibrations was used to estimate the excess pore pressures generated as a function of the energy dissipated in the soil. Coupled consolidation equations were used to simulate soil consolidation. Possible effects of an increase in lateral confining stresses during DC and SC installation were neglected. Such effects may be significant in highly permeable deposits.

Based on numerical simulations of ground response during DC and SC processes using this analytical model, design charts were developed for post-improvement soil densities or penetration resistances. Rational design procedures were developed to use these design charts to choose suitable DC and SC field operational choices to obtain post-improvement density or penetration levels, to mitigate liquefaction potential due to design earthquakes. The sites may or may not be preinstalled with wick drains, for these cases. The design charts were compared with data from instrumented field tests and other available case histories in sand and non-plastic silty soil deposits through collaboration with ground improvement industry partners. Stepwise design procedures and design examples are presented.

TABLE OF CONTENTS

TABLE OF CONTENTS (Continued)

LIST OF FIGURES

LIST OF TABLES

CHAPTER 1
INTRODUCTION

1.1 Overview of Problem

Liquefaction of loose saturated granular soils is a continuing threat to the performance of buildings, highways, bridges, lifelines and other facilities and often causes major economic loss and loss of life and injury in almost every earthquake. The first widespread observations of damage attributed to liquefaction were made in the 1964 Niigata, Japan, and 1964 Alaska earthquakes. Most recently, significant liquefaction-induced damages were observed in Japan (1995), Turkey (1998) and Taiwan (1999). The high incidence of liquefaction during earthquakes, together with its potential for damage, has made the phenomenon a prime subject of concern in earthquake engineering. Liquefaction of ground resulting from earthquake shaking is manifested through surface indications like sand boils and ground cracking; settlement and tilting of buildings and bridge supports; flotation of buried tanks to ground surface; collapse of waterfront structures; lateral spreading and cracking of slopes and embankments; and flow failures of waterfront natural slopes and earth dams.

Liquefaction is defined as a process by which the shear resistance of a loose, saturated, cohesionless soil is reduced by the buildup of excess pore water pressure, which is the pore water pressure rise above the hydrostatic pressure, associated with the undrained cyclic straining induced by earthquake shaking. This buildup of pore pressure is due to the tendency of loose liquefiable soils to densify or contract, upon shearing.

Methods for mitigation of hazards associated with the occurrence of liquefaction deal directly with the factors that cause liquefaction to be initiated, and as liquefaction is triggered by the buildup of excess pore pressures; consequently, methods of prevention of its occurrence must reduce the tendency for buildup of these excess pore pressures. Generally, this can be accomplished by:
  i)   Densification, which historically has been the most commonly used technique, by increasing soil density since the tendency for pore pressure buildup is strongly related to the density of soil.
  ii)   Drainage by enhancing the drainage within the liquefiable soil to prevent the buildup of high pore pressures.
  iii) Physical and chemical modification (mixing and grouting) by increasing the binding of particle-to-particle contacts, and consequently, reducing the amplitude of cyclic strains and the contractive tendency of the soil.

Since most desirable soil properties improve with increasing soil density, densification is one of the most commonly used techniques for soil improvement. A number of different densification methods have been developed and used successfully. This report presents the use of dynamic compaction and vibro-stone columns to densify and mitigate liquefaction in saturated silty soil deposits preinstalled with wick drains.

1.2 Dynamic Compaction and Vibro-stone Columns

Dynamic compaction (DC) (shown in Figure 1-1a), and vibro-stone columns (SC) (shown in Figure 1-1b) are proven ground improvement techniques for liquefaction mitigation and foundation strengthening in sands containing little or no silt content. Saturated loose to medium dense sands densify due to vibration and/or impact-induced liquefaction and the associated expulsion of pore water from the soil through vertical and horizontal dissipation in case of DC, or through the surrounding stone columns during SC installation. The densified soil is more resistant to liquefaction, and has performed well during earthquakes (Mitchell et al. 1995, Andrus and Chung 1995).

Conversely, densification techniques have found limited applications in silty soils. Recent field trials show that such techniques may be extended to silty soils when combined with other supplementary techniques such as prefabricated drains (Dise et al., 1994; Han, 1998; Luehring et al., 2001). An example is shown in Figure 1-2.

(a)	(b)
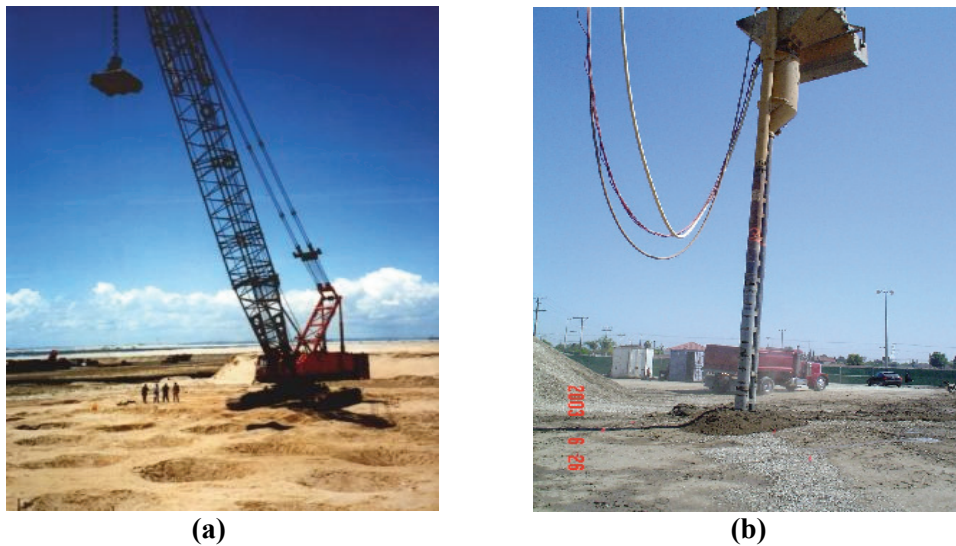
Figure 1-1. Dynamic Compaction and Stone Columns Equipment

Figure 1-2. Supplementary Pre-installed Wick Drains

However, current practice for design, suitability assessment, and determination of optimum field operation parameters for both clean sand sites and silty soil sites rely mainly on field pilot tests, past experience, and empirical equations (Lukas 1986, Lukas 1995, FHWA 2001). No formal theoretical analysis method is currently available to perform a detailed analysis and design for both techniques. A well-developed analysis model and design guidelines are required for design of both techniques to mitigate liquefaction in sand soil deposits and non-plastic silty soil deposits, supplemented with wick drains. Advanced analytical techniques and computational tools need to be developed to aid such design analyses taking into consideration site-specific soil conditions and expected design earthquakes.

1.3 Purpose of Report

The objective of this report is to introduce a rational analysis procedure and design guidelines for liquefaction hazards mitigation in saturated sands and non-plastic silty sands using i) Dynamic Compaction and ii) Vibro-stone Columns. In the case of silty sands, supplementary wick drains are included to expedite drainage and densification during both DC and SC installation projects.

This objective has been achieved through a number of tasks as follows:
  i)   Develop an improved understanding of the behavior of saturated soil deposits containing sands and non-plastic silty sand and sandy silts during DC and SC processes.
  ii)   Develop a computational methodology for simulation of both techniques and quantify the post-improvement densities achievable in: a) sand deposits without wicks, and b) non-plastic silty soil deposits supplemented pre-installed with wick drains.
  iii) Establish design charts, and design guidelines for liquefaction mitigation in silty soils using both techniques.

A numerical model has been developed to simulate the densification processes during both techniques through quantifying pore pressure generation due to vibrations caused by successive impacts on ground surface by DC or vibro-stone columns, pore pressure dissipation, and quantifying the associated concurrent densification of the soil around the impact zone or vibratory probe. The simulation models have been verified through a field study conducted at a silty soil site, Marina del Rey, Los Angeles County, CA in the case of SC. In the case of DC, this is accomplished through comparisons of results of the simulation model with recorded field post-improvement density or penetration resistance data from case histories of previous dynamic compaction projects.

The effects of site-specific conditions such as hydraulic conductivity, fines content, and pre-improvement soil density or penetration resistance on post-improvement density or penetration resistance and resistance to liquefaction have been quantified for a range of energy contents delivered to the soil at specific spacing. In addition, the effects of field operational parameters such as energy per impact, number of impacts, time cycle between impacts, impact grid spacing, impact grid pattern, and wick drain spacing, in the case of DC, or area replacement ratio and wick drains spacing in the case of SC, on post-improvement resistance to liquefaction have been studied. Based on this study, design charts and design guidelines for liquefaction mitigation in silty soils using DC and SC are provided. Design procedures and design examples are provided.

The simulation model and the design guidelines presented herein are expected to advance the use of DC and SC for liquefaction mitigation of silty soils, enhance the confidence of design engineers, and reduce the exclusive reliance on expensive field trials.

This report has been designed to be a general guidance document for liquefaction mitigation in silty soils using both techniques. The focus therefore is on the procedural steps, and decision-making reaching the optimum design parameters. Details of these simulation models and results are presented in Nashed (2005) and Shenthan (2005). The related publications resulting from this work are presented in Appendix A.

1.4 Outline of Report

Current practice and broad design guidelines in the current literature for both techniques are briefly reviewed in chapter 2. Chapter 3 presents the theoretical background for simulating soil densification response in saturated granular soil deposits subjected to DC and SC installations. Chapter 4 presents the numerical simulations of vibro-stone column installation, comparisons of post-improvement densities and penetration resistances with field case histories data, and instrumented field test data, and design charts for determination of post-improvement densities and penetration resistances for a variety of initial soil densities, fines content, hydraulic conductivity, etc. and stone column installation spacing, diameter, etc. Chapter 5 presents the numerical simulations of dynamic compaction, comparisons with field case histories, and design charts for determination of post-improvement densities and penetration resistances for a variety of initial soil densities, fines content, hydraulic conductivity, etc. and impact grid patterns, impact energies, impact spacing, time cycle between impacts, etc. Where relevant, example visualization results depicting progress in changes in densities in the ground at selected points as the dynamic compaction process continues over a site are presented. Chapter 6 presents simple design examples for liquefaction mitigation using these design charts for vibro-stone column and dynamic compaction in sand and silty sand deposits. Chapter 7 presents the conclusions.

CHAPTER 2
REVIEW - CURRENT PRACTICE AND DESIGN GUIDELINES

2.1 Introduction

This chapter presents a brief review of the current practice and the available design guidelines for:
i)   Dynamic compaction (DC) technique, and
ii)   Vibro-stone columns (SC) technique.

Attention is focused on liquefaction mitigation applications.

2.2 Dynamic Compaction

Dynamic compaction is one of the most simple and economically attractive densification techniques used for liquefaction hazard mitigation of saturated loose cohesionless soils with little or no fines content in the open field. Ground improvement and soil densification due to DC results from repeated applications of high-level impact energy at the ground surface. The energy is applied by repeatedly raising and dropping a pounder with a mass ranging from 5 to 35 Mg from heights ranging from 10 to 40 m on a pre-designed impact grid at 4 to 15 m spacing (Figure 2-1 a). Following the high-energy impacts, the soil surrounding the impact zone densifies, except for the surface of the deposit to a depth equal to the depth of the craters caused by the impact. This surface layer is usually compacted with a low-level energy impact called an ironing pass.

(a) DC without wick drains   **(b) DC with wick drains**
(For sand deposits with little or no fines) **(For non-plastic silty deposits)**
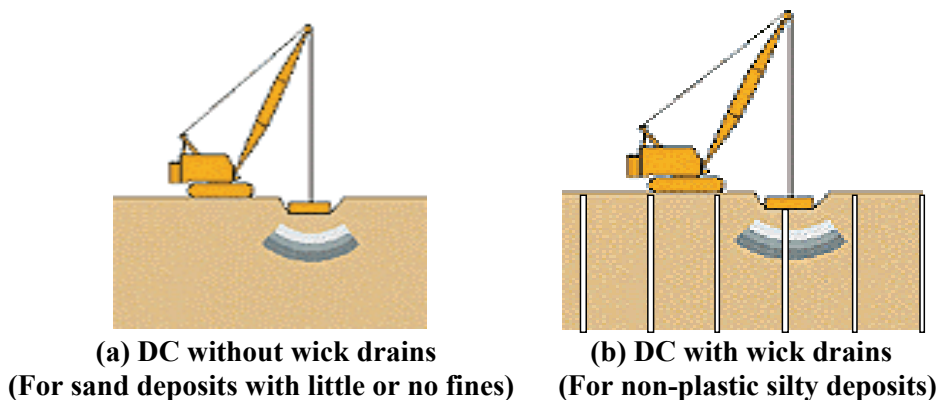
Figure 2-1. Dynamic Compaction

The impact energy applied to the ground surface results in densification due to ground vibration. In saturated loose sands, the vibrations cause a rise in pore water pressures and concurrent consolidation resulting in a denser arrangement of particles. It works well for clean sand sites. For sites containing silty sands, provision of drainage systems such as wick drains (Figure 2-1 b) has been found to enhance dissipation of pore pressures, consolidation of the soil and thus, the efficiency of DC to densify such low permeable soils (Dise et al. 1994, Han 1998). Since the energy is applied at the ground surface, the improvement depths are limited because of energy radiation and attenuation with depth.

A number of cases are reported in the literature where DC was used to reduce liquefaction potential. Most recent examples are found in Atukorala et al. (1992), Fahoum (2001), and Meyer et al. (2001). In these cases, the treated loose sand deposits were densified to a sufficient degree that liquefaction would no longer be a concern.

The earliest use of DC as a soil densification technique was many centuries ago. There is good evidence that compaction of loose deposits by repeatedly lifting and dropping stone weights took place in China around 1000 A.D. (Kramer and Holtz 1991) and later by Romans. In 1871, a Mexican war cannon filled with lead densified the soil for the St. George Mormon Temple in St. George, Utah (Welsh 1986). Cohesionless soils in Germany were compacted with 1.8-Mg tamper and a 1.5 m drop from a steam shovel in 1933. The Corps of Engineers experimented with heavy tamping at the Franklin Falls Dam construction site in 1936. In Russia, heavy tampers were used to compact loessial silty and sandy soils beginning about 1960 (Elias et al. 1999). Nevertheless, not until the early 1970's when the DC technique was finally promoted by the late French engineer Louis Menard with the advent of large crawler cranes that can apply high energy tamping levels, it has been used on a regular basis in France in 1970 and subsequently in Britain 1973 and in North America in 1975 (Slocombe 1993).

2.2.1 Current Practice

2.2.1.1 Suitability of Deposits

Originally, the DC technique was used for granular and fill soils. However, as the technique was proven efficient with time and due to its economic advantages, many other deposits have been considered. Lukas (1986) has categorized different soil deposits for suitability for DC based upon past experience from DC projects by means of conventional index tests. Figure 2-2 shows the range of soil gradation for each categorized zone. Table 2-1 presents the details of the different categories.

2.2.1.2 Design Guidelines

Current practice for design, suitability assessment, and determination of optimum field operation parameters rely on field pilot tests, past experience, and empirical equations relating depth of influence d_{max} to impact energy for various soil types (Lukas 1986, 1995) given by:

$$d_{max} = n\sqrt{WH} \qquad (2\text{-}1)$$

where W is the dropped weight in Mg, and H is the height of drop in m. The value of n was related to soil type and degree of saturation in Table 2-2 for a pounder that is raised and dropped with a single cable for a range of applied energy of 1 to 3 M J/m^2.
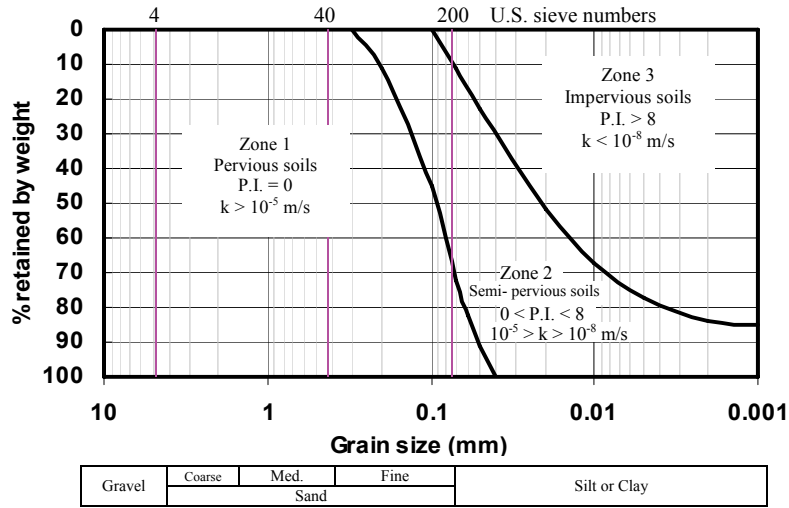
Figure 2-2. Range of Soil Gradation of Deposits Suitable for DC (Lukas 1986)

Table 2-1. Soil Deposit Suitability for DC

Soil Category (Figure 2-2)	Soil Type	Soil properties	Suitability for DC
Zone 1 – Most favorable soil deposits	Pervious soil deposits	$k > 10^{-5}$ m/s, PI = 0	Improvements are achievable
Zone 2 – Intermediate soil deposits	Silty sands, silts, and clayey silts	$10^{-5} > k > 10^{-8}$ m/s, $0 < PI < 8$	With dissipation of induced pore pressures
Zone 3 - Unfavorable soil deposits	Impervious clayey deposits	$k < 10^{-8}$ m/s, PI > 8	Not recommended

Typical average applied energy E_{avg} per cubic meter of improved soil is given by

$$E_{avg} = \frac{N_I * W * H * P}{S^2 * d_{max}} \tag{2-2}$$

where, N_I is number of impacts per location typically 7 to 15 impacts, P is number of passes, and S is grid impact spacing typically, for pervious deposits, 1.5 to 2.5 times pounder diameter. Typical values of E_{avg} for different soil deposits are summarized in Table 2-3. For preliminary design purposes, the typical values for n, E_{avg}, and Eqn. 2-1 are used to determine suitable parameters W, H, N_I, P and S to improve the soil to a desired depth d_{max} at a site. The most important limitation of Eq. 2-1 is that it neither accounts for the pre-improvement relative density or penetration resistance of the deposit nor for the required post-improvement soil density or penetration resistance. Mostly, successful applications of this methodology require field trials and post-improvement penetration resistance verification tests to determine final field operational parameters required to meet a specified minimum penetration resistance profile, before production-level ground improvement is implemented.

Table 2-2. Recommended *n* Values for Different Soil Types (Lukas 1995)

Soil Category (Figure 2-2)	Soil Type	Degree of Saturation	Recommended *n* value*
Zone 1	Pervious soil deposits – Granular soil	High	0.5
		Low	0.5 to 0.6
Zone 2	Semi-pervious soil deposits –Primarily silts with PI < 8	High	0.35 to 0.4
		Low	0.4 to 0.5
Zone 3	Impervious soil deposits –Primarily clayey soils with PI > 8	High	Not recommended
		Low	0.35 to 0.4 Soils should be at water content less than the plastic limit

*For an applied energy of 1 to 3 M J/m^2 and for a tamper drop using a single cable with a free spool drum.

Table 2-3. Applied Energy Guidelines (Lukas 1986)

Soil Category (Figure 2-2)	Type of deposit	Unit applied energy (KJ/m^3)	Standard Proctor energy (%)
Zone 1	Pervious coarse grained soils	200 to 250	33 to 41
Zone 2 & 3	Semipervious fine grained soils and clay fills above the water table	250 to 350	41 to 60
Other deposits	Landfills	600 to 1100	100 to 180

* Standard Proctor energy equals 600 K J/m^3.

a) Initial stages of impacting
b) After densification (including ironing pass)
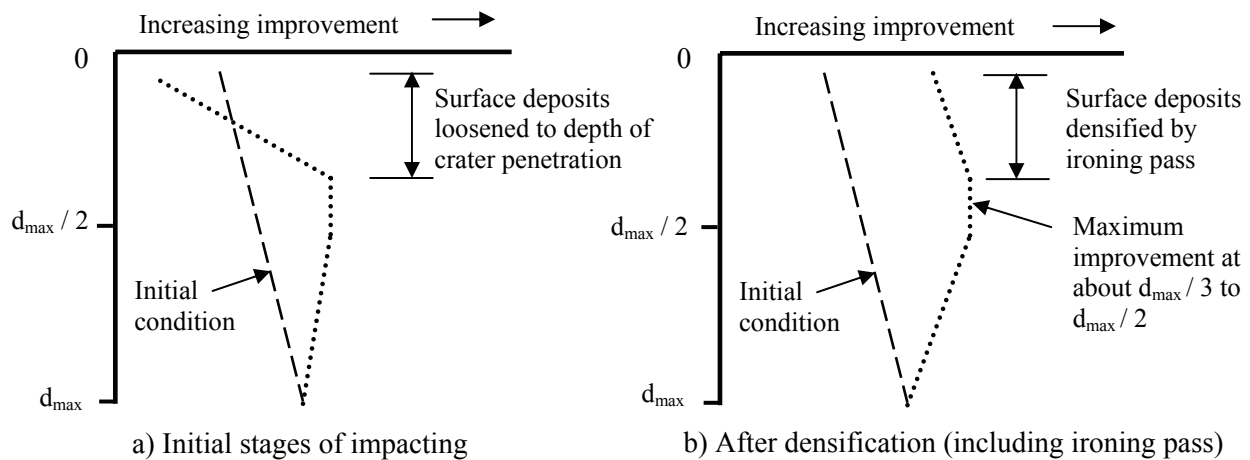
Figure 2-3. Variations of Degree of Improvement with Depth (Lukas 1986)

2.2.1.3 Degree of Improvement

Theoretically, the greatest amount of improvement is generally below the crater depth near the ground surface and then decreasing with depth due to the diminishing effect of the applied impact energy. However, typical test results after DC operations show that the shape of ground improvement tends to be similar to the Boussinesq's distribution of stresses for a circular foundation. The average improvement will be less than the maximum amount, which generally occurs within a zone between one third and one half of the maximum depth of improvement as shown in Figure 2-3. Above this zone, the improvement will be less because of surface disturbance during impacting, but can be improved by an ironing pass. Ironing pass involves a nearly complete coverage of the site with low impact energy.

2.2.1.4 Limits of Improvement

A review of the available case histories indicates that there may an upper limit to the densification that can be achieved by DC. Limit ranges are presented in terms of SPT, CPT, and PMT tests for different soil deposits (Table 2-4).

Table 2-4. Post-improvement Soil Properties - Upper Limits (Lukas 1986)

Soil Category (Figure 2-2)	Soil Type	Maximum test value		
		SPT N (blows/ 300 mm)	CPT (MPa)	Pressure-meter limit pressure (MPa)
Zone 1	Pervious coarse-grained soils sand and gravel	40 to 50	19 to 29	1.9 to 2.4
Zone 2	Semi previous soils i. Sandy silts ii. Silts and clayey silts	34 to 45 25 to 35	13 to 17 10 to 13	1.4 to 1.9 1.0 to 1.4
Zone 3	Partially saturated impervious soils Clay fills and mine spoil	30 to 40*	N/A	1.4 to 1.9
Other deposits	Landfills	20 to 40*	N/A	0.5 to 1.0

* Higher test values may occur due to large particles in the soil mass.

2.2.2 Shortcomings of the Current Practice

Although Eq. 2-1 relating the depth of influence d_{max} to energy level per impact (WH) is a useful guide, design choices such as impact weight, height of drop, number of impacts per location, impact grid spacing, time lag between impacts, total number of passes required to achieve a specified level of relative density or SPT/CPT penetration resistance, etc. are made based on field trials. At present, there are no detailed analytical procedures available to determine the feasibility of this technique and determine densification levels achievable or to analyze the

9

effects of various soil parameters such as silt content, hydraulic conductivity, etc. and dynamic compaction operational parameters on the degree of improvement achievable at a site.

Advanced analytical techniques and computational tools need to be developed to aid such design analyses, taking into consideration site-specific soil conditions, in making the most effective choices of dynamic compaction operational parameters for liquefaction mitigation applications.

2.3 Vibro-stone Columns

Vibro-compaction ground treatment techniques trace back to the 1930s with the development of the first vibrating probe for the compaction of granular soils. The technique was first used in the U.S. in 1948 (Elias et al. 1999). However, the technique was not used on a wide scale until the 1970s. Vibro-stone columns have been in use to reduce liquefaction-induced hazards since 1974, when this technique was first utilized for prevention of liquefaction at a site in Santa Barbara, CA. Dobson (1987) reported several case histories, which give evidence for the usage of vibro-stone columns in sands as well as non-plastic silty soils to mitigate liquefaction hazards.

The vibro-stone column installation process involves insertion of a vibratory probe with rotating eccentric mass (FHWA 2001). Figure 2-4a shows a vibro-stone column arrangement for relatively clean sand sites. The probe (Figure 2-5) plunges into the ground due to its self-weight and vibratory energy, which facilitates penetration of the probe. Once the specified depth (depth of stone column) is reached, the probe is withdrawn in steps (lifts) of about 1 m. During withdrawal of the probe, the hole is backfilled with gravel. During each lift, the probe is then reinserted expanding the stone column diameter. This process is repeated several times until a limiting condition is achieved. In sandy soils, the limiting condition is considered to be achieved when the electric current amperage supply reading to the vibratory probe reaches a high value during reinsertion of the probe, indicating high resistance to penetration into the stone column. This reading is an indirect indication of the extent of the stone column, and soil density and confinement around the stone column. In cases where the amperage readings do not reach high limiting amperage values, construction proceeds until a minimum amount of stones is introduced into the ground to reach a specified minimum stone-column diameter. This happens almost invariably in low permeable soils. It is suspected that this occurs due to lack of sufficient drainage and low densification of the soil and low confinement around the stone column during installation works. Typically, the vibro-stone column technique for densification of soils is limited to sand sites with silt content less than around 15 % by dry weight. For silty soil sites, recent case histories show that provision of pre-installed supplementary wick drains around the vibro-stone columns (Figure 2-4b) enhance densification during installation (Andrews 1998, and Luehring et al. 2001).

(a) SC without wick drains
(For sand deposits with little or no fines)

(b) SC with wick drains
(For non-plastic silty deposits)
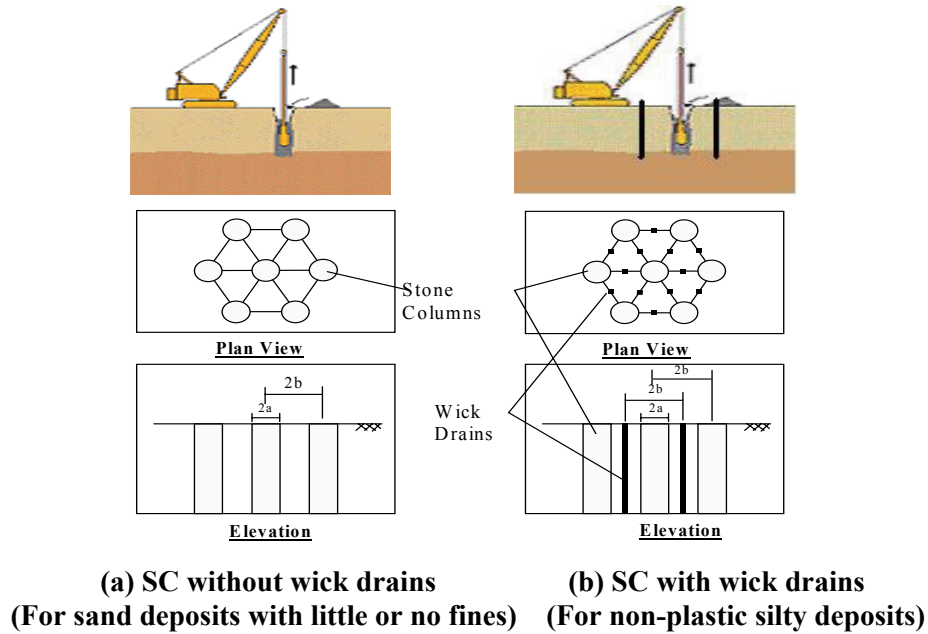
Figure 2-4. Vibro-stone Columns
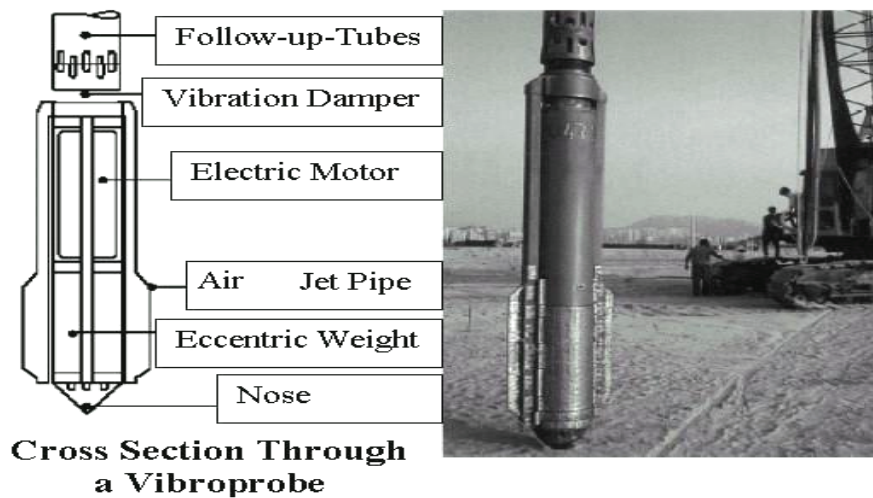
Figure 2-5. The Vibratory Probe

The stone columns also act as reinforcements increasing the stiffness of the improved ground and reducing the magnitude of shear stress caused in the improved soil due to an earthquake. In highly permeable soils, the insertion of the probe also causes an increase in lateral stresses in the ground. During an earthquake, the induced pore pressures also dissipate through the stone columns. All of the above processes reduce the liquefaction potential of the site. Past experience indicates that sandy soils improved using vibratory stone columns have performed well during earthquakes.

11

2.3.1 Current Practice

2.3.1.1 Suitability of Deposits

Liquefaction mitigation applications of vibro-stone columns have been mainly confined to densification of relatively granular soils containing less than 15% passing sieve #200 (74 µm) and less than 2% of clayey particles (<2 µm) (FHWA 2001). If the soil contains excessive fines, it has been considered difficult to densify using vibro-stone columns.

2.3.1.2 Design Guidelines

Although stone columns are used to improve soils over a long time, there is no unique design method available for liquefaction mitigation applications. In the U.S., vibro replacement stone column designs are primarily limited to their capability of soil densification (Baez and Martin, 1992; Baez, 1995). A simplified densification prediction model considering the initial density state of the soil was first introduced by Baez (1995). Prior to that, the selection of stone column diameter and spacing relied on the personal experience of the engineers and contractors, or on a preliminary design chart introduced by Barksdale and Bachus (1983), which does not consider the initial state of the soil (Drumheller et al., 1997).

Seed and Booker (1977) were the first to develop a simple design method to assess the drainage effect of stone columns used as gravel drains. However, the Seed-Booker method did not quantify the soil densification that occurs during installation and its effect on increasing the resistance to liquefaction of the soil. Their design method focused on consideration of the stone column as a pore pressure relieving well and on prediction of maximum pore pressure that would develop in the soil deposit improved by stone columns, which were assumed infinitely permeable during an earthquake. This method has since then been refined to include the effects of soil smearing and well resistance on pore pressure dissipation rates (Onoue, 1988).

Later, Baez and Martin (1993) introduced an approximate method to introduce the reinforcement effect by the stone columns on the cyclic shear stress caused by an earthquake. The reinforcement effect becomes predominant especially when the soils being treated is of very low permeability (e.g. silts) as the drainage efficiency will be very low.

Based on SPT and CPT data obtained before and after SC installation from 18 case histories, Baez (1995) developed an empirical relationship between pre- and post-improvement SPT blow counts $(N_1)_{60cs}$ for different stone columns spacings, expressed in terms of area replacement ratio A_r (Figure 2-6). The replacement area ratio, A_r, is defined as the ratio of stone column area to the tributary area per stone column. This approach is purely based on the regression analysis of available data, and represents average conditions. It is applicable to sands and fine to medium silty sand with fines less than 15% and little or no clay content.
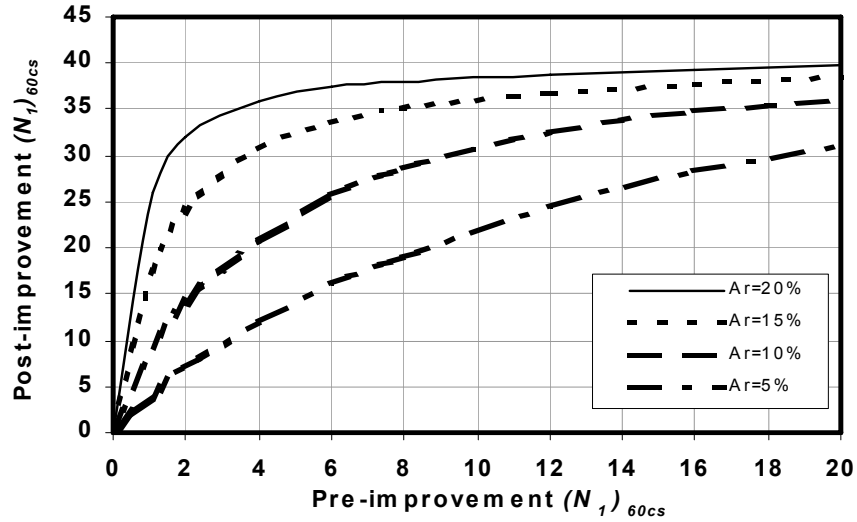
Figure 2-6. Pre- and Post-improvement $(N_1)_{60cs}$ **(Baez 1995)**

Although not explicitly introduced in Figure 2-6, the post-improvement $(N_1)_{60cs}$ is also dependent on the energy rating of the vibratory probe and the method of installation. At present, there are no detailed analytical procedures available to determine the densification or post-improvement penetration resistance achievable or to analyze the effects of various soil parameters and vibro-stone column parameters on the degree of improvement achievable at a site. Modifications are also needed to this design chart to include soils containing high non-plastic silt contents.

CHAPTER 3
DYNAMIC COMPACTION AND VIBRO-STONE COLUMN -
NUMERICAL SIMULATION MODELS

3.1 Conceptual Model

Improvement of loose saturated sands and non-plastic silty soils by vibro-stone column and dynamic compaction is essentially a process involving vibration of the soil, causing excess pore pressure development, possible liquefaction, and consolidation of the soil leading to concurrent densification. The vibro-stone column also involves expansion of a zero cavity and associated rise in pore pressures and densification of the soil. In cases where the soil permeability is very high, the excess pore pressures generated may dissipate almost instantaneously, causing a fully drained condition. In such a case, both dynamic compaction and vibro-stone columns tend to increase the soil density as well as the lateral confining stresses around the impact zones and vibratory stone columns. In medium to low permeable soils, after a certain level of soil densification is achieved, subsequent repeated impacts by a tamper or vibratory insertions of the vibro-probe may also cause an increase in lateral confining stresses in the soil. In all cases, the increase in soil density and confinement leads to an increase in resistance to liquefaction during a post-improvement earthquake. In the case of vibro-stone columns, the stone columns may also act as drainage pathways to reduce accumulation of excess pore pressures during earthquakes, and hence further increase the soil resistance to liquefaction.

Liquefaction of saturated granular soils is a process involving energy dissipation due to frictional loss along grain contacts during cyclic loading, leading to contact slips and instability of the soil structure and an increase in excess pore pressures. The energy required to cause liquefaction depends on the density of packing of the grains, effective confining stress, etc. Studies have shown that the magnitude of induced excess pore pressure due to undrained cyclic loading in a saturated granular soil is related to cumulative energy dissipated per unit volume of soil (e.g. Nemat-Nasser and Shokooh 1979, Davis and Berrill 1982, Law et al. 1990, Figueroa et al. 1994, Desai 2000, Green and Mitchell 2004, and Thevanayagam et al. 2002). If the energy dissipated in a saturated loose deposit due to an earthquake exceeds the energy required to cause liquefaction on a per volume of soil basis, the soil liquefies. Similarly, if the energy dissipated in a saturated loose granular soil due to vibratory tamping during dynamic compaction or vibro-stone column installation exceeds the energy required to cause liquefaction, pore pressure approaches 100 percent of confining stress at localized locations around the impact zone or vibratory probe zone.

Based on this concept, there have been suggestions to use an energy-based approach to design liquefaction mitigation using vibratory densification methods (Thevanayagam and Martin 2002, Green and Mitchell 2004, Thevanayagam et al. 2005). The objective of a vibratory densification scheme is to impart sufficient energy to the soil to be improved by repeated applications of vibratory energy to repeatedly liquefy and densify the soil until its density increases sufficiently and its resistance to liquefaction exceeds the would-be-dissipated energy due to an anticipated future design earthquake. Figure 3-1 illustrates this concept, where $(E_L)_{pre-Den}$, $(E_L)_{post-Den}$ are the energy per unit volume of soil required to cause liquefaction pre and post densification, respectively. E_{EQ} is the dissipated energy per unit volume due to the design earthquake, and

$\mathit{\Sigma E_{Den}}$ is the increase in energy required to cause liquefaction of a soil from its initial pre-improvement state, and is equal to the difference between $(E_L)_{post\text{-}Den}$ and $(E_L)_{pre\text{-}Den}$. The cumulative energy per unit volume of soil applied during DC or SC typically would be much higher than ($\mathit{\Sigma E_{Den}}$ x volume of soil improved) due to energy losses at the far field beyond the immediate vicinity of the impact zone or vibro-probe zone.
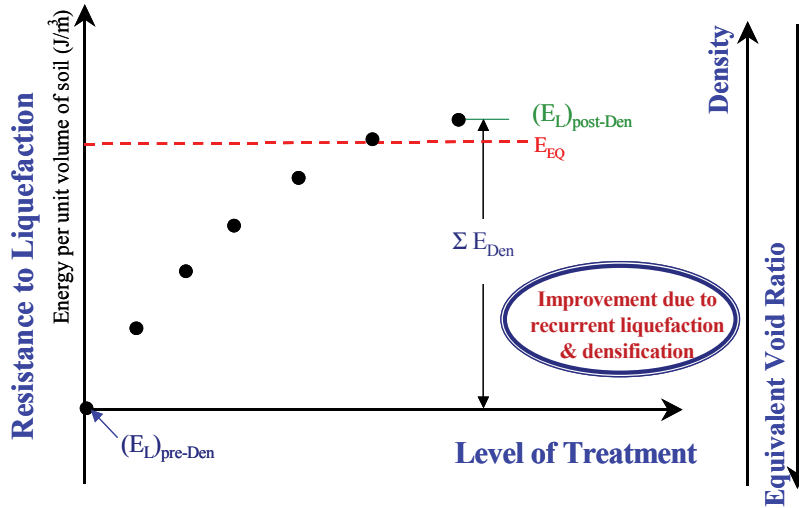
Figure 3-1. Energy-based Liquefaction Mitigation
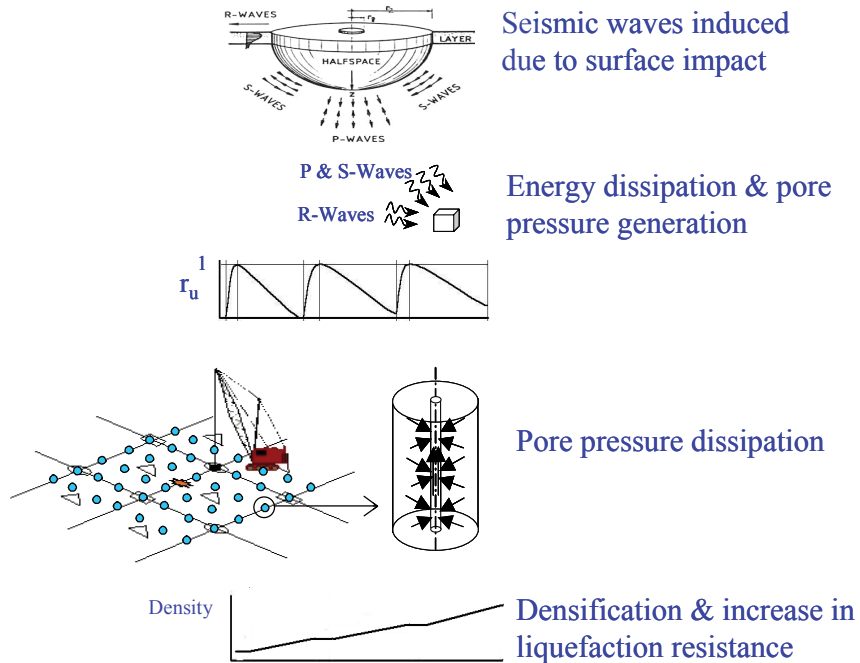
(a) Dynamic Compaction in Silty Sands supplemented with Wick Drains

Figure 3-2. Soil Densification Process During DC and SC

16

Vibratory energy delivery

VibroProbe

Energy dissipation &
Pore pressure generation

Body-Waves

(Outer) Stone
Column

Center Column

Wick Drain

Pore pressure dissipation

Density

Densification & increase in
liquefaction resistance
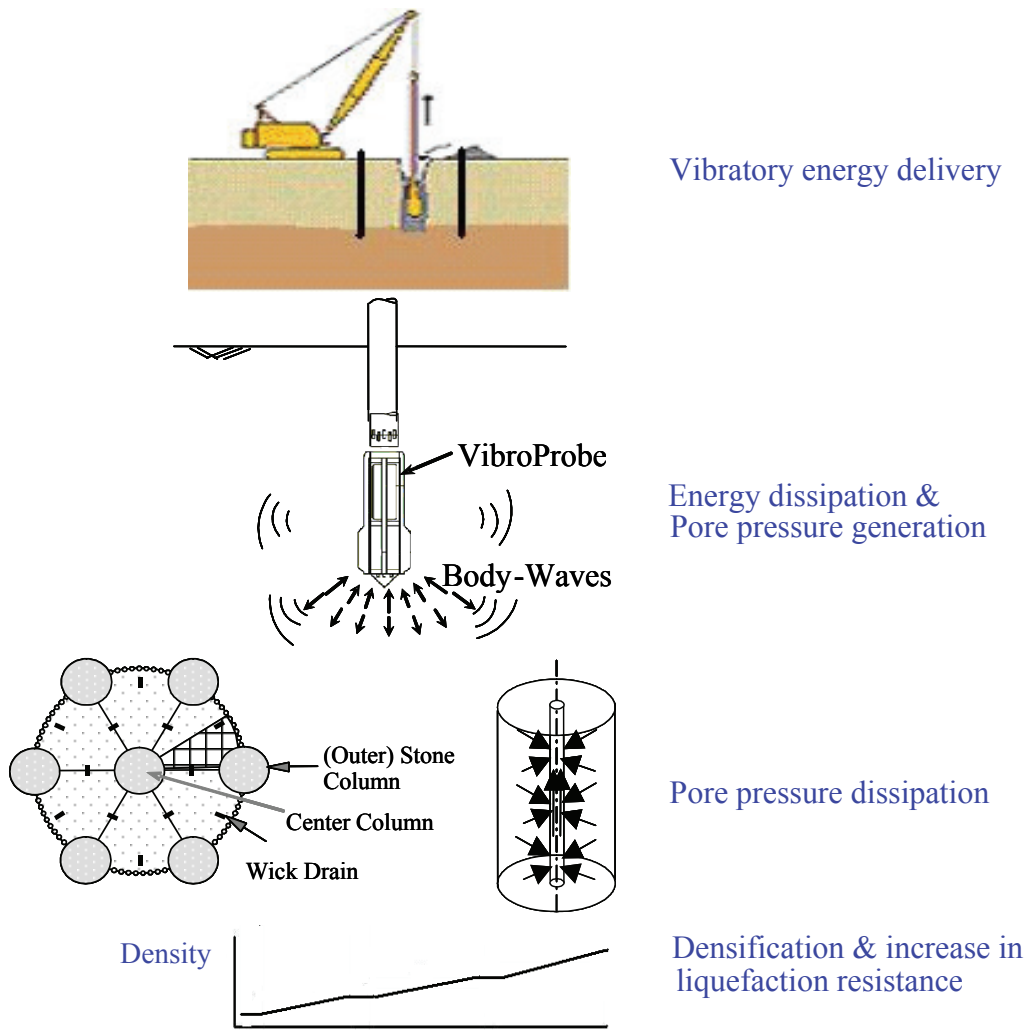
(b) Vibro-stone Column in Silty Sands supplemented with Wick Drains

Figure 3-2. (Continued) Soil Densification Process During DC and SC

Figure 3-2 schematically illustrates the densification process during DC and SC installation projects. In the case of DC, energy is delivered through successive surface impacts, generating seismic waves. The generated waves radiate through the soil deposit, causing vibrations of soil grains. The wave energy dissipates due to material damping, generating pore pressures around the impact zone. During the time cycle between successive impacts, the generated pore pressure dissipates. In the case of sands, the excess pore pressure induced due to impact dissipates outward from the impact zone. In the case of silty sands supplemented with wick drain, the excess pore pressures dissipate towards the wick drains. As the pore pressure dissipates, the soil consolidates in denser density packing that then increases the soil liquefaction resistance. A similar process occurs during repeated insertion and expansion of the vibro-stone column as illustrated in Figure 3-2b.

This chapter presents a methodology to simulate pore pressure developments in the soil due to vibratory energy imparted during dynamic compaction and vibro-stone column installation project in saturated sands and silty sands, and to quantify subsequent consolidation of the soil and densification. The effects of possible increase in confining stress in the soil as described before are not included. Energy partitioning models based on elastic half space coupled with simple attenuation models to account for material damping are used to estimate the energy dissipated in the soil surrounding the impact zone or vibratory probe. An energy-based pore pressure model developed based on experimental data is used to estimate the pore pressures generated around the impact zone or vibratory probe as a function of the energy dissipated in the soil during impact DC or vibro-stone column installation. Coupled consolidation equations are used to quantify densification. A finite difference numerical scheme is developed to simulate this process. This model is used to simulate a few selected case histories of dynamic compaction and vibro-stone columns, as well as to study the effects of various soil parameters and design/construction choices on the degree of improvement achievable for various simplified soil profiles.

3.2 Vibratory Energy Radiation and Attenuation

Consider vibro-stone column (SC) (Figure 3-3) and dynamic compaction (DC) impact (Figure 3-4) processes. The energy delivered at the source by the vibratory probe and by a falling weight propagates through the surrounding soil as body waves (compressional and shear waves) for SC, and body waves and surface waves (Rayleigh waves) for DC, respectively. Field observations indicate that the ground vibration caused by SC is in the range of 30 to 50 Hz (FHWA 2001) and between 2 to 20 Hz (Mitchell 1981, Mayne 1985) for DC. A solution for energy dissipated (per unit volume of soil), the associated pore water pressures, and densification at any point in the soil requires a reasonably accurate quantification of energy partitions in the above three categories and their spatial attenuation relationships. The problem is complex due to non-uniformity in the stress field, stress and density dependent soil properties, and changes in the stress field, pore water pressures, and soil densities in the ground during and immediately following the energy delivery. In order to circumvent this problem, as a first order approximation, models for energy partition in the elastic half space coupled with field observation based attenuation models that account for material damping are used herein.

3.2.1 Dynamic Compaction

Past studies indicate that the energy partitioning in the form of shear, compressional, and Raleigh waves due to a harmonic uniform vertical stress on a flexible disk of radius r_0 acting on an elastic half-space is dependent on the frequency parameter a_0 (= $\omega r_0 / c_s$, where, ω = angular frequency in Hz., and c_s = shear wave velocity in m/s) (Figure 3-5) and Poisson's ratio (Miller and Pursey 1955, Meek and Wolf 1993). Further, Richart et al. (1970) show that Raleigh wave amplitude varies with dimensionless depth (depth/L_R) as shown in Figure 3-6 where, L_R = wavelength of Rayleigh wave. Rayleigh wave amplitude ratio attenuates with depth very rapidly to about 10% at a depth of about 1.6 L_R. As a first order approximation, if the above model is used to determine the energy partitioning for DC, the frequency parameter a_0 tends to be less than 1 for typical values of r_o corresponding to impact weights used in dynamic compaction, c_s of soils, and

frequencies in the range of 2 to 20 Hz, and hence Rayleigh waves account for about two thirds of impact energy transfer and body waves account for the remaining one third. For DC, further, considering radiation damping, the energy content of the body wave is assumed to be uniformly distributed on a hemispherical surface of the wave front, while the energy content of the Rayleigh wave is assumed to be radially spreading along a cylindrical surface, and is also assumed to attenuate with depth as shown in Figure 3-6 for various Poisson's ratios.

(a) **Cross Section Through a Vibroprobe**

(b) **Radiation of Vibratory Energy - Schematic**
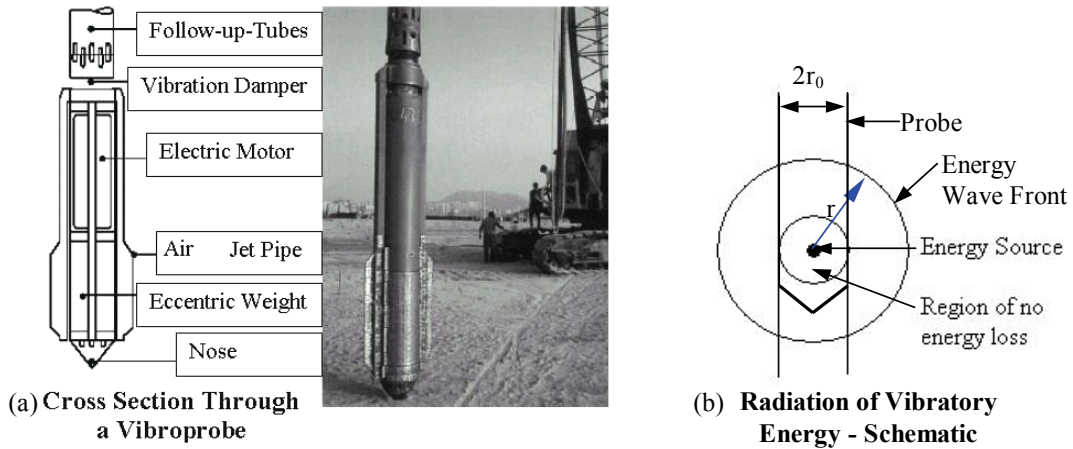
Figure 3-3. Vibratory Probe and Energy Propagation
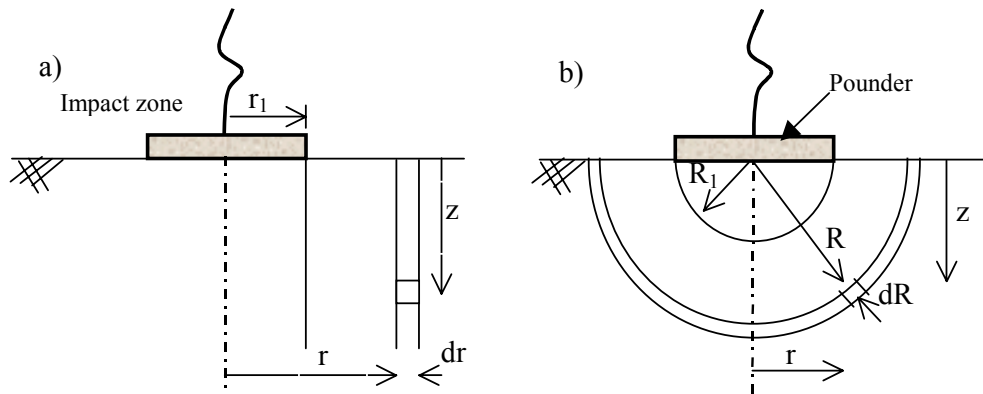
Figure 3-4. Energy Partitioning – Dynamic Compaction
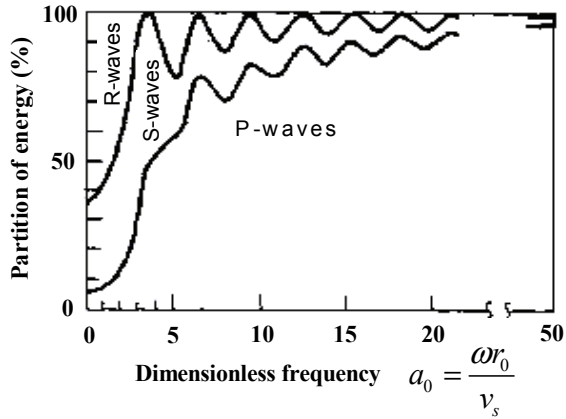
Figure 3-5. Partition of Energy – Surface Load
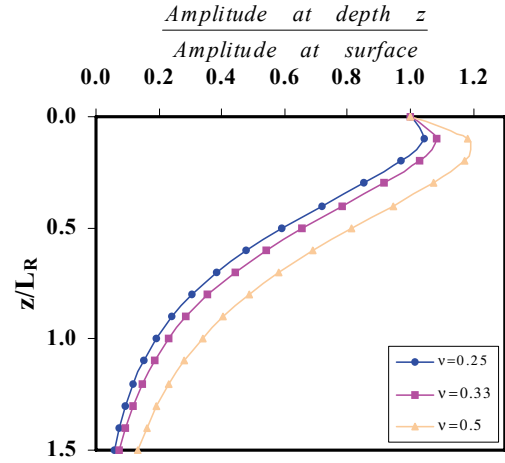
Figure 3-6. Wave Amplitude (Rayleigh Wave)

Material damping occurs as a result of energy loss due to hysteresis damping and internal sliding of soil particles. The energy loss depends on frequency of loading, soil type, stress conditions, and strain level. Field observations indicate surface wave attenuation due to material damping is given by (Richart et al. 1970, Dowding 1996):

$$a = a_1 . \, e^{-\alpha(r-r_1)} \tag{3-1}$$

where, a_1 = amplitude of vibration at distance r_1 from the source, a = amplitude of vibration at distance r, and α = attenuation coefficient due to material damping. Energy attenuation is related to the square of the amplitude of vibration; the corresponding energy attenuation relationship is given by

$$E = E_1 . \, e^{-2\alpha(r-r_1)} \tag{3-2}$$

where, E_1 = energy content at a distance r_1 from the source, E = energy content at a distance r.

Based on the above considerations, the energy loss per unit volume of soil due to Rayleigh waves w_R and body waves w_B, respectively, in the case of DC, are given by

$$w_R(r,z) = F(0.67WH)\frac{\alpha e^{-2\alpha r}}{\pi r} \tag{3-3}$$

$$F = \frac{f^2\left(\dfrac{z}{L_R}\right)}{\displaystyle\int_0^\infty f^2\left(\dfrac{z}{L_R}\right)dz} \tag{3-4}$$

$$w_B(r,z) = (0.33WH)\frac{\alpha e^{-2\alpha R}}{\pi R^2} \tag{3-5}$$

where, $R = \sqrt{(r^2+z^2)}$, f=amplitude ratio given by Figure3-6, and r and z are radial and vertical coordinates, respectively.

3.2.2 Vibro-stone Columns

In the case of SC, assuming that radiation damping is due to body waves spreading along a spherical wave front (Figure3-3b) and it is uniformly distributed on a spherical surface of the wave front, the energy loss per unit time per unit volume of soil takes the form:

$$w = W_0 \frac{\alpha e^{-2\alpha(r-r_0)}}{2\pi r^2} \tag{3-6}$$

where, $W_o = \eta_0 P_0$, P_0= power rating of the vibratory probe, η_0=probe efficiency. As excess pore pressure develops due to vibration during SC process, the soil becomes weak. Since the amplitude of vibration of the probe is limited (FHWA 2001), the energy imparted to the surrounding soil would decrease, resulting in a reduced efficiency. When the pore pressures dissipate, and the soil is sufficiently densified, the energy transfer rate would increase. In this paper, this phenomenon was taken into account considering the energy transfer rate to decay with increasing excess pore pressure:

$$w = W_0 \frac{\alpha e^{-2\alpha(r-r_0)}}{2\pi r^2} \cdot e^{-\beta(r_e)_{av}} \tag{3-7}$$

where $(r_u)_{av}$=the average excess pore pressure ratio within the soil surrounding the probe up to an effective radial distance r_e, and β=a constant. A detailed discussion on the applicability and limitations of the above attenuation relationships are reported in Shenthan (2005), and Nashed (2005).

3.3 Pore Pressure Generation

Based on a large experimental database and theoretical considerations, excess pore water pressure generated due to undrained cyclic loading has been related to frictional energy loss in the soil by Thevanayagam et al. (2002) as:

$$r_u = 0.5\log_{10}\left(100\frac{w_c}{w_L}\right), \quad \frac{w_c}{w_L} \rangle 0.05 \tag{3-8}$$

where, r_u=excess pore pressure ratio (u/σ_0'), σ_0'=initial mean effective confining pressure, w_c = cumulative energy loss per unit volume of soil, and w_L = energy per unit volume required to cause liquefaction.

In the case of the SC process, in addition to vibration-induced excess pore pressure, a significant amount of pore pressure is generated due to cavity expansion as well. Initial insertion of the

probe into the ground can be considered as expanding a zero cavity to a diameter the same as that of the probe. Filling of this cavity by stones and inserting the probe further expands the cavity by pushing the stone backfill radially outwards. Lifting the probe causes slight contraction of the cavity. Repeated lifting, filling, and insertion of the probe cause repeated cavity expansions. Shenthan et al. (2004d) outline a simplified approach to estimate excess pore pressures induced during such cavity expansions and contractions.

3.4 Pore Pressure Dissipation and Densification

The governing equation for pore pressure dissipation in the soil is:

$$\frac{\partial u}{\partial t} = \frac{k_h}{\gamma_w m_v}\left(\frac{\partial^2 u}{\partial r^2} + \frac{1}{r}\frac{\partial u}{\partial r} + \frac{1}{r^2}\frac{\partial^2 u}{\partial \theta^2}\right) + \frac{k_v}{\gamma_w m_v}\frac{\partial^2 u}{\partial z^2} + \frac{\partial u_g}{\partial t} \tag{3-9}$$

where k_h and k_v are hydraulic conductivity of the soil in horizontal and vertical directions, respectively; m_v=volume compressibility of the soil; u=excess pore water pressure at coordinates (r, θ, z); u_g=excess pore pressure generated due to vibration and cavity expansion (in the case of SC); t=time; γ_w=unit weight of water; r, θ, and z are radial, angular, and vertical coordinates, respectively. In the case of the vibro-stone column, the term u_g stands for time dependent pore pressure generation as in the case due to vibratory energy during SC installation. In the case of cavity expansion/contraction during vibro-probe insertion and impact during DC, the excess pore pressures are assumed to be induced instantaneously.

Volumetric densification of a soil element due to excess pore pressure dissipation may be obtained by:

$$\varepsilon_v = \int m_v . d\sigma' \tag{3-10}$$

where, ε_v=volumetric strain, and σ'=mean effective confining pressure. Seed et al. (1976) suggests that m_v values for clean sands increase from its initial value according to the following relationship, and do not decrease from the highest value obtained:

$$\frac{m_v}{m_{v0}} = \frac{\exp(y)}{1 + y + y^2/2} \geq 1; \quad y = a.r_u^b; \quad a = 5(1.5 - D_r); \quad b = 3(4)^{-D_r} \tag{3-11}$$

where, m_v and D_r are initial volume compressibility and relative density of clean sand, respectively. For silty sands, the above equation is modified using an equivalent relative density $(D_{rc})_{eq}$ instead of D_r to take into account the effects of fines on volume compressibility (Shenthan 2005). Typical values for m_{v0} are adopted from Thevanayagam and Martin (2001).

3.5 SPT Blow Count $(N_1)_{60cs}$ vs Clean Sand Relative Density $(D_r)_{cs}$

The numerical simulations of the above theoretical relationships require soil density parameters in terms of relative density for clean sands and equivalent clean sand relative density $(D_{rc})_{eq}$ for silty soils (Thevanayagam et al. 2002, Shenthan 2005). Details about the relationship of $(D_{rc})_{eq}$ to void ratio e, fines content FC, and soil gradation are presented elsewhere (Thevanayagam et al.

2002, 2003, Kanagalingam and Thevanayagam 2006). However, most field data describing soil conditions are expressed in terms of normalized overburden-stress-corrected SPT blow counts $(N_1)_{60}$ and silt content. For simulation of field sites, the reported $(N_1)_{60}$ and fines content need to be converted to $(D_{rc})_{eq}$. Conversely, for practical field applications of results from numerical simulations of simple soil profiles, the results obtained from such simulations must be converted to normalized clean sand SPT blow counts $(N_1)_{60cs}$.

For this purpose, the relationship proposed by Tokimatsu and Seed (1984) for clean sand relative density $(D_r)_{cs}$ and normalized clean sand blow count $(N_1)_{60cs}$ shown in Figure 3-7 was used (Nashed 2005). For non-plastic silty soils, $(N_1)_{60cs}$ is related to the normalized overburden-stress-corrected SPT blow counts $(N_1)_{60}$ and fines content FC by:

$$(N_1)_{60cs} = A + B(N_1)_{60} \tag{3-12}$$

where A = 0 and B = 1.0 for FC ≤ 5 % by weight, and A = 5.0 and B =1.2 for FC ≥ 35 % (NCEER 1997). For FC between 5 and 35%, A and B are given by:

$$A = e^{\left[1.76 - \frac{190}{(FC)^2}\right]} \tag{3-13a}$$

$$B = \left[0.99 + \frac{(FC)^{1.5}}{1000}\right] \tag{3-13b}$$
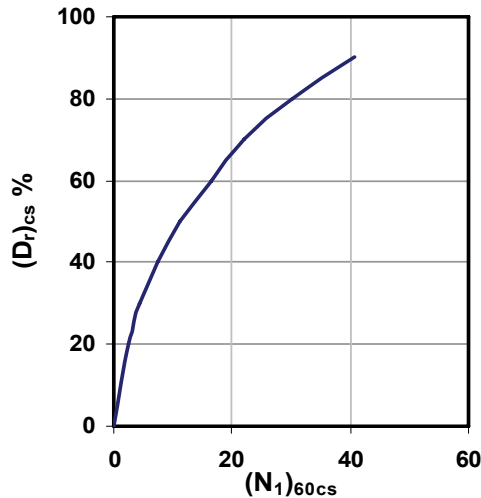
Figure 3-7. Relationship Between Relative Density $(D_r)_{cs}$ and $(N_1)_{60cs}$ for Clean Sands

CHAPTER 4
VIBRO-STONE COLUMN - NUMERICAL SIMULATIONS
AND DESIGN CHARTS

4.1 Introduction

The numerical model outlined in Chapter 3 was used to simulate the vibro-stone column installation process in saturated sands and silty sands to: (i) verify its predictive capabilities, (ii) study the effects of soil parameters such as hydraulic conductivity and silt content, area replacement ratio, wick drains, and initial soil density or penetration resistance on post-improvement density or penetration resistance, and (iii) develop simplified charts for design of vibro-stone columns for liquefaction mitigation. Figure 4-1 shows the vibro-stone column layout used for these numerical simulations. The spacing between vibro-stone columns is 2b (Figure 2-4). The spacing between wick drains is b (Figure 2-4). The radius of the stone columns and the equivalent radius of pre-installed wick drains are a and r_w, respectively. The wick drains are installed first over the entire site before vibro-stone columns are constructed. Two different effects of stone column installation processes, (i) vibration-induced excess pore pressure development and densification, and (ii) cavity-expansion-induced pore pressure development and densification, were considered separately. In the case of vibration-induced pore pressures, it was assumed that the perimeter stone columns shown in Figure 4-1 are installed first and the center stone-column is installed last. A finite-difference numerical scheme was developed to simulate vibro-stone column installation and the densification process in the soil surrounding the center column. Boundaries of symmetry allow reducing the computational time by requiring calculations to be done for only the representative area shown in Figure 4-1. Details of the simulation scheme are presented in Shenthan (2005).
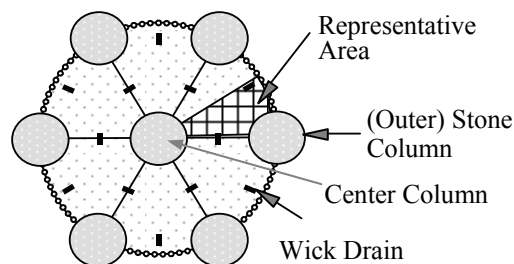
Figure 4-1. Composite Stone Column Layout

First, the numerical model was used to simulate the densification process in clean sands with no pre-installed wick drains. The relationship between pre- and post-improvement penetration resistances were obtained and compared with known case-history based data. This is described in Section 4.2. Secondly, simulations were done to study the effect of silt content and permeability on post-improvement equivalent clean sand relative densities achievable using vibro-stone columns with preinstalled wick drains and without wick drains, respectively. Based on experimental data available in the literature (Shenthan 2001), hydraulic conductivity k was obtained as a function of silt content. This is presented in Section 4.3. In these simulations, the

effect of cavity expansion was neglected and the effect of vibration induced pore pressure generation and dissipation was included.

In the third set of simulations, the effect of cavity expansion was included and the vibration induced pore pressures were neglected. The effect of cavity expansion on post-improvement equivalent clean sand relative densities was studied. This is reported in Section 4.4. Fourth, based on the above results, simplified design charts were developed, as presented in Section 4.5. This was followed by comparisons of the design chart-based predictions with results from a field study described in Section 4.6. In all the simulations, dissipation of excess pore pressures in the vertical direction was neglected in order to reduce the computational time. Possible effects of changes in confining stresses due to stone column installation were not included in this study.

4.2 Vibro-stone Columns in Sand without Wicks

The simulations presented herein consider soil densification due to dissipation of vibration induced pore pressures only. The simulations herein consider installation of vibro-stone columns in uniform clean sand with no wick drains (Figure 2-4a). Three different pre-improvement soil densities were used: (a) D_r=40%, (b) D_r=48%, and (c) D_r=59%. The hydraulic conductivity was assumed to be $5x10^{-6}$ m/s, representative for sand. Three different area replacement ratios (A_r=5.6, 10.0, and 22.5%) were simulated for each initial density, where A_r=(A_c/A_e)*100%, A_c is area of the stone column, A_e is the tributary area (=$\pi*D_e^2/4$), and D_e=equivalent diameter of the tributary area=1.05 times the center-to-center spacing between stone columns installed in a triangular pattern. These A_r values correspond to center-to-center stone column spacing of 4 diameters, 3 diameters, and 2 diameters, respectively. Table 4-1 summarizes the probe characteristics used for the simulation. Table 4-2 summarizes simulation parameters.

Table 4-1. Vibratory Probe Specifications

Length	Frequency	Power Rating P_0	η_0	β	Avg. Penetration Rate
m	Hz	kW	%		cm/s
3	50	120	50	4	3

Table 4-2. Simulation Parameters – Vibro-stone Column

Column Dia. (m)	Column Spacing (m)			k (m/s)
	A_r=5.6%	A_r=10.0%	A_r=22.5%	
0.9	3.6	2.7	1.8	$5x10^{-6}$

Note: Initial effective confining pressure at the depth considered is about 100 kPa.

The post-improvement relative densities are compared against pre-improvement densities for the three different area replacement ratios in Figure 4-2a. The results indicate that the area replacement ratio has a significant influence on post-improvement density. This influence diminishes as the initial density increases. Although not shown herein, it was also found that hydraulic conductivity also plays an important role. Higher hydraulic conductivity leads to higher densification for the same vibratory duration. Post-improvement densification diminishes as the hydraulic conductivity decreases (Shenthan 2005, Thevanayagam et al. 2001).
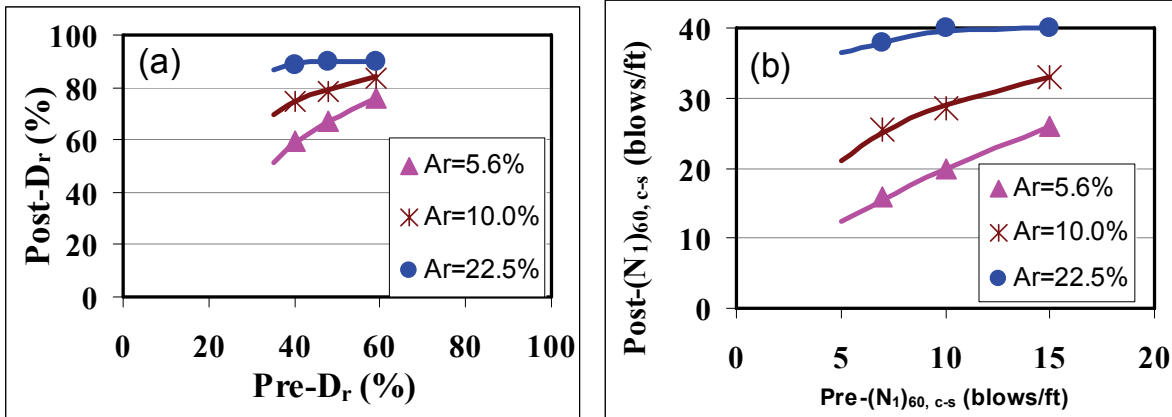
Figure 4-2. Vibro-stone Column Simulation Results

For qualitative comparison purposes, the data in Figure 4-2a may be converted to equivalent SPT blow counts $(N_1)_{60c-s}$ using Tokimatsu and Seed (1984) relationship for $(N_1)_{60c-s}$ and $(D_r)_{cs}$ for clean sands, as shown in Figure 4-2b. This can be compared with the field-case history database for pre- and post-improvement SPT blow counts compiled by Baez (1995) shown in Figure 4-3. The regression curves for post-improvement SPT blow counts obtained by Baez (1995) were based on an analysis of a number of case histories, where vibro-stone columns were used to improve sandy soil sites with less than 15% silts. Although direct comparisons are not possible due to lack of site-specific data, the trend found in Figure 4-2b agrees well with the trend in Figure 4-3.
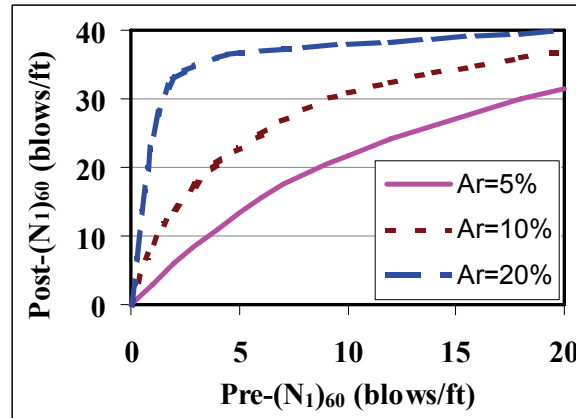
Figure 4-3. Vibro-stone Column Design Curves (Baez 1995)

4.3 Vibro-stone Columns in Silty Sand with Wicks

A number of simulations were conducted to assess the effects of hydraulic conductivity and silt content, and area replacement ratio A_r on post vibro-stone column installation soil density of silty soils preinstalled with wick drains (Figure 2-4b). Wick drains were assumed to be 100 mm x 5 mm in size with an equivalent diameter of 5 cm, installed at the center point between adjacent vibro-stone column locations (Figure 4-1). The soil sites were considered to be uniform sites. Three different pre-improvement equivalent clean sand relative densities $((D_r)_{eq}=40, 48$ and 59%, Shenthan 2005) were considered. Two different area replacement ratios $(A_r=10.0$, and

27

22.5%) were simulated. Silt content dependent soil input parameters (compressibility m_v, hydraulic conductivity k, energy required to cause liquefaction E_L) based on an experimental database for silty soils (Shenthan 2001, and Thevanayagam et al. 2001) were used. For direct comparison purposes, the same simulations were repeated for vibro-stone columns in the same soil without pre-installed wick drains (Figure 2-4a).

Figures 4-4a-b show the simulation results for post-improvement equivalent clean sand relative densities for $A_r=10$, and 22.5%, respectively, for the three different initial equivalent clean sand relative densities $(D_r)_{eq}$ considered. Without wick drains, no significant improvement is achieved for soils with hydraulic conductivity less than about 10^{-6} m/s. Although not shown in this Section, at low A_r, wick drains do not contribute to any further increase in post-improvement density for all initial densities (Shenthan et al. 2004a-c). In this case, the spacing of stone columns and wick drains are too large and wick drains are far from the stone columns to be effective in relieving the excess pore pressures generated during vibro-stone column installation and to facilitate repeated cycles of densification. As the area replacement ratio increases, both stone column spacing and wick drain spacing become smaller and the influence of wick drains in relieving the excess pore pressures become significant. At a high area replacement ratio of about 20% or above (Figure 4-4b), wick drains significantly contribute to the drainage and repeated densification occurs during vibro-stone column installation, even for silty soils with hydraulic conductivity as low as 10^{-8} m/s. However, the degree of improvement is dependent on hydraulic conductivity.
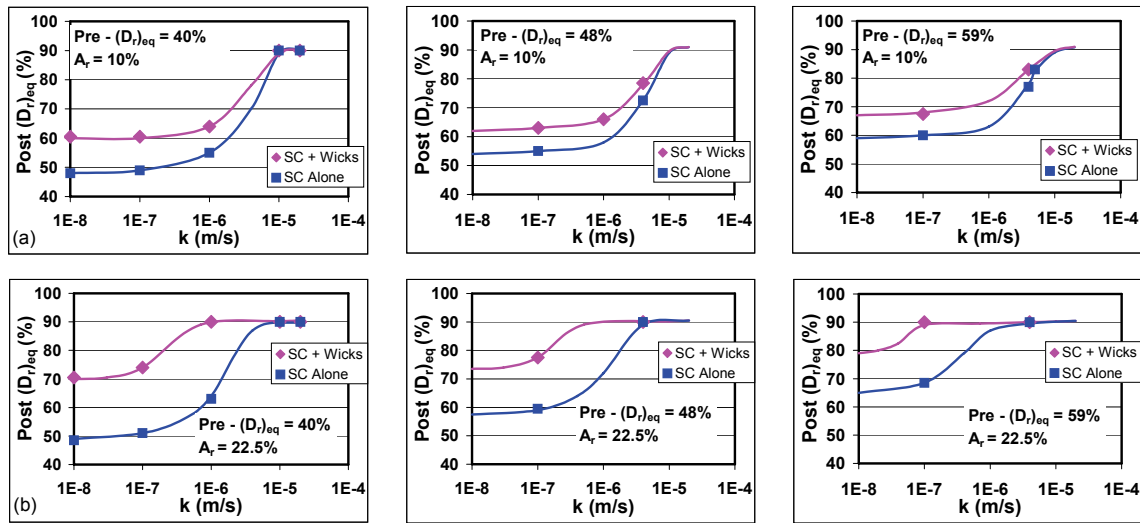
Figure 4-4. Composite Vibro-stone Columns – Simulation Results
(SC=Vibro-stone Column without Wicks, SC + Wicks= Vibro-stone Column with wick drains)

4.4 Cavity Expansion and Densification

The simulations presented herein consider soil densification due to dissipation of cavity expansion induced pore pressures only. These simulations involved two cases: (i) vibro-stone columns with wick drains, and (ii) vibro-stone columns without wick drains. The initial equivalent clean sand relative density $(D_r)_{eq}$ of soils was 40%. Three different area replacement ratios ($A_r=10$, 15, and 25%) were considered. Probe characteristics used for the simulation are

the same as those summarized in the Table 4-1. Table 4-3 summarizes simulation parameters relevant to this analysis. Vibratory probe diameter was 0.36 m. The probe was reinserted 7 times, in lifts of 1m, to build a stone column of 0.95 m diameter. Field experience indicates that this process takes about 4 to 5 minutes per lift of 1 m.

Table 4-3 Simulation Parameters - Cavity Expansion

Column Diameter (m)	Column Depth (m)	Column Spacing (m)			Depth Simulated (m)
		A_r=10%	15%	25%	
0.95	15	2.85	2.3	1.8	12

Note: Initial effective confining pressure at the depth considered is about 100 kPa.

The post-improvement densification results are shown in Figures 4-5a, b, and c for A_r=10, 15, and 25, respectively. Without wick drains, highest improvement is achieved for highly permeable soils at or above 10^{-5}m/s. The post-improvement density depends on hydraulic conductivity and area replacement ratio. Addition of wick drains does not significantly affect the degree of improvement due to cavity expansion. It appears that the cavity expansion induced pore pressures do not extend far enough from the stone column and hence wick drains do not significantly contribute to drainage in this case, except for large A_r (Figure 4-5c).
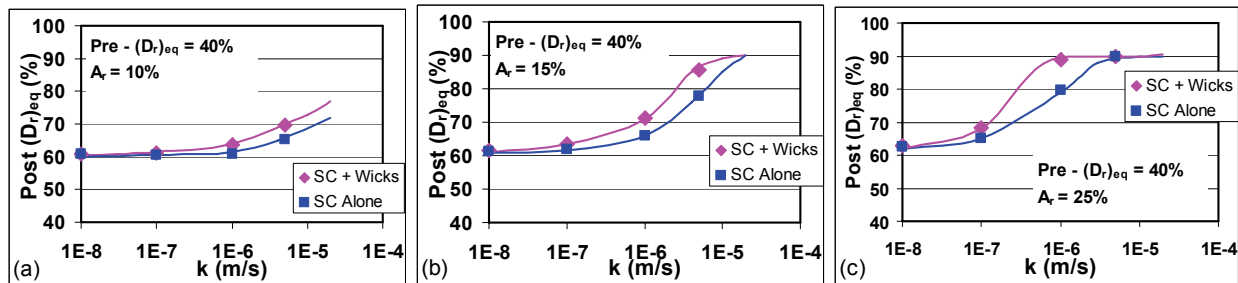
Figure 4-5. Post-improvement Densification - Due to Pore Pressures Induced by Cavity Expansion

The above results shown in Figures 4-4 and 4-5 indicate that both cavity expansion process and ground vibration contribute to densification. Post-improvement densities due to the coupled effect of both cavity expansion and vibratory energy should be higher than those obtained by considering cavity expansion only.

4.5 Simplified Design Charts

Based on the above simulation models, additional studies were conducted to develop simplified design charts to obtain the relationships between pre- and post-improvement soil densities for various uniform soil sites containing sands to non-plastic silty soils improved by SC pre-installed with wick drains. For convenient field applications, the results were converted in a form to present them in terms of equivalent pre- and post-improvement normalized clean sand SPT blow counts $(N_1)_{60cs}$ (Nashed 2005). The numerical simulations were conducted for uniform silty soil deposits with three different pre-improvement $(N_1)_{60cs}$ of 7, 11 and 16. For each $(N_1)_{60cs}$, three different area replacement ratios (A_r = 5.6, 10, and 22.5%) were considered. For each case, simulations were done for stone column installation process (i) without pre-installed wick drains, and (ii) with pre-installed wick drains, respectively. The effect of fines content was reflected by

varying the hydraulic conductivity (k) from 10^{-4} to 10^{-8} m/s, representing clean sands to non-plastic sandy silts. It was assumed that the vibro-stone columns are installed in a triangular pattern with wick drains pre-installed at midpoints between stone column locations as previously indicated in Figure 4-1. The power rating of the vibratory probe was set at 120 kW, operating at 50 Hz. The wick drains were assumed to be 100 mm x 5 mm in size with an equivalent diameter of 5 cm.

Figures 4-6 and 4-7 show the simulation results for pre- and post- improvement $(N_1)_{60cs}$ soils at a depth with effective vertical stress of 100 kPa for a range of k values. Solid lines in Figure 4-7 refer to soils improved with stone columns preinstalled with wick drains. The dashed lines refer to soils improved by stone columns alone without pre-installed wick drains. Figure 4-7 shows a similar trend shown in Figure 4-3 observed from stone column case histories for soils containing silt content up to 15%. However, Figure 4-7 is applicable for silty sands containing a large range of silt contents. Results show that, at a low area replacement ratio, the effect of supplementary wick drains is negligibly small and soil densification is primarily affected by stone columns. No significant additional densification is achieved by stone columns with wick drains compared to stone columns without wick drains in soils with hydraulic conductivities less than about 10^{-6} m/s. At a high area replacement ratio of about 22.5%, wick drains significantly contribute to the drainage of excess pore pressures induced during stone column installation and soil densification. The combined system is effective for soils containing non-plastic silt and hydraulic conductivity as low as 10^{-8} m/s. However, the degree of improvement decreases with increasing silt content and decreasing hydraulic conductivity.
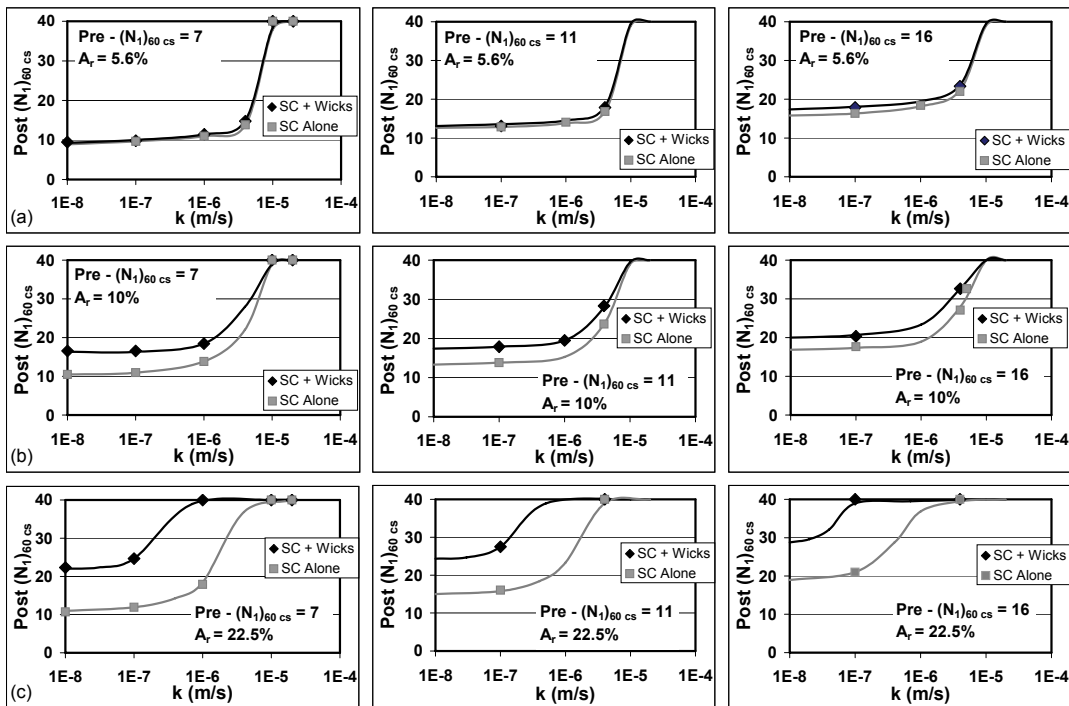
Figure 4-6. Vibro-stone Columns Design Charts
(SC + Wicks = vibro-stone column with wicks; SC = vibro-stone column without wicks)

Figures 4-8a,b show the relationship for pre- and post-improvement $(N_1)_{60cs}$ for a fixed $A_r =$ 22.5%, for soils with k values ranging from 10^{-4} m/s to 10^{-8} m/s, for stone columns without wicks and with wicks, respectively. The soils at high k values refer to sands and low values refer to sandy silts. Without wick drains, for high k values which are relevant for sandy soil sites with little or no silt content, the results agree with field observations reported in Figure 4-3. The post-improvement $(N_1)_{60cs}$ values are significantly affected by k. For low k values which are relevant for silty sands and sandy silts, the post-improvement $(N_1)_{60cs}$ values are much smaller than those observed for sands (Figure 4-8a). When wick drains are included, the post-improvement $(N_1)_{60cs}$ values are significantly improved (Figure 4-8b).
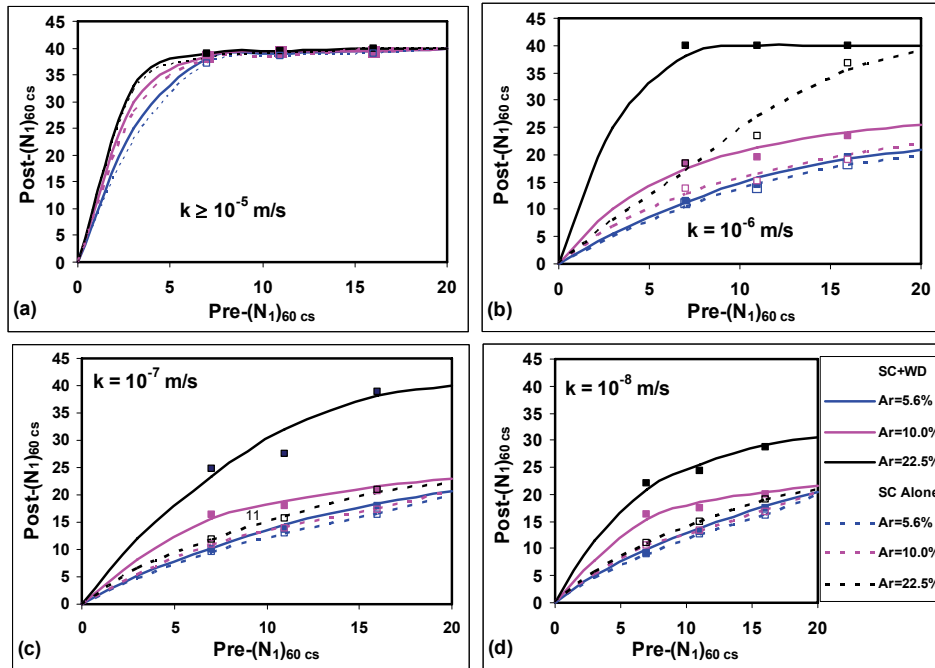
(SC + WD = vibro-stone column with wicks; SC Alone = vibro-stone column without wicks)

Figure 4-7. Vibro-stone Columns Design Charts

a) SC without wicks   b) SC with wicks
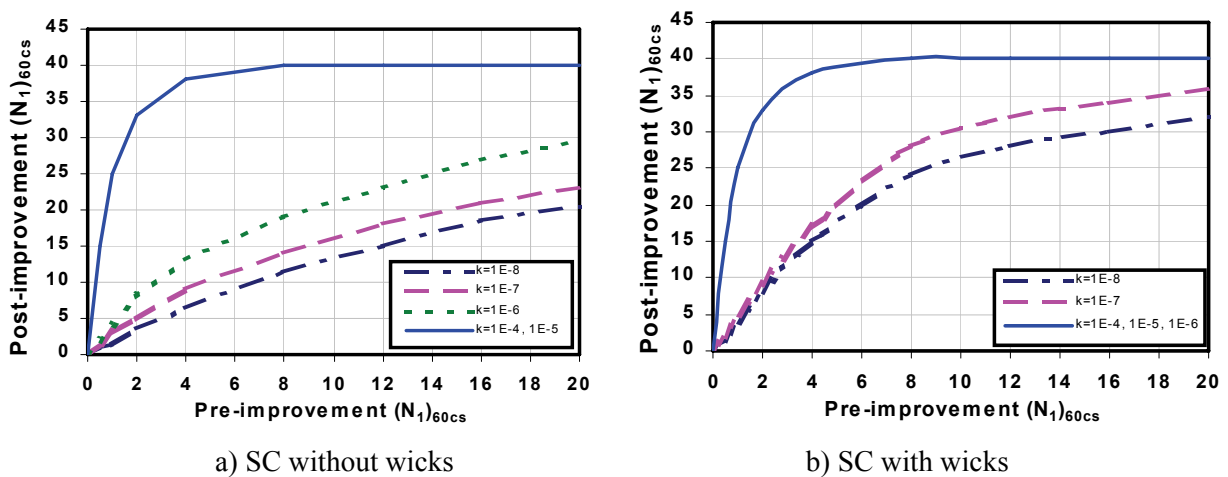
Figure 4-8. Pre- and Post-improvement $(N_1)_{60cs}$ for $A_r =$ 22.5% (Note: 1E-6 means $k = 10^{-6}$ m/s)

4.6 Field Comparisons

As part of this effort, a field test was conducted to verify the applicability of the above design charts for field conditions. The field tests were done in collaboration with Hayward Baker, Inc. and Advanced Geosolutions, Inc. at a site in Marina Del Rey, CA. The site consists of loose sands, silts, and clayey layers. The average soil profile within the test section is shown in Figure 4-9. The soil profile throughout the site is similar to the one shown in Figure 4-9 with varying layer thicknesses. The silt layer to be improved had a silt content ranging from 20 to 40 %. The hydraulic conductivity was estimated to be in the range 10^{-6} to 10^{-7} m/s. Liquefaction risk analysis suggested soil layers from 2.7 m up to about 6.0 m depth (approximate depth range of 2.9 to 4.1 m at the test section) in the site were liquefiable for a design earthquake of $M = 7.5$ and $a_{max} = 0.35g$. Ground improvement using vibro stone columns preinstalled with wick drains was recommended (Baez 2004, Personal communications).
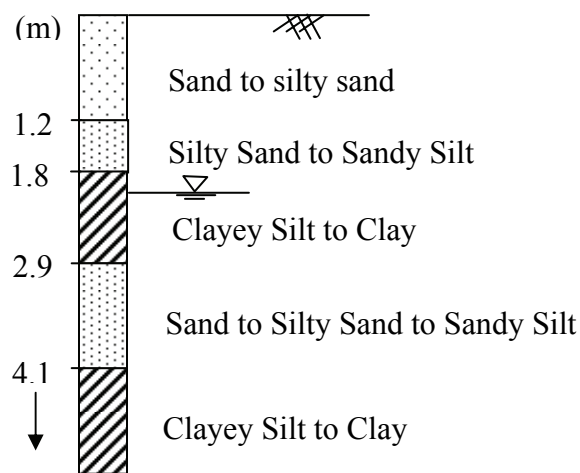
Figure 4-9. Soil Profile, Marina Del Rey, CA

Figure 4-10 shows the field setup. Red flags in this figure show the locations for stone columns. The dry vibro compaction (or stone column) method was used at this site. It involved the use of a bottom feed ("S" type) depth vibratory probe comprising an electrically powered eccentric weight assembly enclosed in a heavy tubular steel casing. The probe was powered by a 250 kVA diesel generator and develops high centrifugal forces in a horizontal plane at 30 Hz. Length of the probe was about 2.7 m, which was connected to follower tubes to a total length of about 10 m for this particular project. The diameter of the probe was about 0.45 m, and that of the stone columns was 0.9 m. Spacing between stone columns was 2.4 m, and the area replacement ratio was about 11 %. Wick drains dimensions were 100 mm x 5 mm (Baez 2004, Personal communications).

(a) Instrumentation and Wick Drains (b) Installation of Stone Columns begins   (c) Stone Column Installation

Figure 4-10. Instrumented Field Tests at Marina Del Rey

Plan View
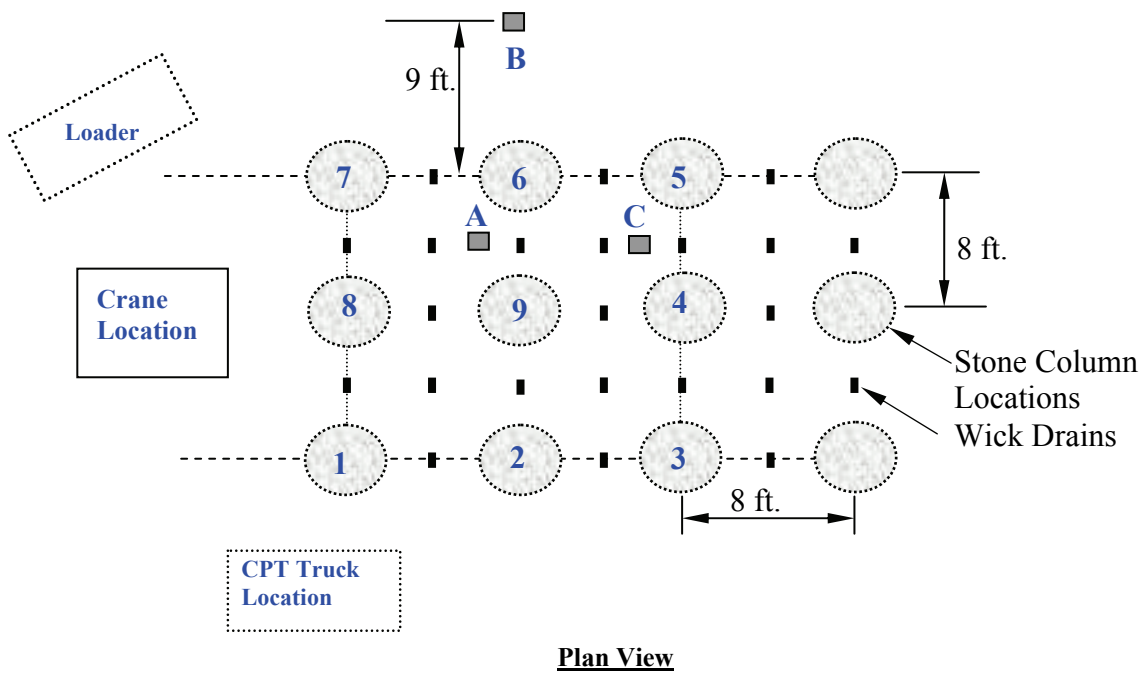
Figure 4-11. Site Layout and Instrumentation Locations
(Stone columns were installed at the numbered sequence shown)

Figure 4-11 shows a schematic diagram of the test area. Stone columns were installed at the numbered sequence 1 to 9. Pore pressures, ground vibrations, and energy delivered to the soil during stone column installation were monitored using a CPT mounted seismic piezocones (Fugro Geosciences, Inc., CA) at locations A, C (Figure 4-11), retrievable seismic accelerometers (www.nees.ucla.edu) at location B, and a current sensor mounted on the power cable of the crane, respectively. Details of the site, field test, instrumentation, and data are presented elsewhere (Shenthan 2005).

Three pre-improvement CPT tests and two post-improvement CPT tests were completed at the test location. The average pre- and post-improvement CPT profiles are shown in Figure 4-12a, and the corresponding soil profile is shown in Figure 4-12b. A detailed analysis of these data is

33

presented elsewhere (Shenthan 2005). Approximate average water table at the time of CPT tests and stone column installation is shown on the soil profile using dashed-line (Figure 4-12b). CPT test results were interpreted following the procedures outlined by Youd et al. (2001). Normalized CPT resistance results were converted to clean sand equivalent normalized SPT blow counts, $(N_1)_{60cs}$, using correlations recommended by Robertson and Wride (1998). The field results are shown in the simulation chart developed for $A_r = 10\%$, which is slightly different from the field A_r of 11%, in Figures 4-13a and b. The field results are in good agreement with the simulation results. Additional field data are needed to further validate the range of applicability of the simulation results.
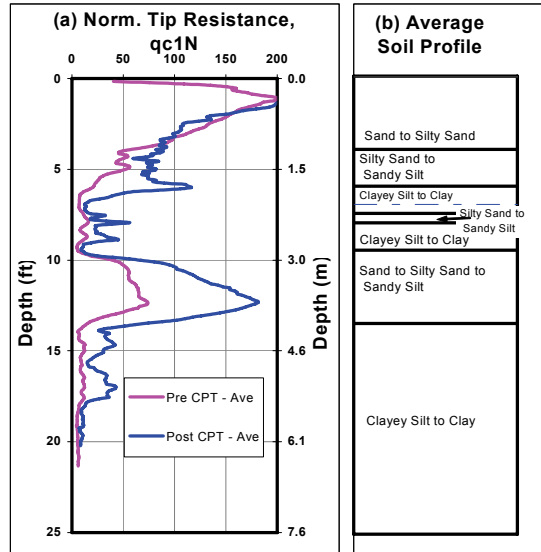
(a) Pre- and Post-Improvement CPT Profiles (b) Soil Profile

Figure 4-12. Cone Penetration Test Data
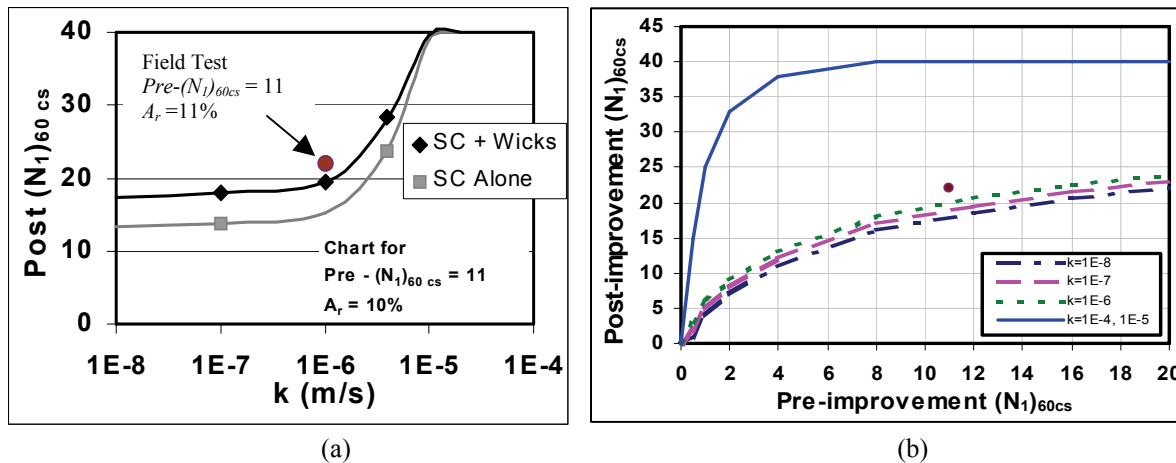
(a)   (b)

Figure 4-13 Comparison of Field Test Results with Numerical Simulations for $A_r = 10\%$
(Notation – k=1E-6 = 10^{-6} m/s)

34

CHAPTER 5
DYNAMIC COMPACTION - NUMERICAL SIMULATIONS
AND DESIGN CHARTS

5.1 Introduction

The numerical model outlined in Chapter 3 was used to simulate the dynamic compaction process in saturated sands and silty sands to: (i) verify its predictive capabilities, (ii) study effects of various soil properties and DC operational variables on degree of improvement achievable, and (iii) develop simplified design charts for dynamic compaction.

The flowchart in Figure 5-1 shows the DC stimulation procedure. Numerical simulation of the densification process begins with delivering energy to the ground surface through one impact of the pounder. The energy delivered to the ground surface is calculated considering a free drop of weight W from a given height H on the ground surface. Parameters such as cable drag and air resistance that restrict free fall are not considered. Such factors should be taken into account in the field by increasing drop height to achieve the design energy delivery per drop. The spatial distribution of the energy dissipated per unit volume of soil and the excess pore pressure distribution generated due to surface impact is determined based on the procedures outlined in Sections 3.2 and 3.3. The changes in pore pressures and associated changes in soil density are calculated based on consolidation equations presented in Chapter 3. A time-step finite difference scheme is used to simulate these processes until the next impact. It is recognized that all the excess pore pressure may not fully dissipate during the interval between the impact cycles. Therefore, the simulation model considers the residual excess pore pressure as well as the decaying energy transfer efficiency as soil approaches liquefaction. As the excess pore pressure dissipates and the soil density increases, the soil properties also change with time during the impact cycles. The soil parameters are continuously updated during this simulation to take these changes into consideration. Further details of this numerical simulation procedure are presented in Nashed (2005).

First, the numerical model was used to simulate a few known case histories of dynamic compaction. The results were compared with field data from these case histories. Following reasonably good comparisons, the simulation procedure was used to assess the effects of the following parameters on the depth of improvement and degree of improvement in sands and silty sands: (i) hydraulic conductivity k and fines content FC, (ii) number of impacts, (iii) time cycle between impacts, (iv) impact grid pattern and print spacing, (v) wick drains spacing, and (vii) initial density or standard penetration resistance. The results from this study are presented in Nashed (2005). This was followed by development of design charts for dynamic compaction.

```
                    New Impact
        Calculate energy delivered to ground surface

                            │
                            ▼
                    Partition of energy  ◄──────────────┐
                            │                           │
                            ▼                           │
              Calculate the energy dissipated           │
                  per unit volume of soil               │
                            │                           │
                            ▼                           │
              Calculate the induced pore pressure       │
              taking into account the already existing  │
                        pore pressure                   │
                            │                           │
                            ▼                           │
            Simulate dissipation of pore pressure throughout
              time cycle between impacts/drop passes    │
                            │                           │
                            ▼                           │
                Calculate changes in density            │
                            │                           │
                            ▼                           │
                  Update soil properties                │
                            │                           │
                            ▼                           │
                                      No     ┌──────────┤
                  ◄ All impacts ─────────────│ Additional│
                    completed ?              │  Impact   │
                            │                └──────────┘
                      Yes   ▼
                          END
```

Figure 5-1. Modeling of DC Processes

5.2 Comparisons with Case Histories

This section presents comparisons of numerical simulation results for two case histories of dynamic compaction: (a) Kampung Pakar (Chow et al. 1992), and (b) Steinaker dam (Dise et al. 1994). The Kampung site is a clean sand site, improved by DC without any wick drains. The Steinaker dam site is a silty sand site improved by DC preinstalled with wick drains.

5.2.1 Kampung Pakar – Clean Sand Site

The Kampung Pakar site is in the Sungei Besi area near the Kuala Lumpur-Seremban Highway, approximately 15 km from Kuala Lumpur, Malaysia. The site consisted of 14 m of relatively clean, uniform, homogeneous and highly permeable loose sand, except for a layer of silty clay at a depth of 10 to 12 m. The site is underlain by limestone bedrock at 14 m depth (Figure 5-2). The groundwater level was at a depth of about 3 m below the surface. The dynamic compaction program at this site involved two high-energy passes over a 6 m x 6 m grid pattern using a 1.83 m x 1.83 m square pounder weighing 15 Mg (Figure 5-4). The number of impacts per location was 10 for the first pass and six for the second pass. The details of the compaction program are summarized in Table 5-1. No wick drains were installed at this site. Pre- and post-improvement CPT tests were performed at the center of the 6 m x 6 m square impact grid pattern shown in

Figure 5-4. The relative density profile at the site has been estimated from the CPT measurements based on Meyerhof's 1957 and 1976 correlations between cone resistance; friction angle; and relative density for clean sand reported in Chow et al. (1994). Details of the numerical simulations are presented in Nashed (2005). The post-improvement density profile obtained from numerical simulations is compared with the density profile deduced from CPT data in Figure 5-3. The simulation results agree reasonably well with the field data.
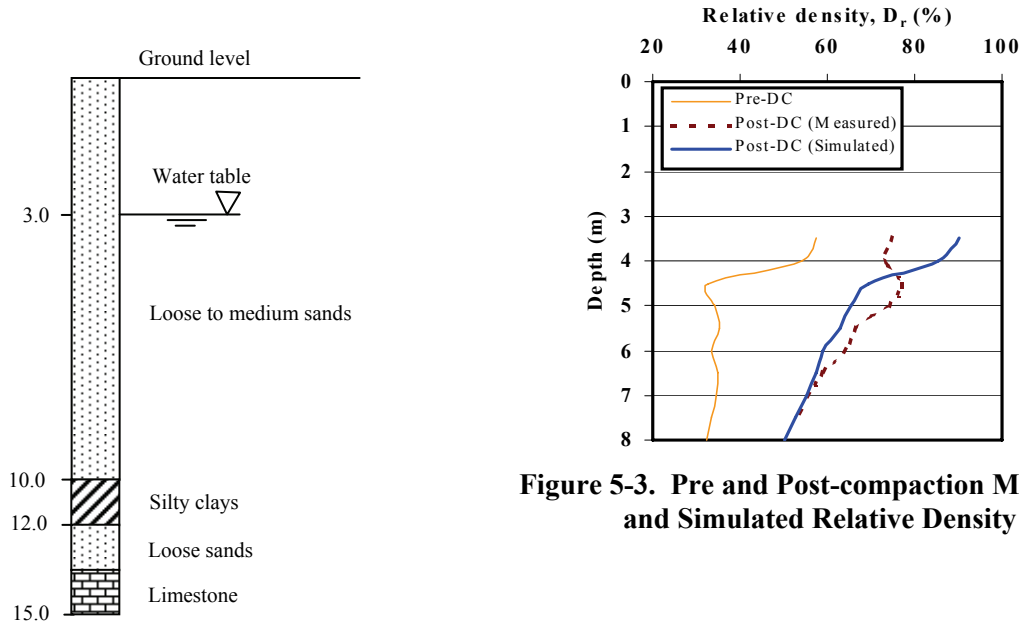
Figure 5-3. Pre and Post-compaction Measured and Simulated Relative Density

Figure 5-2. Soil Profile
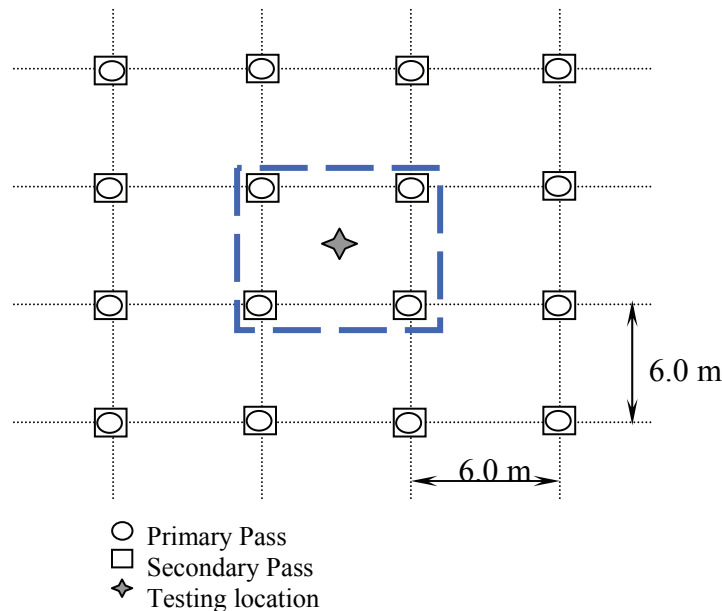
Figure 5-4. Impact Grid Pattern

Table 5-1. Impact Parameters – Dynamic Compaction

Parameters	Kampung Paker Site, Malaysia		Steinaker dam modification project, Utah			
	1st pass	2nd pass	Initial ironing	1st phase	2nd phase	3rd phase
Pounder weight (Mg)	15.0	15.0	30.0	30.0	30.0	30.0
Drop height (m)	20.0	25.0	18.0	30.0	30.0	30.0
No. of impacts at each grid point	10	6	2	30	30	20

The further illustrate the utility of the numerical simulation method developed in this work, additional simulations were conducted for a representative area marked in Figure 5-4 to obtain the progressive changes in density profiles during dynamic compaction. Figure 5-5 shows subsurface relative density contours for a section between impact location points 1 and 3 as illustrated in Figure 5-5 b.   Figures 5-6 to 5-12 demonstrate the progressive changes in subsurface relative density contours due to repeated impacts at the impact location where the crane shown in the adjunct diagrams. For example, Figure 5-6 illustrates the subsurface relative density contours for section 1 – 3 immediately after the tenth impact on location 1 of the first pass, Figure 5-7 illustrates the subsurface relative density contours for same section immediately after the tenth impact on location 2 of the first pass, while Figure 5-10 illustrates the subsurface relative density contours for same section immediately after the sixth impact on location 1 of the second pass.
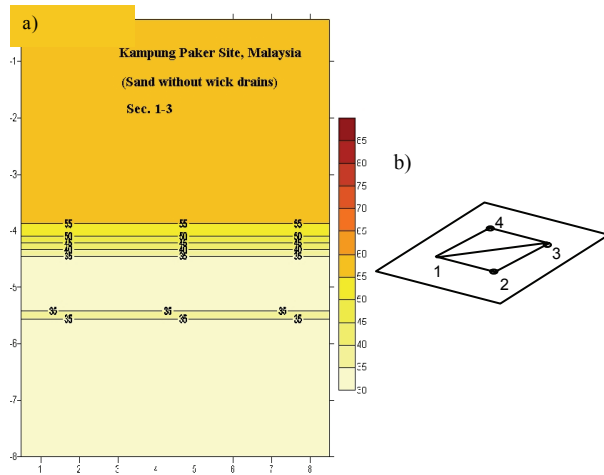
Figure 5-5. a) Pre-compaction Soil Density Profile, b) Impact Grid Pattern
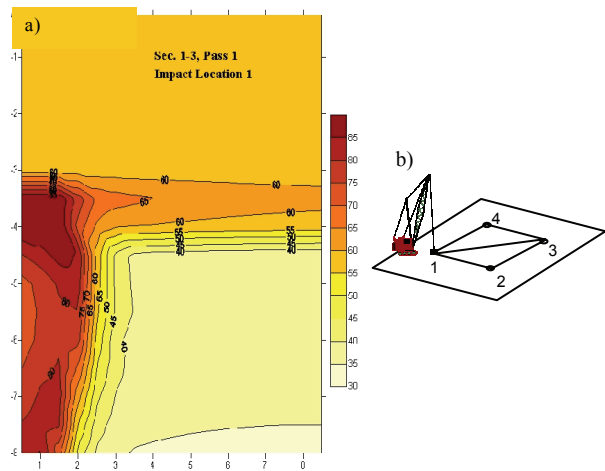
Figure 5-6. a) Soil Density Profile after Impacts on Location 1, 1st Pass, b) Impact Location
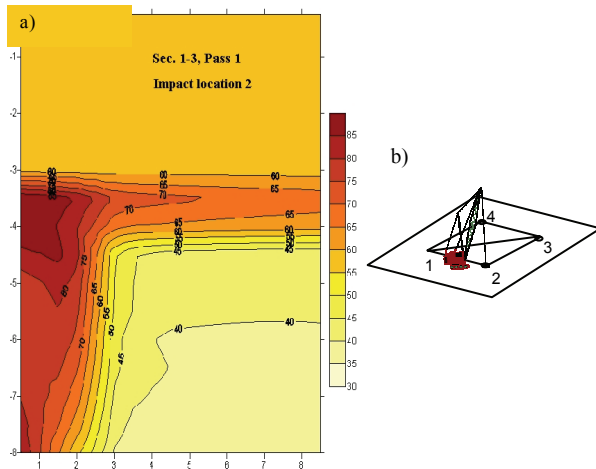
Figure 5-7. a) Soil Density Profile after Impacts on Location 2, 1st Pass; b) Impact location
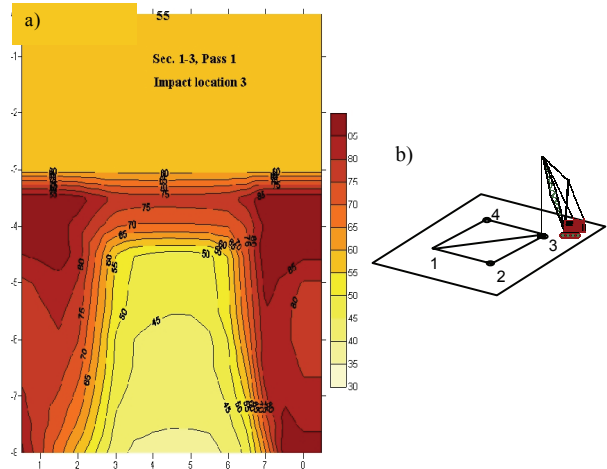
Figure 5-8. a) Soil Density Profile after Impacts on Location 3, 1st Pass; b) Impact Location
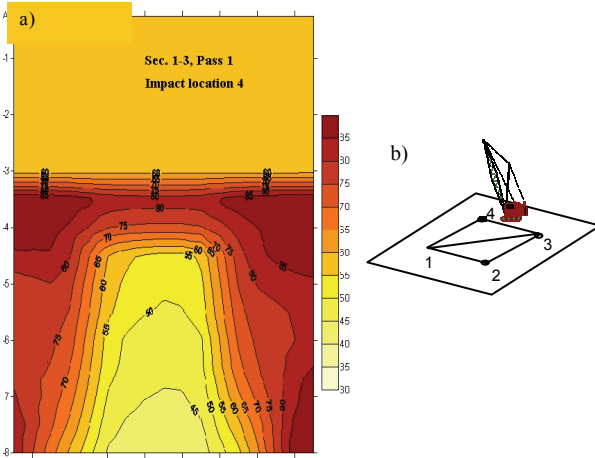
Figure 5-9. a) Soil Density Profile after Impacts on Location 4, 1st Pass; b) Impact Location
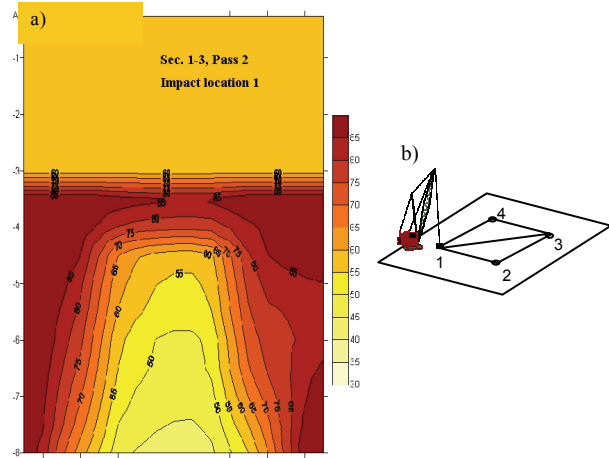
Figure 5-10. a) Soil Density Profile after Impacts on Location 1, 2nd Pass; b) Impact Location
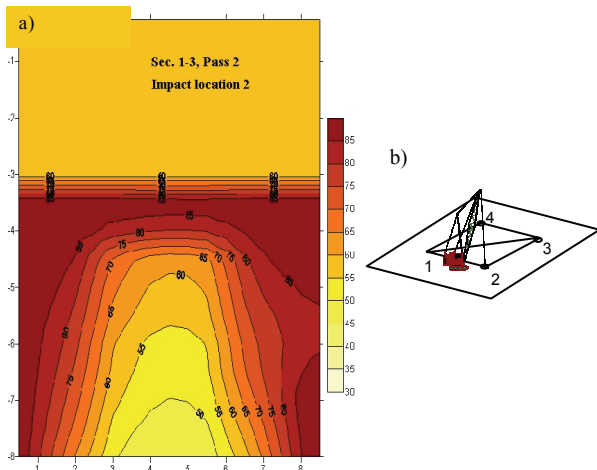
Figure 5-11. a) Soil Density Profile after Impacts on Location 2, 2nd Pass; b) Impact Location
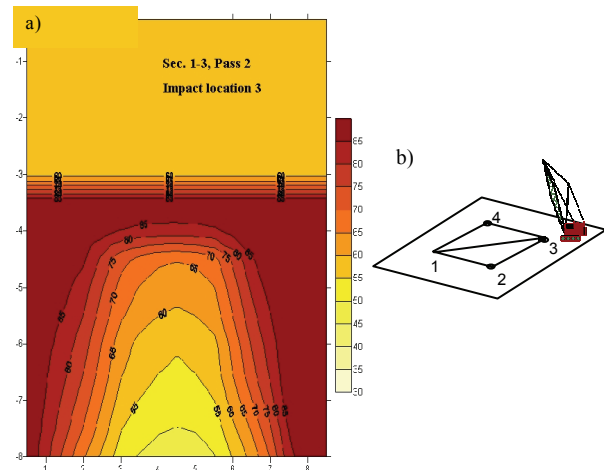
Figure 5-12. a) Soil Density Profile after Impacts on Location 3, 2nd Pass; b) Impact Location

5.2.2 Steinaker Dam – Silty Sand Site

Steinaker dam was built as an earth fill dam in the 1960's. Alluvial materials form the foundation beneath the main dam section including a deep layer of non-plastic silty sand with an average fines content of 45 % underlain by stiff, fat clay lying directly on bedrock (Dise et al. 1994). Testing conducted in 1986 under the safety of dams program determined that the sandy silt layer beneath the dam was liquefiable, and that the dam would fail should the design maximum credible earthquake of magnitude 6.5 occur. Alternatives were investigated and the remedial modification selected was a stability berm placed on treated foundation material at the downstream toe of the dam. Dynamic compaction was selected to treat approximately 9.5 m of liquefiable sandy silt. Figure 5-13 shows the soil profile at the site, 1.5 m thick compaction pad was placed on top of the sandy silt layer. Perimeter well points were installed to lower the water table at least 3.7 m below the top of the compaction pad. Wick drains were installed on 1.5 m centers to a depth of 9.0 m from the top of the compaction pad.

The dynamic compaction program involved an initial ironing pass and three high-energy passes (primary, secondary, and tertiary). The impact grid pattern is shown in Figure 5-15. The primary and secondary drop points were located at the corners of 7.6 m x 7.6 m squares. The primary and secondary grid spacing is 15.2 m. Tertiary points were located at the center of each 7.6 m x 7.6 m square. The pounder weight was 30.0 Mg. The initial ironing pass included two impacts from a drop height of 18.0 m at each primary, secondary, and tertiary impact location. The drop height was 30.0 m for the primary, secondary, and tertiary passes. The number of impacts per grid location was 30 for the primary and secondary passes, and 20 for the tertiary pass. The details of the compaction program are summarized in Table 5-1. The primary pass was completed over the entire site before drops were allowed in the secondary pass. The secondary pass was completed before the tertiary pass. To further prevent pore pressure build up, drops were completed on each row before impacting locations on the next.
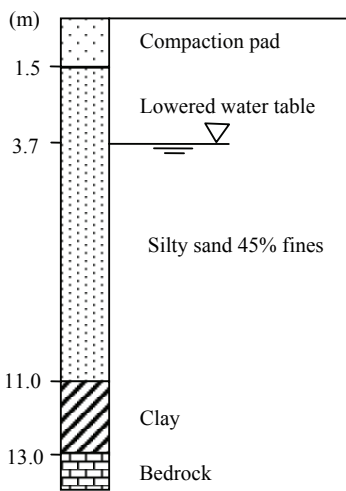
Figure 5-13. Soil Profile
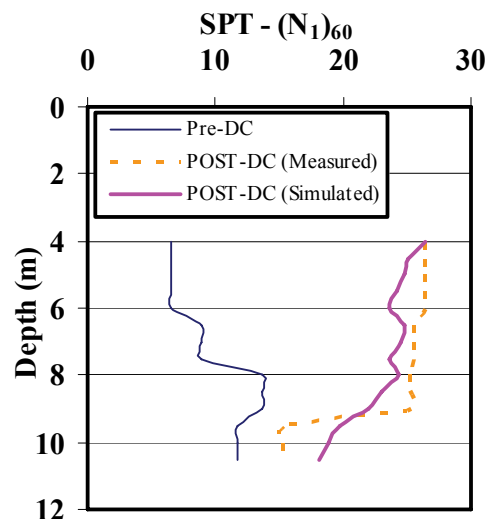
Figure 5-14. Pre- and Post-compaction Measured and Simulated $(N_1)_{60}$
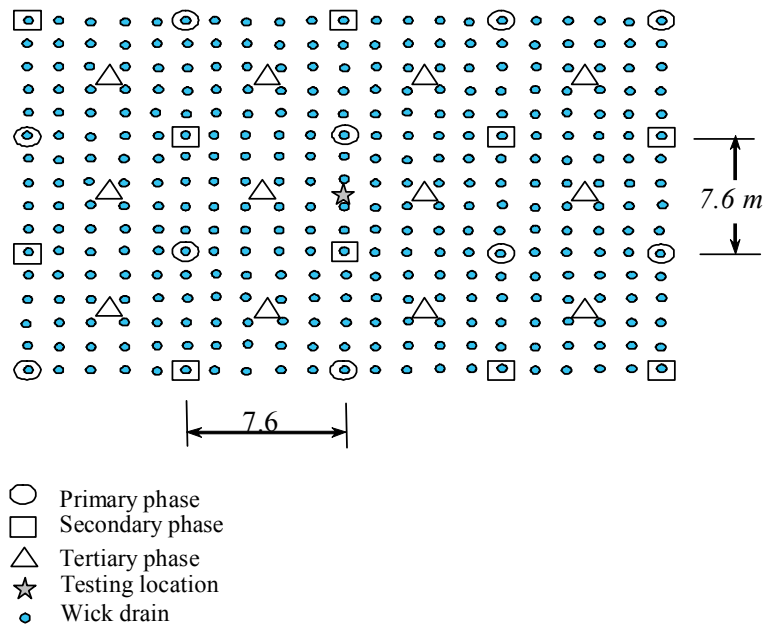
Figure 5-15. Impact Grid Pattern for Steinaker Dam Modification Project, Utah

Numerical simulations were conducted for this site using the above compaction parameters. The hydraulic conductivity was unknown, and it was assumed to be 10^{-8} m/s based on other available data for silty sands at 45% silt content (Thevanayagam and Martin 2001).

The pre- and post-improvement field SPT corrected blow count for overburden pressure $(N_1)_{60}$ obtained at a location midway between primary and secondary drop locations (as illustrated in Figure 5-15) are shown in Figure 5-14 (records obtained through collaboration with Hayward Baker Inc., also Dise et al., 1994). The measured post-improvement SPT $(N_1)_{60}$ are compared with post-improvement simulation results in this figure. The simulation results follow the trend observed in the field.

5.3 Parametric Studies

Parametric studies were conducted to study the effects of hydraulic conductivity and wick drain spacing on the effective depth of influence of ground improvement by dynamic compaction. In each simulation, the site was considered as a uniform soil site with a specified value of $(N_1)_{60c-s}$. The groundwater table was assumed to be at 2 m below the ground surface. The studies reported herein were limited to the impact grid pattern used in Section 5.2.2 (shown in Figure 5-15). Three energy delivery passes (primary, secondary, and tertiary) were made. Each grid point received a total of 12 impacts per pass. The time cycle between subsequent impacts was selected as 2 minutes. The cumulative energy applied at the sites ranged from 1 to 3 MJ/m^2. In all simulations, the energy (WH) per impact was varied from 250 to 750 Mg.m. The hydraulic conductivity (k) and wick drain spacing were varied to represent the variation in silt content and drain spacing. The equivalent diameter of the wick drains was 5 cm. The center-to-center wick drain spacing was set at 1.5 m. For comparison purposes, one set of simulations was done for a sand deposit at the same $(N_1)_{60c-s}$ as the silty sand sites, without wick drains. The hydraulic

41

conductivity of this soil was set at 10^{-5} m/s representing sand. The spacing between the impact points was 6 m for the sand site. The energy (WH) per impact was varied from 200 to 500 Mg.m.

The depth of improvement d_{max} is considered as the depth at which 10 % improvement in the equivalent relative density is achieved. For the silty soil sites, d_{max} was considered at a location midway between primary and secondary drop locations (as illustrated in Figure 5-15), while for sand sites, d_{max} was considered at the center of the square impact grid pattern as shown in Figure 5-4.

Figure 5-16 shows the effect of the hydraulic conductivity and fines content of the soil on the achievable depth of improvement d_{max} by DC. Figure 5-16a shows the depth of improvement d_{max} versus WH (energy per impact) for the two silty soil sites, with preinstalled wick drains. The hydraulic conductivity of the soil at these two sites was 10^{-7} m/s and 10^{-8} m/s, respectively. The pre improvement $(N_1)_{60c-s}$ value for these two sites was 7.5. Although not shown in this figure, simulations of these silty soils without wick drains indicated little or no improvement. Figure 5-16b shows d_{max} versus WH for the clean sand site at the same pre improvement $(N_1)_{60c-s}$, without wick drains. The empirical relationship (d_{max} =n(WH)$^{0.5}$; Lukas 1986, 1995) applicable for highly permeable sandy sites assuming n=0.5 (without wick drains) is also shown in these figures.

When compared with Figure 5-16b, the results indicate that, with the provision of preinstalled wick drains, silty soils can be improved up to comparable depths of improvement achievable in clean sands. It is also interesting to note the effects of hydraulic conductivity on d_{max} in silty soils, even with preinstalled wick drains. A decrease in hydraulic conductivity reduces the effective depth of influence d_{max}.

Although further details of this study are not reported herein, results indicated that DC is ineffective in silty soils with hydraulic conductivity less than 10^{-6} m/s, without preinstalled wick drains. With wick drains, however, silty soils with hydraulic conductivities as low as 10^{-8} m/s could be densified using DC by pre-installing wick drains at a spacing of 1.0 m to 1.5 m.

(a) Silty soil with wick drain   (b) Sand without wick drain
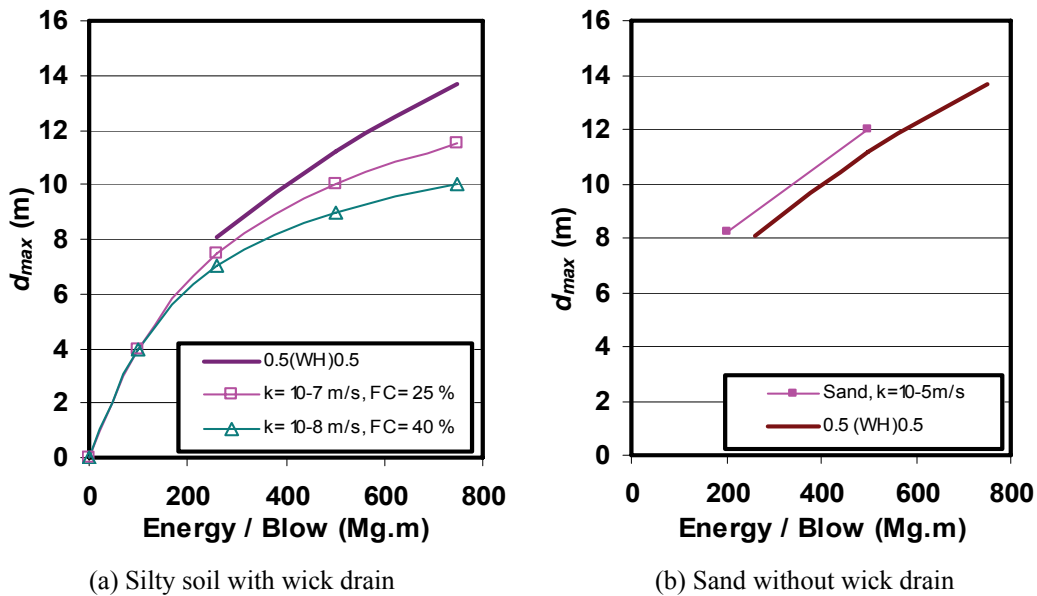
Figure 5-16. Effect of Hydraulic Conductivity and Fines Content on Depth of Influence

Figure 5-17a shows the effect of wick drain spacing on the achievable depth of improvement d_{max} by DC for a silty soil deposit with k of 10^{-7} m/s and pre-improvement $(N_1)_{60c-s}$ of 7.5, preinstalled with wick drains at three different spacing, 1.0, 1.5, and 2.0 m, respectively. Figure 5-17b shows the effect of wick drain spacing on the achievable depth of improvement d_{max} at two different spacing 1.0 and 1.5 m, respectively, for energy per blow range of 250 to 750 Mg.m. Wick drains at close spacing improve the efficiency of DC. However, spacing closer than 1 m may not be practical. Further details are reported in Nashed et al. (2004).

(a)   (b)
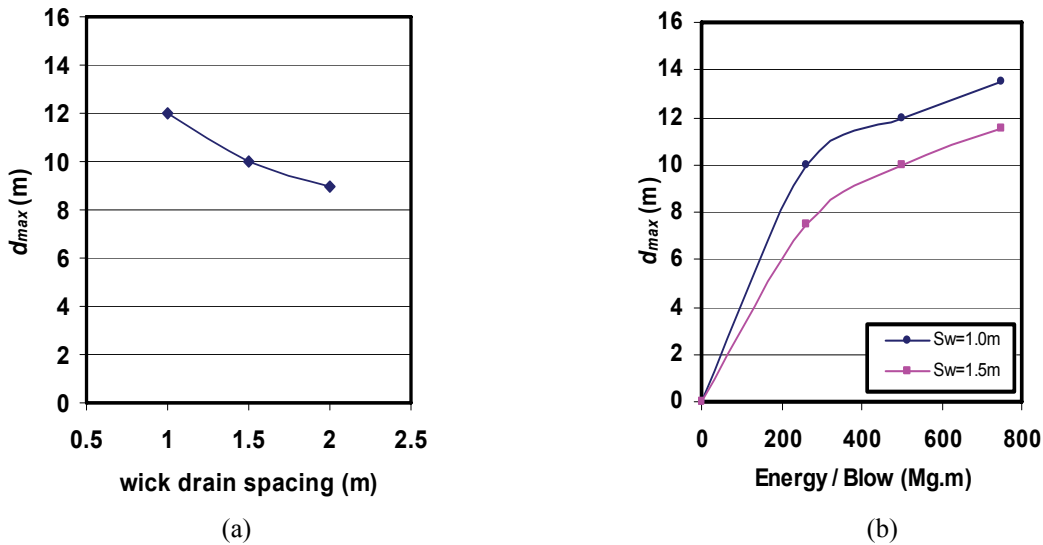
Figure 5-17. Effect of Wick Drains Spacing on Depth of Influence

5.4. Visualization Tools

Visualization tools have also been developed to display and view changes in pore pressures and soil densities in the subsurface around the impact zones during DC process. This section presents an example simulation results to illustrate the utility of the visualization tools.

The soil site chosen for this example consists of uniform silty sand at a silt content of 25% and hydraulic conductivity k of 10^{-7} m/s. The pre-improvement $(N_1)_{60-cs}$ value was 7.5 (Nashed 2005). Wick drains were pre-installed in a square pattern at 1.5 m spacing. The impact grid pattern is shown in Figure 5-18. The grid spacing S is 15.0 m. Dynamic compaction was done in three phases: primary, secondary and tertiary. Impacts were carried out row by row. The primary phase was completed first, followed by secondary and tertiary phases. Each phase consisted of eight impacts (N_I) per grid location. The time cycle T between impacts at each grid point was 2.0 min. The energy delivery per impact WH was 260 Mg.m.

○ Primary phase
□ Secondary phase
△ Tertiary phase
• Wick drain
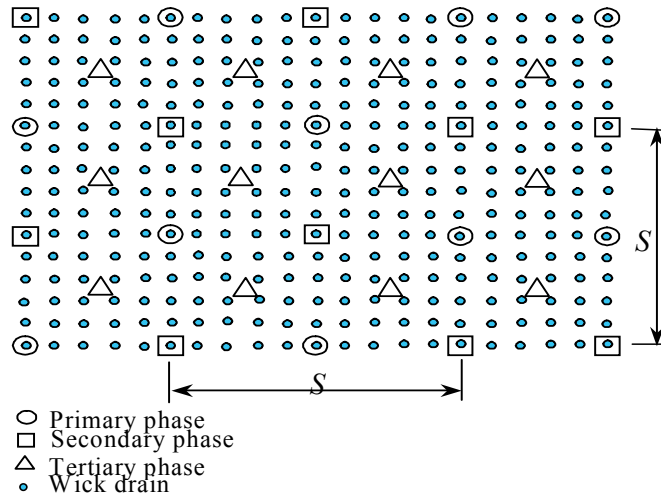
Figure 5-18. Impact Grid Pattern

5.4.1 Example Results during Primary Phase

Consider the beginning of the primary phase of improvement starting with impacts at a primary starting grid point (next to the crane) shown in Figure 5-19. Consider a reference wick drain located at the center between the primary grid point and the adjacent secondary grid point as shown in Figure 5-19. The results below show the subsurface excess pore pressures and densities in the vicinity of this reference wick drain at specific times during and after certain impacts in the primary impact phase. The horizontal axis in these figures refers to distance from the axis of the reference wick drain in meters up to half distance (0.75 m) between adjacent wick drains. Figure 5-19a shows the excess pore pressure contours around a wick drain immediately after the eighth impact at the last primary grid point close to the referenced wick drain. Figure 5-19b shows the pore pressures two minutes after the eighth impact. Figure 5-19c shows the soil density profile around the same wick drain location two minutes after the eighth impact before any further impacts at the secondary grid points.

5.4.2 Example Results during Secondary Phase

The numerical simulations were continued through the entire primary phase and into the secondary phase. Consider the secondary phase impact at the last secondary grid point adjacent (Figure 5-20) to the same reference wick drain described before. The results below show the subsurface excess pore pressures and densities in the vicinity of this reference wick drain at specific times during and after certain impacts at the grid point in the secondary phase. Figure 5-20a shows the excess pore pressures around the reference wick drain immediately after this eighth impact. Figure 5-20b shows the excess pressures two minutes after impact. Figure 5-20c shows the density profile two minutes after the eighth impact before any further impact at the tertiary grid points. Comparison of Figures 5-19c and 5-20c illustrates the changes in density from the end of the primary phase to the end of the secondary phase.

44
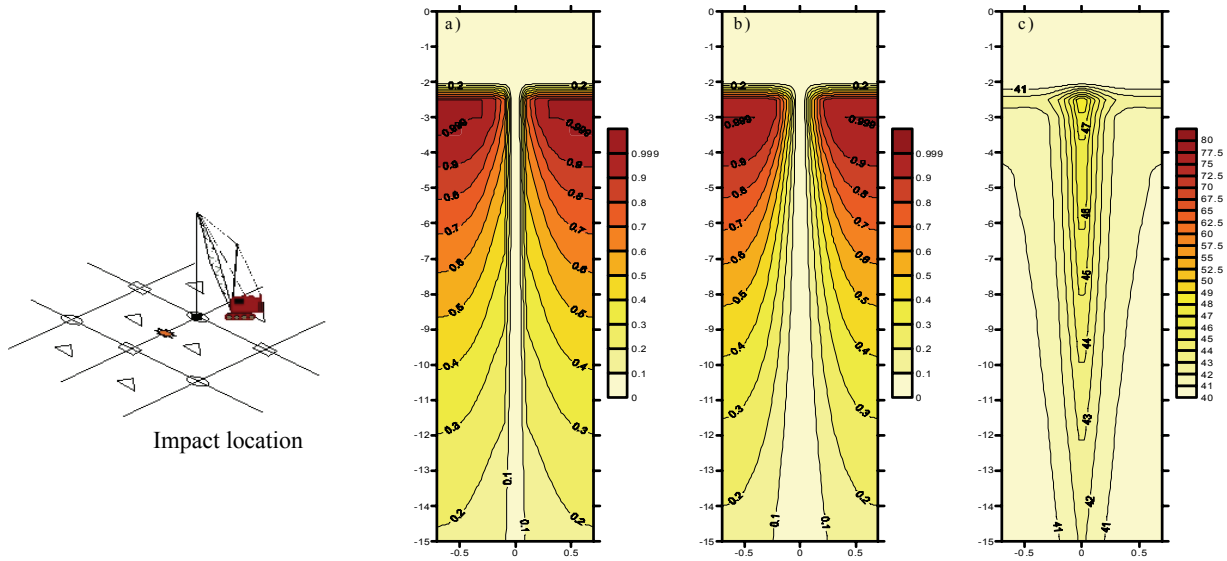
Figure 5-19. Primary Phase: a) Pore Pressure Profile after 8th Impact at the Primary Location Shown: b) Pore Pressure Profile at 2 Minutes after 8th Impact; c) Soil Density Profile $(D_r)_{eq}$ at 2 Minutes after 8th Impact
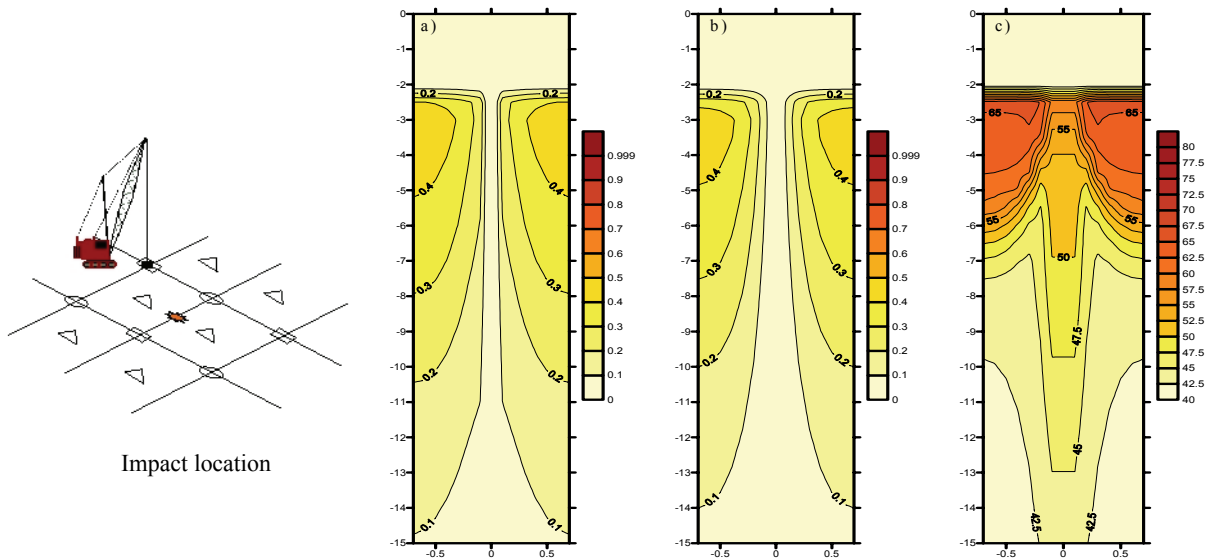
Figure 5-20. Secondary Phase: a) Pore Pressure Profile after 8th Impact at the Secondary location Shown; b) Pore Pressure Profile at 2 Minutes after 8th Impact, c) Soil Density Profile $(D_r)_{eq}$ at 2 Minutes after 8th Impact

5.4.3 Example Results during Tertiary Phase

The numerical simulation was continued past completion of the secondary phase into the tertiary phase. Consider the beginning of the tertiary phase impact at the last tertiary grid point adjacent (Figure 5-21) to the same reference wick drain previously described. The results below show the subsurface excess pore pressures and densities in the vicinity of this reference wick drain at specific times during and after certain impacts at the last grid point in the tertiary phase. Figure 5-21a shows the excess pore pressures around the reference wick drain immediately after this

45

eighth impact. Figure 5-21b shows the excess pressures two minutes after impact. Figure 5-21c shows the density profile after two minutes the eighth impact. Comparison of Figure 5-20c and 5-21c illustrates the changes in density from the end of the secondary phase to the end of the tertiary phase.
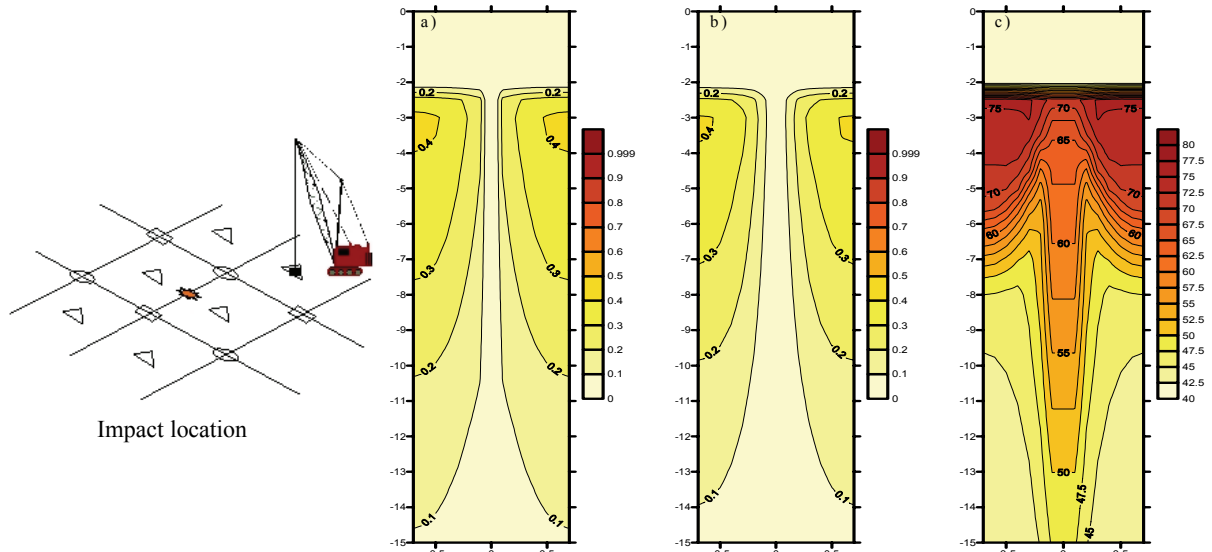
Figure 5-21. Tertiary Phase: a) Pore Pressure Profile after 8th Impact at the Tertiary Location Shown; b) Pore Pressure Profile at 2 Minutes after 8th Impact; c) Soil Density Profile $(D_r)_{eq}$ at 2 Minutes after 8th Impact

5.4.4 Summary

These figures illustrate the progress in consolidation and gradual increase in density of the soil around the reference wick drain during the DC process. This is illustrative of the changes occurring around each wick drain at the site. The density increases significantly near the ground surface and close to the wick drains. The changes in soil density decay gradually as the depth increases. The presence of the wick drains facilitates drainage and enhances the increase in soil density. The visualization tool is not sufficiently developed to be user friendly software yet. When sufficiently developed, it can serve as a design tool aided with visualization effects.

5.5 Simplified Design Charts

Based on the above simulation model, additional studies were conducted to develop simplified design charts to obtain the relationships between pre- and post-improvement equivalent clean sand SPT blow counts (or equivalent clean sand soil densities) for a set of selected uniform silty sand soil sites, for a range of hydraulic conductivities, improved by DC and preinstalled wick drains. Groundwater level was assumed to be at 2.0 m depth from impact surface. For convenient field applications, the results are presented in terms of equivalent pre- and post-improvement normalized clean sand SPT blow counts $(N_1)_{60cs}$.

For all simulations, the impact grid pattern was assumed to be as shown in Figure 5-18. In each case, the DC process involved a single pass involving three phases of impact (primary, secondary, and tertiary), at the grid locations shown in this figure. *WH, S, N_I,* wick drain spacing

S_w, and time cycle between impacts T were varied for each simulation. The size of the wick drains was assumed to be 100 mm x 5 mm with an equivalent diameter d_w of 5 cm.

5.5.1 Example Post-Improvement $(N_1)_{60cs}$ Charts

A total of eight example charts are presented in Figures 5-22 and 5-23. Figure 5-22 presents the charts for grid spacing of 15 m. Figure 5-23 shows the charts for grid spacing of 12 m. For all charts, each grid point received 12 impacts during each phase. The time cycle between subsequent impacts was two minutes. The wick drains was assumed to be pre-installed at 1.5 m spacing in a rectangular pattern.

Figure 5-22a shows the post-improvement $(N_1)_{60cs}$ profile for various values of energy per impact (WH) for a silty sand site with a uniform pre-improvement $(N_1)_{60cs}$ of 7.5 and $k=1\times10^{-7}$ m/s. Figure 5-22b shows the results for a uniform pre-improvement $(N_1)_{60cs}$ of 16 and $k=1\times10^{-7}$ m/s. Figure 5-22c presents the results for a silty sand site with a uniform pre-improvement $(N_1)_{60cs}$ of 7.5 and $k=1\times10^{-8}$ m/s. Figure 5-22d shows the results for pre-improvement $(N_1)_{60cs}$ of 16 and $k=1\times10^{-8}$ m/s. Figures 5-23a-d show a similar set of results as in Figures 5-22a-d, except for S=12 m. Each curve in these figures refers to post improvement $(N_1)_{60cs}$ profile for a different value for *WH* ranging from 100 to 750 Mg.m.

a) $k=10^{-7}$m/s, pre-$(N_1)_{60cs}$=7.5   b) $k=10^{-7}$m/s, pre-$(N_1)_{60cs}$=16   c) $k=10^{-8}$m/s, pre-$(N_1)_{60cs}$=7.5 d) $k=10^{-8}$m/s, pre-$(N_1)_{60cs}$=16
(N_1 = 12, T = 2 min, S_w = 1.5m, d_w = 5 cm for all charts)
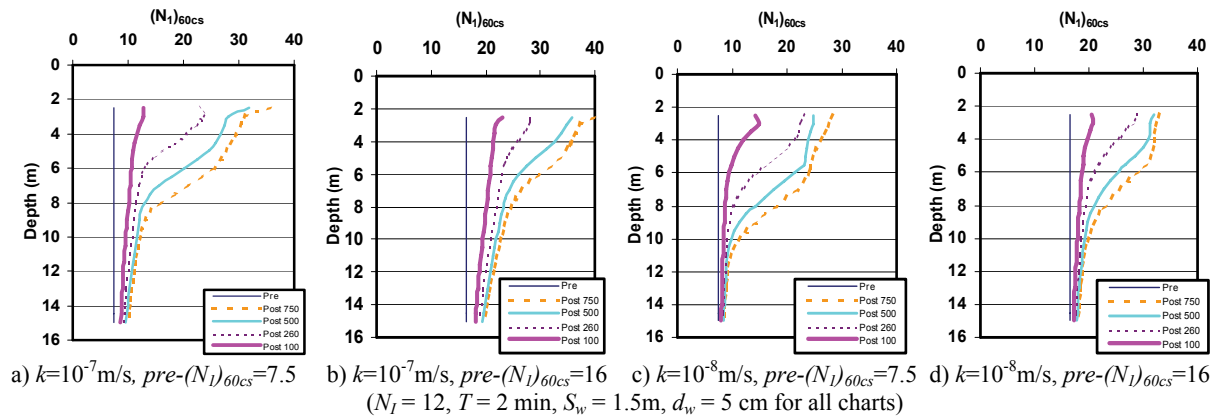
Figure 5-22. Pre- and Post-improvement $(N_1)_{60cs}$ for S = 15 m (Post 750 = WH = 750 Mg. m)

a) $k=10^{-7}$m/s, pre-$(N_1)_{60cs}$=7.5   b) $k=10^{-7}$m/s, pre-$(N_1)_{60cs}$=16   c) $k=10^{-8}$m/s, pre-$(N_1)_{60cs}$=7.5 d) $k=10^{-8}$m/s, pre-$(N_1)_{60cs}$=16
(N_1 = 12, T = 2 min, S_w = 1.5m, d_w = 5 cm for all charts)
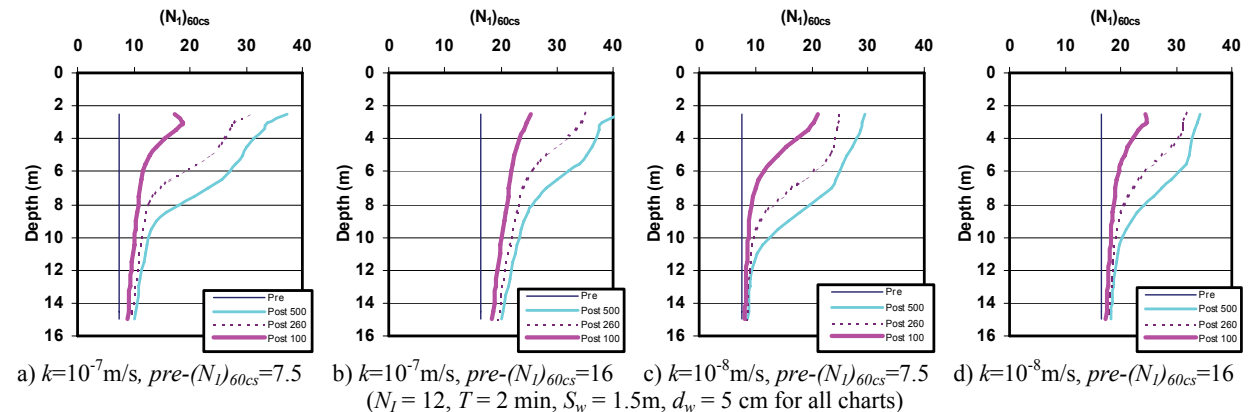
Figure 5-23. Pre- and Post-improvement $(N_1)_{60cs}$ for S = 12 m (Post 500 =WH = 500 Mg. m)

5.5.2 Post-Improvement $(N_1)_{60cs}$ Charts

Additional sets of design charts for other sets of (H, S, N_I, T, S_w, d_w and k) for different uniform soil deposits are presented in this section. The use of these charts to determine DC operational parameters WH, S, N_I, T, S_w and d_w for liquefaction mitigation design at a site is illustrated in Chapter 6 using stepwise design examples.

(a) $N_I = 12$, $S_w = 1.5$ m, $T = 2$ min   (b) $N_I = 12$, $S_w = 1.5$ m, $T = 4$ min   (c) $N_I = 12$, $S_w = 1.0$m, $T = 4$min

(d) $N_I = 8$, $S_w = 1.5$ m, $T = 2$ min   (e) $N_I = 8$, $S_w = 1.5$ m, $T = 4$ min   (f) $N_I = 8$, $S_w = 1.0$ m, $T = 4$ min
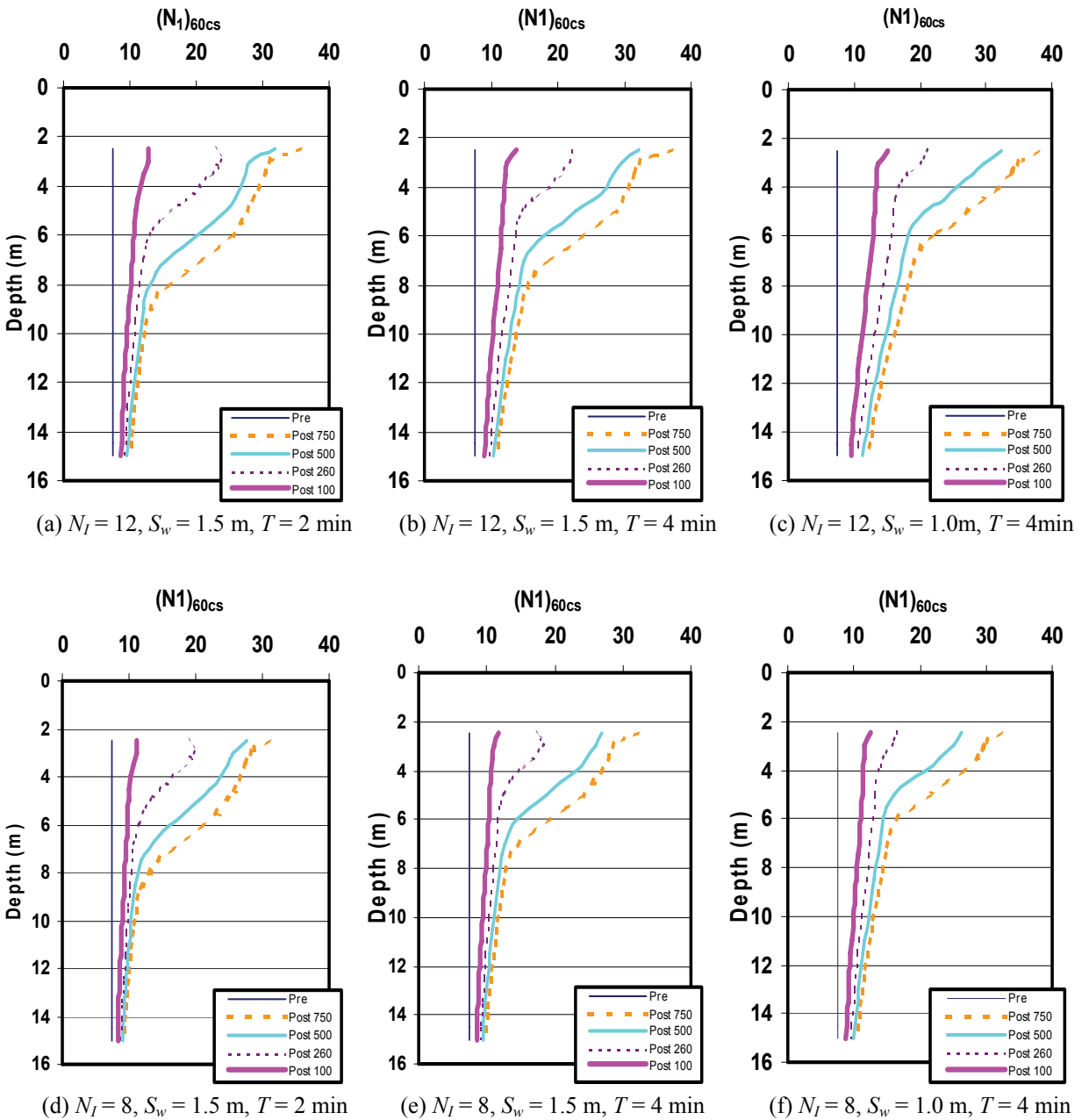
Figure 5-24. DC Design Charts for $k=10^{-7}$ m/s, $FC=25$ %, $pre\_(D_r)_{eq}= 40$ % ($pre-(N_1)_{60cs}=7.5$), $S=15.0$ m (Post 750: $WH = 750$ Mg.m)

48

(a) $N_I = 12$, $S_w = 1.5$ m, $T = 2$ min   (b) $N_I = 12$, $S_w = 1.5$ m, $T = 4$ min   (c) $N_I = 12$, $S_w = 1.0$m, $T = 4$min

(d) $N_I = 8$, $S_w = 1.5$ m, $T = 2$ min   (e) $N_I = 8$, $S_w = 1.5$ m, $T = 4$ min   (f) $N_I = 8$, $S_w = 1.0$ m, $T = 4$ min

Figure 5-25. DC Design Charts for $k=10^{-7}$ m/s, $FC=25$ %, $pre\_(D_r)_{eq}= 60$ % ($pre\text{-}(N_1)_{60cs}=16.0$), $S=15.0$ m (Post 750: $WH = 750$ Mg.m)

49
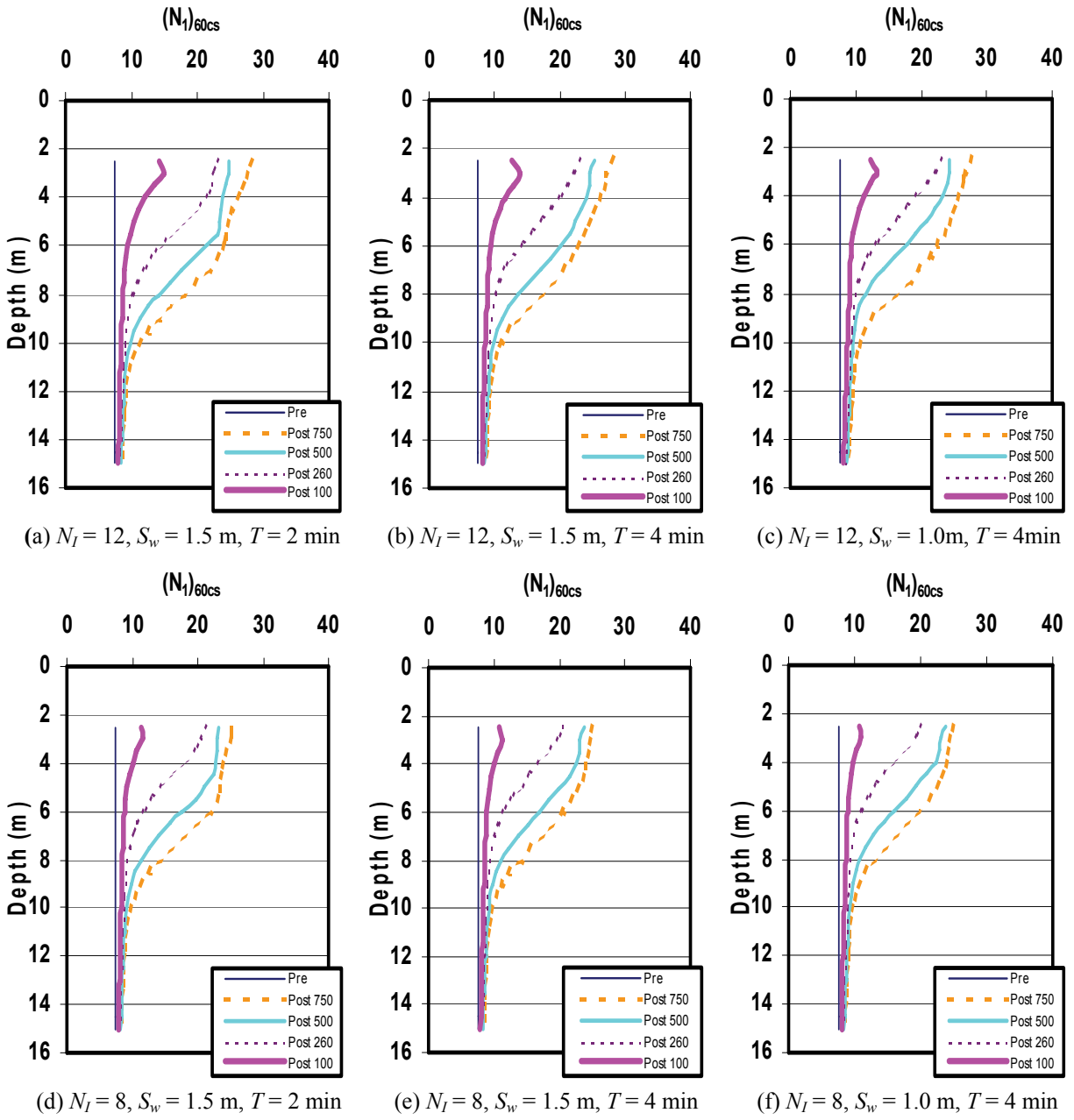
Figure 5-26. DC Design Charts for $k=10^{-8}$ m/s, FC=40 %, $pre\_(D_r)_{eq}$= 40 % (pre-$(N_I)_{60cs}$=7.5), S=15.0 m (Post 750: WH = 750 Mg.m)

50

(a) $N_I = 12$, $S_w = 1.5$ m, $T = 2$ min   (b) $N_I = 12$, $S_w = 1.5$ m, $T = 4$ min   (c) $N_I = 12$, $S_w = 1.0$ m, $T = 4$ min

(d) $N_I = 8$, $S_w = 1.5$ m, $T = 2$ min   (e) $N_I = 8$, $S_w = 1.5$ m, $T = 4$ min   (f) $N_I = 8$, $S_w = 1.0$ m, $T = 4$ min

Figure 5-27. DC Design Charts for $k=10^{-8}$ m/s, $FC=40$ %, $pre\_(D_r)_{eq}= 60$ % ($pre\text{-}(N_1)_{60cs}$=16.5), S=15.0 m (Post 750: $WH = 750$ Mg.m)

(a) $N_I = 12$, $S_w = 1.5$ m, $T = 2$ min   (b) $N_I = 12$, $S_w = 1.5$ m, $T = 4$ min   (c) $N_I = 12$, $S_w = 1.0$m, $T = 4$min

(d) $N_I = 8$, $S_w = 1.5$ m, $T = 2$ min   (e) $N_I = 8$, $S_w = 1.5$ m, $T = 4$ min   (f) $N_I = 8$, $S_w = 1.0$ m, $T = 4$ min
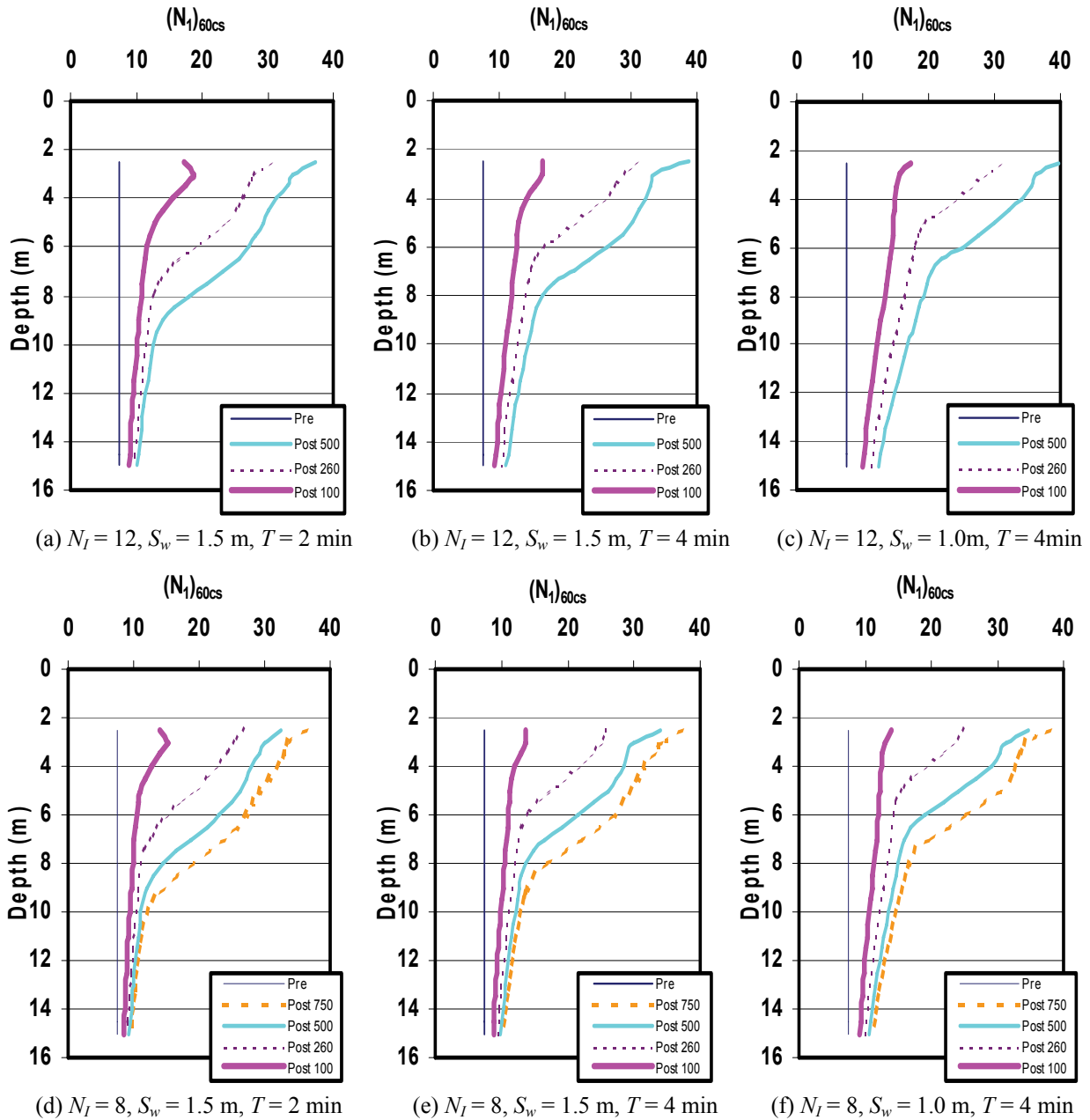
Figure 5-28. DC Design Charts for k=10^{-7} m/s, FC=25 %, $pre\_(D_r)_{eq}$= 40 % (pre-$(N_1)_{60cs}$=7.5), S=12.0 m   (Post 750: WH = 750 Mg.m)

(a) $N_I = 12$, $S_w = 1.5$ m, $T = 2$ min   (b) $N_I = 12$, $S_w = 1.5$ m, $T = 4$ min   (c) $N_I = 12$, $S_w = 1.0$m, $T = 4$min

(d) $N_I = 8$, $S_w = 1.5$ m, $T = 2$ min   (e) $N_I = 8$, $S_w = 1.5$ m, $T = 4$ min   (f) $N_I = 8$, $S_w = 1.0$ m, $T = 4$ min
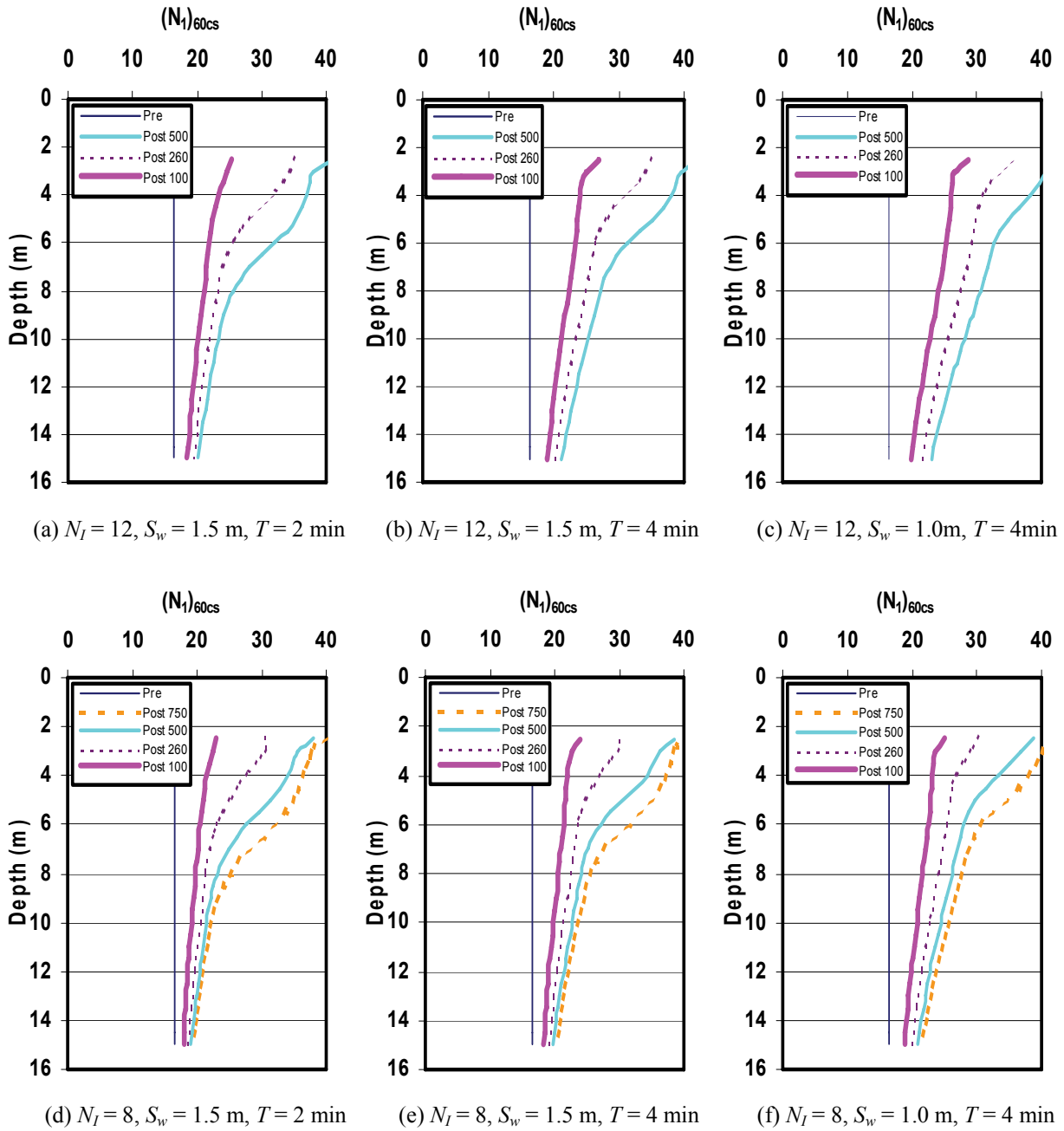
Figure 5-29. DC Design Charts for $k=10^{-7}$ m/s, $FC=25$ %, $pre\_(D_r)_{eq}= 60$ % ($pre\text{-}(N_1)_{60cs}=16.5$), $S=12.0$ m (Post 750: $WH = 750$ Mg.m)
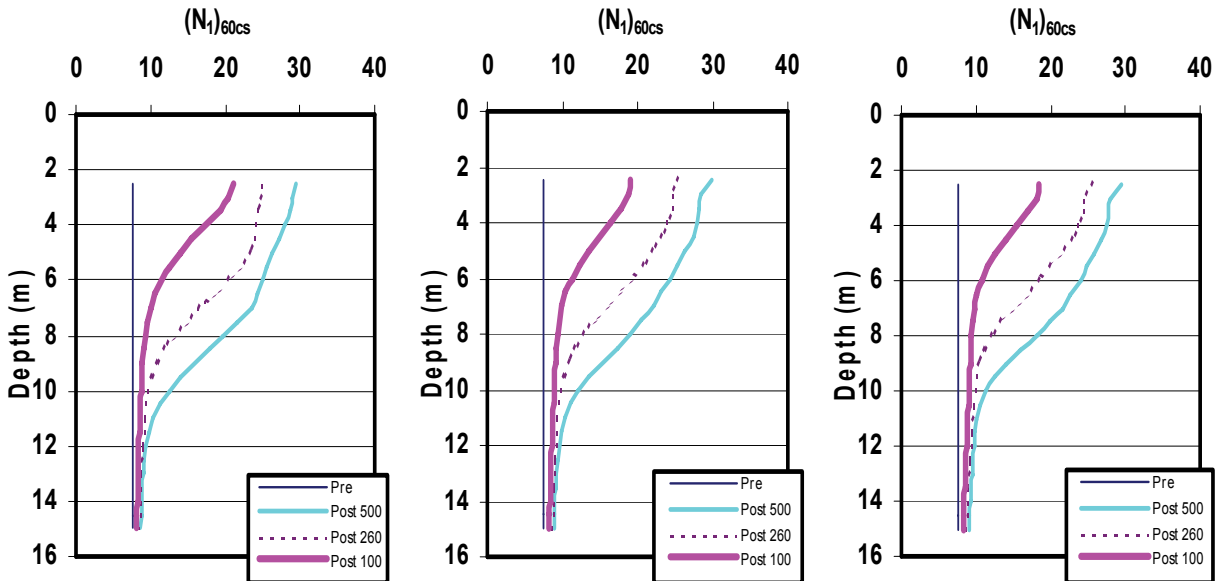
53
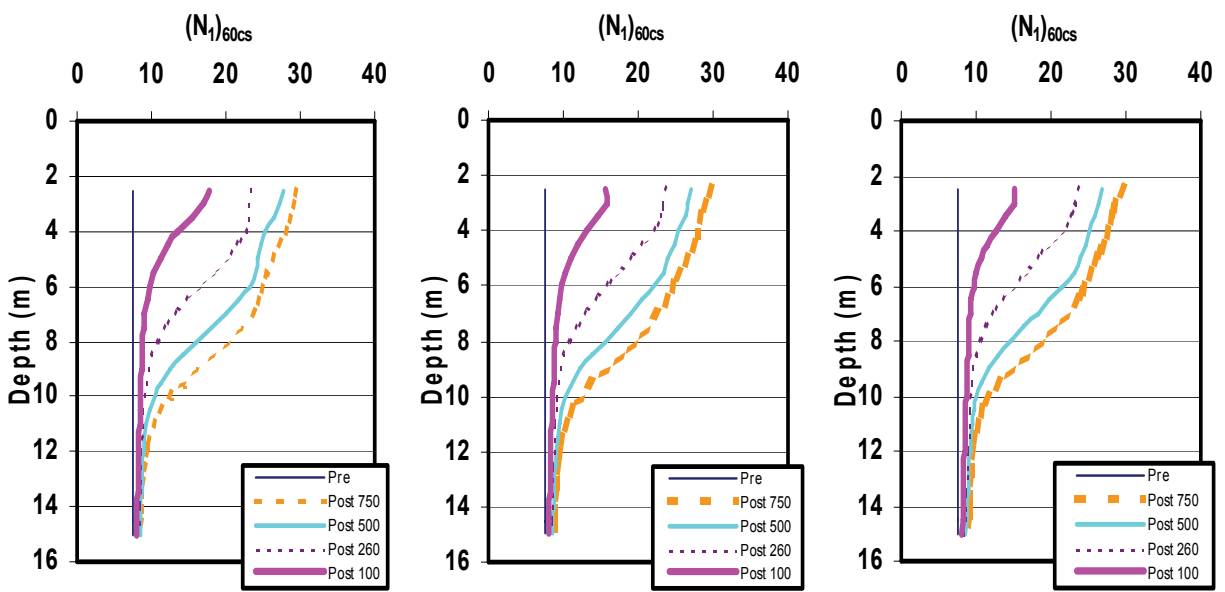
Figure 5-30. DC Design Charts for k=10⁻⁸ m/s, FC=40 %, $pre\_(D_r)_{eq}$= 40 % (pre-$(N_1)_{60cs}$=7.5), S=12.0 m (Post 750: WH = 750 Mg.m)

54

(a) N_I = 12, S_w = 1.5 m, T = 2 min

(b) N_I = 12, S_w = 1.5 m, T = 4 min

(c) N_I = 12, S_w = 1.0m, T = 4min

(d) N_I = 8, S_w = 1.5 m, T = 2 min

(e) N_I = 8, S_w = 1.5 m, T = 4 min

(f) N_I = 8, S_w = 1.0 m, T = 4 min
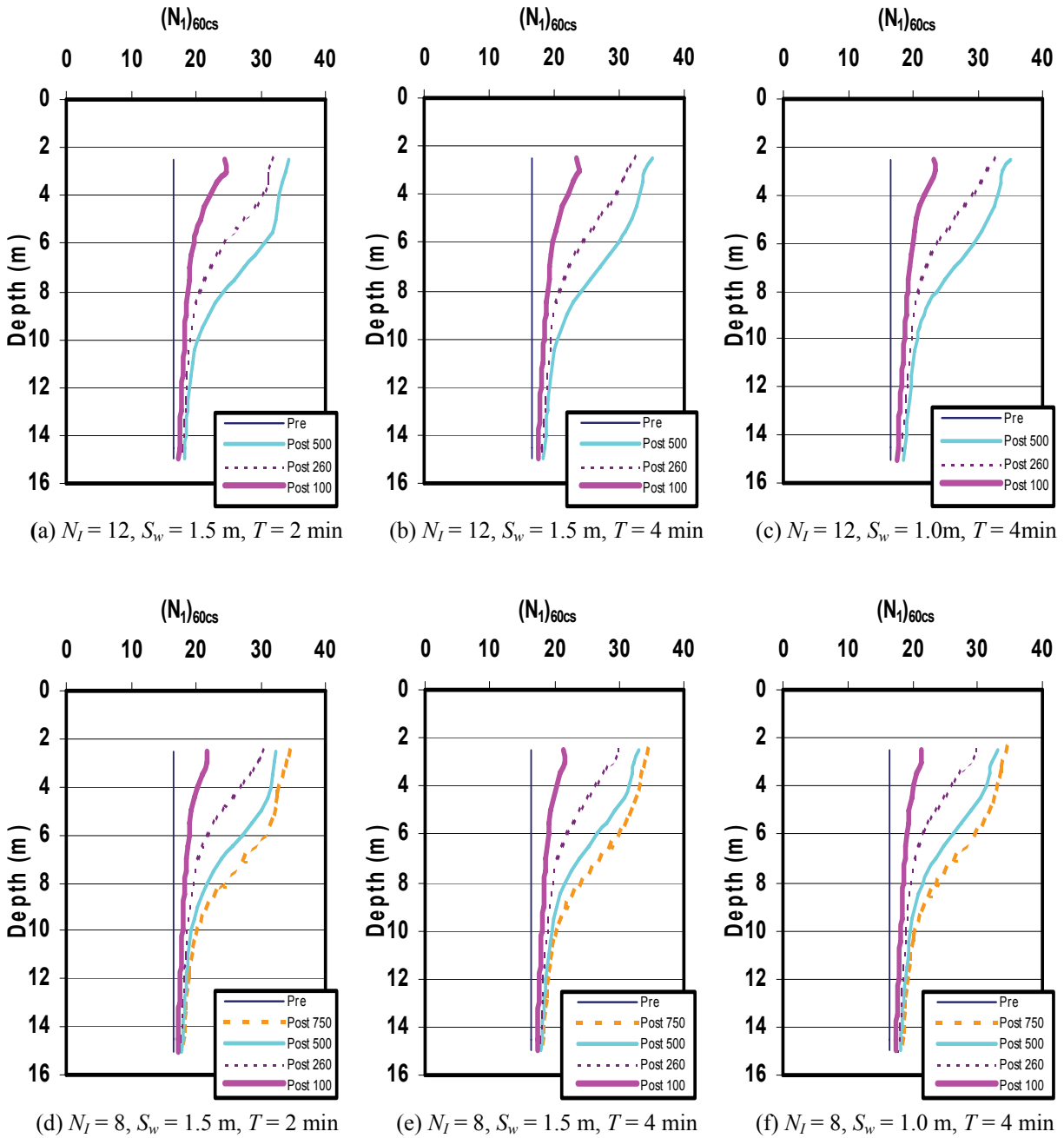
Figure 5-31. DC Design Charts for k=10^{-8} m/s, FC=40 %, $pre\_(D_r)_{eq}$= 60 % ($pre\text{-}(N_1)_{60cs}$=16.5), S=12.0 m (Post 750: WH = 750 Mg.m)

55

CHAPTER 6
DESIGN EXAMPLES

6.1 Introduction

This section considers liquefaction potential at a few example sites, and presents design examples to illustrate the use of the simplified design charts to determine either dynamic compaction parameters or vibro-stone column parameters required to mitigate liquefaction at these sites for a given earthquake magnitude and maximum ground acceleration.

6.2 Dynamic Compaction

The post-improvement penetration resistance charts presented in Section 5.5.2 are directly applicable for a uniform silty sand deposit with: (i) pre-improvement $(N_1)_{60cs}$ values of 7.5 or 16; (ii) energy per impact (WH) of 100, 250, 500, and 750 Mg.m; (iii) three phases of impact (primary, secondary, and tertiary), each phase consisting of a single pass of 8 or 12 impacts per grid location (N_I) completed row-by-row; (iv) grid spacing S of 12.0 or 15.0 m (Figure 5-18); (v) time cycle between impacts T of 2 or 4 min; and (vi) wick drains spacing S_w of 1.5, 1.0 m (rectangular pattern). The size of wick drains was assumed to be 100 mm x 5 mm with an equivalent diameter of 5 cm. The charts were developed for two values of hydraulic conductivities of 10^{-7} m/s and 10^{-8} m/s, respectively. The groundwater is at a depth of 2 m below the working surface. The radius of the pounder ranges from 1.5 m to 2.5 m (Elias et al. 1999). In all cases, $(N_1)_{60cs}$ is related to $(N_1)_{60}$ and fines content by the relationship presented in Section 3.5.

This section presents a few examples on the use of these charts for liquefaction mitigation, for uniform soil profiles. Figure 6-1 presents a flowchart describing the use of post-improvement penetration charts. For other soil profiles or other values of soil parameters, these charts may be interpolated appropriately as shown in a few examples below.

```
┌─────────────────────────────────────────┐
│  Choose charts set for deposit k & pre-(N₁)₆₀cs │
│       Start with trial parameters:      │
│  S = 15.0 m, Sᵥ =1.5 m, N_I = 8 & T = 2 min │
└─────────────────────────────────────────┘
                    │
                    ▼
┌─────────────────────────────────────────┐
│   Overlay the min. req. (N₁)₆₀cs profile  │
│   Find (d_max)_dsn for different impact energies │
└─────────────────────────────────────────┘
                    │
                    ▼
           ⟨ (d_max)_dsn ≥ (d_max)_req ⟩  ──── Yes ───┐
                    │ No                              │
                    ▼                                 │
        ┌──────────────────────┐                      │
        │    Use chart with     │                      │
        │  higher N_I and/or T   │                      │
        │          OR            │                      │
        │  smaller Sᵥ and/or S   │                      │
        └──────────────────────┘                      │
                    │                                 │
                    ▼                                 │
   Yes ──── ⟨ N_I, T, Sᵥ, S are practical? ⟩          │
                    │ No                              │
                    ▼                                 │
        ┌──────────────────────┐                      │
        │ Consider another technique │                 │
        └──────────────────────┘                      │
                                                      │
        ┌──────────────────────┐                      │
        │ Print final design parameters │ ◄───────────┘
        │      W, H, N_I, T, Sᵥ, S       │
        └──────────────────────┘
```
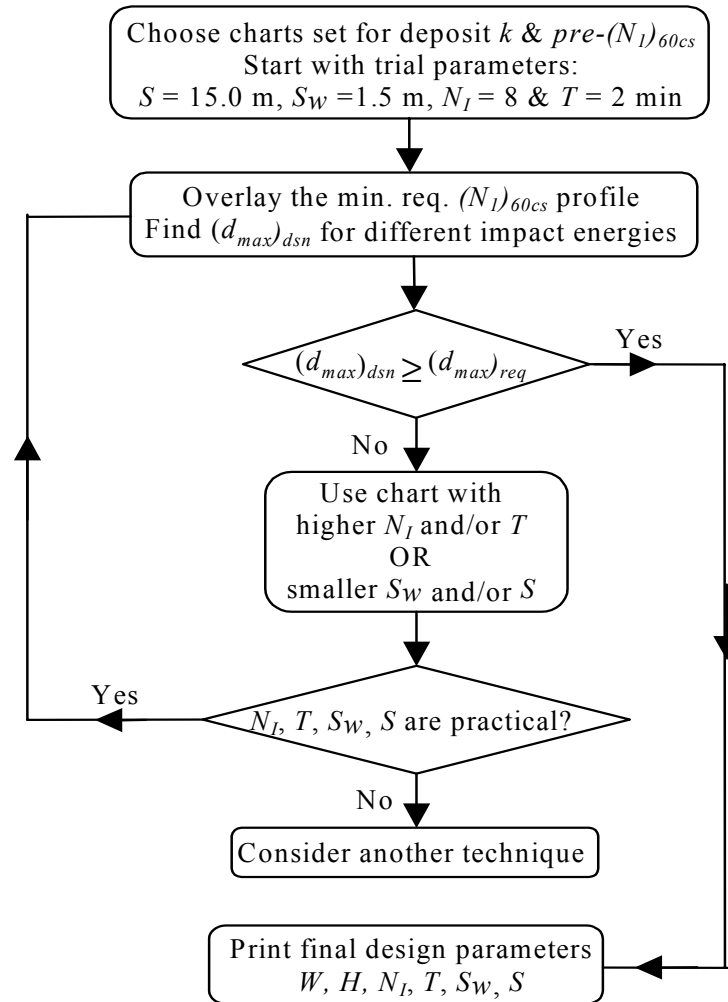
Figure 6-1. Design Example Procedure

6.2.1 Design Example 1

In this design example, a silty sand site with pre-improvement $(N_1)_{60cs}$ shown in Figure 6-2 is considered. The fines content and the hydraulic conductivity are estimated to be about 25% and 10^{-7} m/s, respectively. The groundwater level is at 2.0 m below the working surface. Based on liquefaction potential analysis using a procedure outlined by Youd et al. (2001), the required minimum $(N_1)_{60cs}$ to mitigate liquefaction at the site was estimated for a design earthquake of M = 7.5 and a_{max} = 0.25g. This minimum profile is also shown in Figure 6-2. This analysis indicates that the pre-improvement $(N_1)_{60cs}$ is less than the required minimum values for the silty sand layer between 2.0 to 6.0 m depth is liquefiable.

The average $(N_1)_{60cs}$ for the liquefiable layer in Figure 6-2 located between 2 and 6 m is 7.5. The post-improvement charts corresponding to $(N_1)_{60cs}$ = 7.5 and k = 10^{-7} m/s were chosen from Section 5.5.2 The minimum required $(N_1)_{60cs}$ profile to resist liquefaction obtained from the liquefaction potential analysis was overlaid on these charts. The charts which will provide post-improvement $(N_1)_{60cs}$ profile exceeding the minimum required $(N_1)_{60cs}$ for the layer at 2 to 6 m depth was chosen. This chart is shown in Figure 6-3.

Based on Figures 6-2 and 6-3, the recommended liquefaction mitigation solution is to use dynamic compaction supplemented with wick drains with the following characteristics: impact grid pattern as shown in Figure 5-18; Grid spacing $S = 15$ m; Impact phases: primary, secondary and tertiary completed row by row; Energy per impact (WH) = 750 Mg.m; Impact per grid location/phase (N_I)= 12; Time cycle between impacts (T) = 2 min; wick drain spacing (S_w) = 1.5 m; and wick drain equivalent diameter = 5 cm.

Figure 6-2. Pre- and Required $(N_1)_{60cs}$ Figure 6-3. Post-improvement $(N_1)_{60cs}$ Figure 6-4. Simulation Results Chart ($k=10^{-7}$m/s, $Pre-(N_1)_{60cs}$=7.5)

In order to further assess the use of simplified post-improvement charts, one set of numerical simulations was also conducted for the actual pre-improvement $(N_1)_{60cs}$ soil profile shown in Figure 6-2, for the chosen compaction parameters and grid spacing. The post-improvement $(N_1)_{60cs}$ profile obtained from this simulation is shown in Figure 6-4. The simulation results indicate that the post-improvement $(N_1)_{60cs}$ is indeed higher than the minimum required $(N_1)_{60cs}$ to resist liquefaction at all depths.

6.2.2 Design Example 2

A nonuniform 9.0 m silty sand deposit is considered in this example with fines content and hydraulic conductivity of 25% and 10^{-7} m/s, respectively. The groundwater level is at 1.0 m. A 1.0 m thick compacted granular working pad was constructed over the site (Figure 6-5), making the ground water at a depth of 2.0 m below the working surface. The pre-improvement equivalent clean sand normalized SPT profile $(N_1)_{60cs}$ is shown in Figure 6-6. The depth values shown in this figure refer to depth below the working surface.

Based on liquefaction potential analysis using SPT procedures (Youd et al. 2001), the minimum required $(N_1)_{60cs}$ profile to resist liquefaction at this site was estimated for a design earthquake of magnitude $M = 7.5$ and peak horizontal accleration $a_{max} = 0.25g$. This minimum required $(N_1)_{60cs}$ profile is also shown in Figure 6-7 . Two layers located between depths of 2.0 m to 4.0 m and 6.0 m to 10.0 m were found to be susceptible to liquefaction. The combined average $(N_1)_{60cs}$ for these two layers is 16.0. The depth of improvement requiring ground improvement is 10 m.
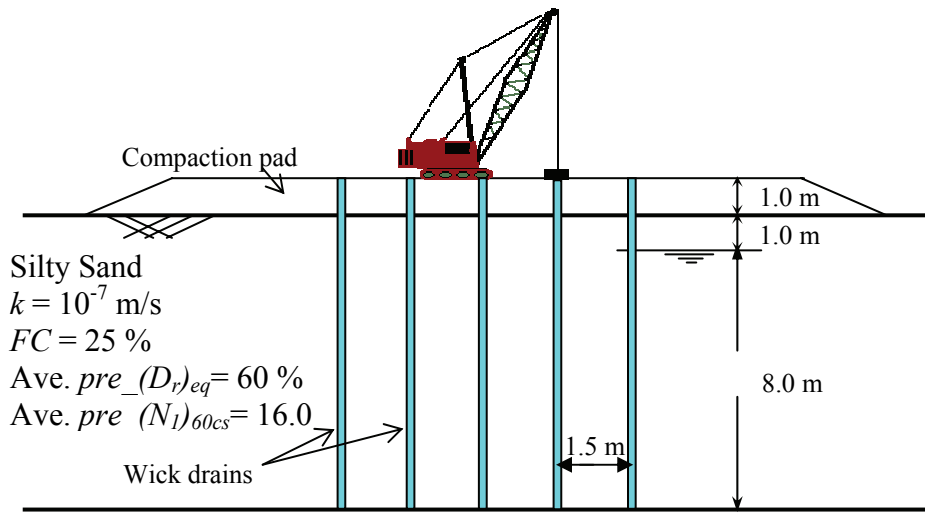
Figure 6-5. Design Example 2

The post-improvement charts corresponding to $(N_1)_{60cs}$ = 16 and $k = 10^{-7}$ m/s were chosen from Section 5.5.2. The minimum required $(N_1)_{60cs}$ profile to resist liquefaction obtained from the liquefaction potential analysis was overlaid on these charts. The charts which will provide post-improvement $(N_1)_{60cs}$ profile exceeding the minimum required $(N_1)_{60cs}$ was chosen. This chart is shown in Figure 6-7.

Based on Figures 6-6 and 6-7, the recommended liquefaction mitigation solution is to use dynamic compaction supplemented with wick drains with the following characteristics: impact grid pattern as shown in Figure 5-18; Grid spacing S = 15 m; Impact phases: primary, secondary and tertiary completed row by row; Energy per impact (WH) = 570 Mg.m; Impact per grid location/phase (N_I)= 12; Time cycle between impacts (T) = 4 min; wick drain spacing (S_w) = 1.5 m; and wick drain equivalent diameter = 5 cm.
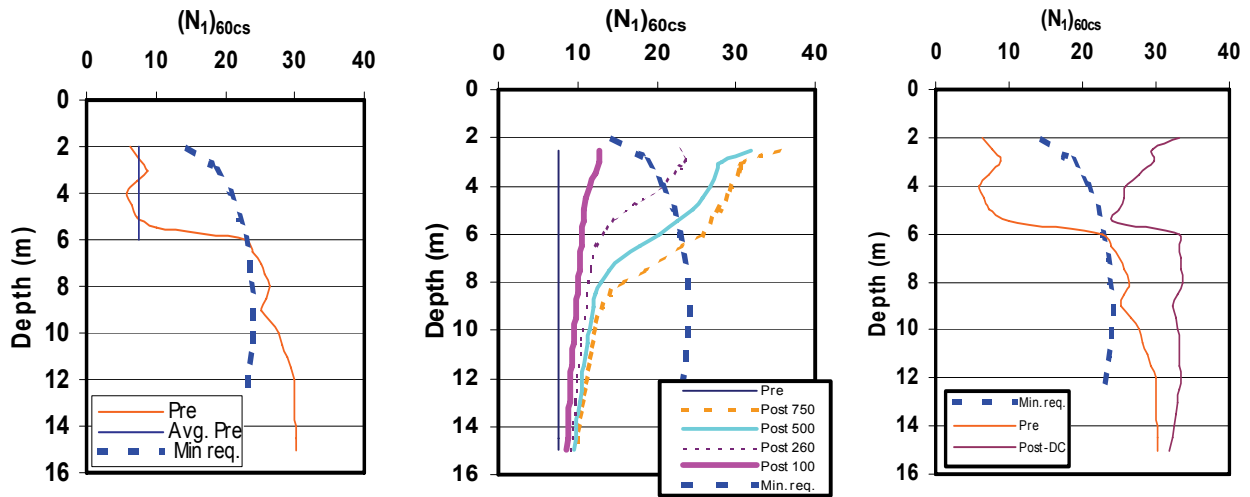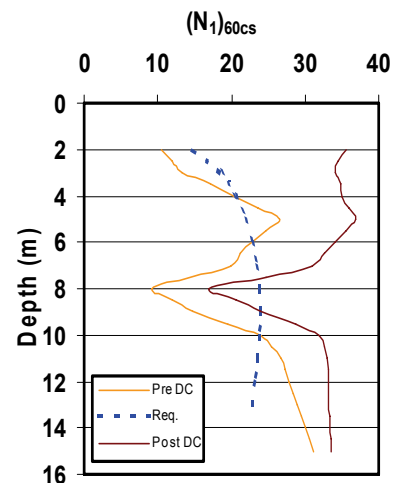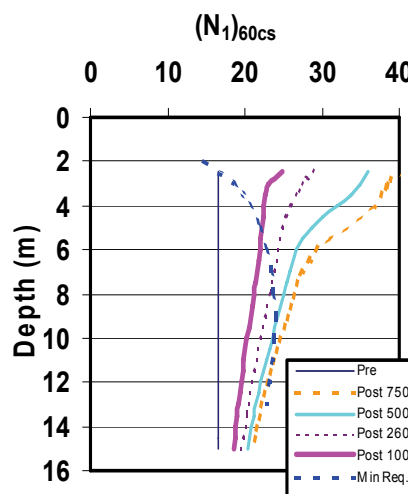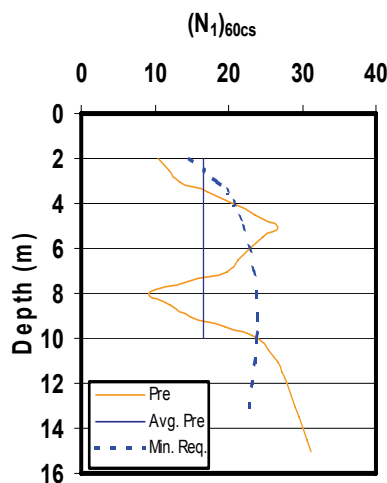

Figure 6-6. Pre- and Required $(N_1)_{60cs}$ Figure 6-7. Post-improvement $(N_1)_{60cs}$ Figure. 6-8 Simulation Results Chart (k=10^{-7} m/s, _Pre-($N_1)_{60cs}$=16.0)

60

In order to further assess the use of simplified post-improvement charts, one set of numerical simulations was also conducted for the actual pre-improvement $(N_1)_{60cs}$ soil profile shown in Figure 6-6, for the chosen compaction parameters and grid spacing. The post-improvement $(N_1)_{60cs}$ profile obtained from this simulation is shown in Figure 6-8. The simulation results indicate that the post-improvement $(N_1)_{60cs}$ is higher than the minimum required $(N_1)_{60cs}$ at all depths except for a weak layer from 7.5 to 9.0 m. This indicates that it would be appropriate to use the values for the weakest layer in the design to determine the compaction parameters and ascertain exceedance of minimum required post-improvement $(N_1)_{60cs}$ profile.

A reanalysis of this case assuming the weak layer from 7.5 to 9.0 m as governing the design ground improvement, the required compaction parameters were found to be $WH= 750$ Mg.m, $N_I=12$, $S=15$m, $S_w=1.0$ m, and $T=4$ min.

6.2.3 Design Example 3

In this example, the soil deposit is a dense silty sand deposit having a weak layer in the vicinity of 6 to 12 m depth as shown in Figure 6-9. The fines content and the hydraulic conductivity for the silty sand layer are estimated to be about 25% and 10^{-7} m/s, respectively. The groundwater level is at 2.0 m. The minimum required $(N_1)_{60cs}$ profile to resist liquefaction due to a design earthquake of magnitude $M = 7.5$ and peak horizontal accleration $a_{max} = 0.25g$ is also shown in Figure 6-9. Soil layer between depthes 6.0 and 12.0 m is liquefiable for the design earthquake. The average $(N_1)_{60cs}$ for this liquefiable layer is 16.0.

The post-improvement charts corresponding to $(N_1)_{60cs} = 16$ and $k = 10^{-7}$ m/s were chosen from Section 5.5.2. The minimum required $(N_1)_{60cs}$ profile to resist liquefaction obtained from the liquefaction potential analysis was overlaid on these charts. The charts which will provide post-improvement $(N_1)_{60cs}$ profile exceeding the minimum required $(N_1)_{60cs}$ was chosen. This chart is shown in Figure 6-10.
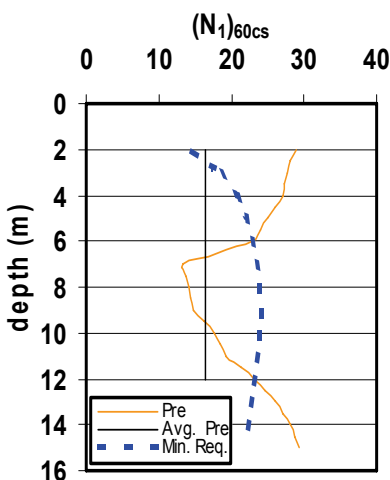
Figure 6-9. Pre- and Required $(N_1)_{60cs}$ **Figure 6-10. Design chart**   **Figure 6-11. Simulation Results**
$(k=10^{-7}$m/s, *Pre-$(N_1)_{60cs}$*=7.5)
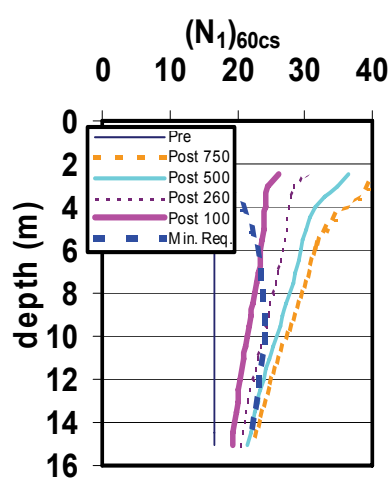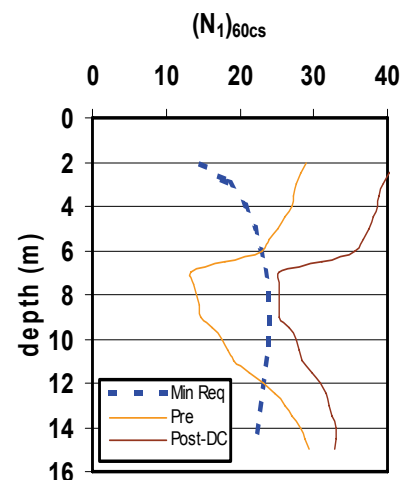
61

Based on Figures 6-9 and 6-10, the recommended liquefaction mitigation solution is to use dynamic compaction supplemented with wick drains with the following characteristics: impact grid pattern as shown in Figure 5-18; Grid spacing S = 15 m; Impact phases: primary, secondary and tertiary completed row by row; Energy per impact (WH) = 410 Mg.m; Impact per grid location/phase (N_I)= 12; Time cycle between impacts (T) = 4 min; wick drain spacing (S_w) = 1.0 m; and wick drain equivalent diameter = 5 cm. Figure 6-11 shows the post-improvement $(N_1)_{60cs}$ profile based on numerical simulation using the actual pre-improvement $(N_1)_{60cs}$ profile. The post-improvement $(N_1)_{60cs}$ exceeds the required minimum values at all depths.

6.2.4 Summary

The design process shown in Figure 6-1 for the selection of field dynamic compaction parameters involves the following steps:
  o Choosing design chart sets corresponding to the average pre-improvement $(N_1)_{60cs}$ of the liquefiable layer and deposit's hydraulic conductivity, and fines content.
 o Starting with, as an optimal choice (least cost operational parameters), S = 15.0 m, S_w = 1.5 m, N_I = 8, and T = 2 min.
  o Overlaying the minimum required $(N_1)_{60cs}$ profile, concluded from the liquefaction assessment study of the site due to the design earthquake, on the relevant design chart.
  o Determining the maximum depth of liquefaction mitigation for different impact energies and defining the final design operational parameters.
  o In case the design depth depicted from design chart did not cover the required depth of liquefaction mitigation, repeat the process with charts of higher N_I and/or T, or smaller S_w and/or S.

If the required depth of liquefaction mitigation was not achieved using any of the operational parameter combinations, a different improvement technique should be considered.

6.3 Vibro-Stone Columns

The post-improvement penetration resistance charts presented in Section 4.5 are directly applicable for loose saturated uniform silty sand deposits with: (i) pre-improvement $(N_1)_{60cs}$ values of up to 20; (ii) energy rating of the vibratory probe of 120 kW operating at 50 Hz; (iii) vibro-stone columns and wick drains installed in a triangular pattern as shown in Figure 6-1; and (iv) vibro-stone column diameter of about 0.9 m. The size of the wick drains was assumed to be 100 mm x 5 mm with an equivalent diameter of 5 cm. The charts were developed for a range of hydraulic conductivities from 10^{-4} m/s to 10^{-8} m/s. In all cases, $(N_1)_{60cs}$ is related to $(N_1)_{60}$ and fines content by the relationship presented in Section 3.5.

This section presents a few examples on the use of these charts for liquefaction mitigation, for similar soil profiles chosen in the examples for DC. Figure 6-12 presents a flowchart describing the use of these post-improvement penetration charts.

Choose charts set for deposit $pre\text{-}(N_1)_{60cs}$
Start with SC alone

Consider trial
A_r of 5.6 %

Enter chart with k (m/s)
Find $post\text{-}(N_1)_{60cs}$

$(N_1)_{60cs\,des} \geq (N_1)_{60cs\,req}$ — Yes

No

Increase A_r

A_r is practical? — Yes

No

Use SC with wick drains

Consider another technique

Print final design parameters
$Wicks, A_r,$ SC diameter, spacing
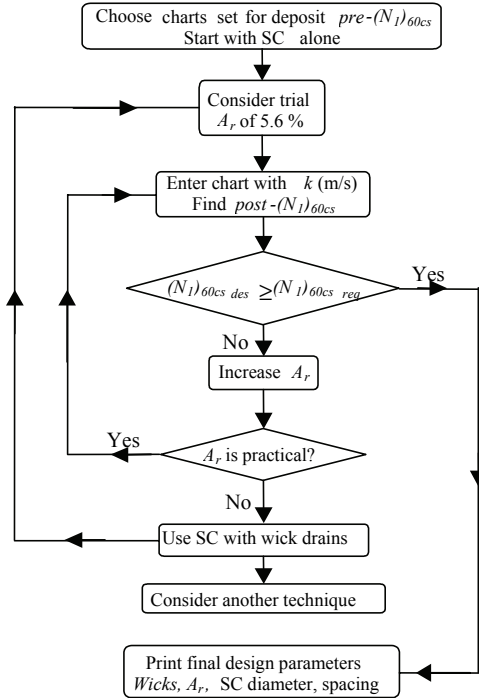
Note: $(N_1)_{60cs,req}$ = minimum $(N_1)_{60cs}$ profile required to mitigate liquefaction at the site, obtained using a liquefaction potential analysis; $pre\text{-}(N_1)_{60cs}$ = average pre-improvement $(N_1)_{60cs}$ for the liquefiable layer at the design site; $post\text{-}(N_1)_{60cs} = (N_1)_{60cs,des.}$ average post-improvement $(N_1)_{60cs}$ for the liquefiable layer at the design site obtained from the chart; chart = Figures 4-6 and 4-7.

Figure 6-12. SC Design Flowchart

As shown in Figure 6-12, the design process for selection of field design parameters involves:
- o Choosing design charts set corresponding to the defined site-specific conditions from soil investigations of the deposit under treatment (average pre-improvement $(N_1)_{60cs}$ of the liquefiable layer and the deposit's hydraulic conductivity, and fines content).
- o Starting as an optimal choice with SC without wick drains, and considering an area replacement ratio of 5.6 %, use the deposit's hydraulic conductivity to find the corresponding post-densification $(N_1)_{60cs}$.
- o If the post-densification $(N_1)_{60cs}$ is found to be lower than the required $(N_1)_{60cs}$, use a chart with a higher area replacement ratio A_r.
- o In case the post-densification $(N_1)_{60cs}$ still did not satisfy the minimum required, use curves corresponding to SC with wick drains starting with lower A_r; if required, repeat the process with a higher A_r.

6.3.1 Design Example 1

In this design example, a 13.0 m deep saturated loose silty sand site with pre-improvement $(N_1)_{60cs}$ shown in Figure 6-13 is considered. The groundwater level is at a depth of 2.0 m. Based on SPT based liquefaction potential analysis (Youd et al. 2001), the minimum required $(N_1)_{60cs}$ profile to resist liquefaction for a design earthquake of $M = 7.5$ and $a_{max} = 0.25g$ is also shown in Figure 6-13. The soil layer from 2 m up to a depth of about 12 m is liquefiable for the design earthquake. The average $(N_1)_{60cs}$ for this liquefiable layer is about 7. The fines content and the hydraulic conductivity are 25% and 10^{-7} m/s, respectively.
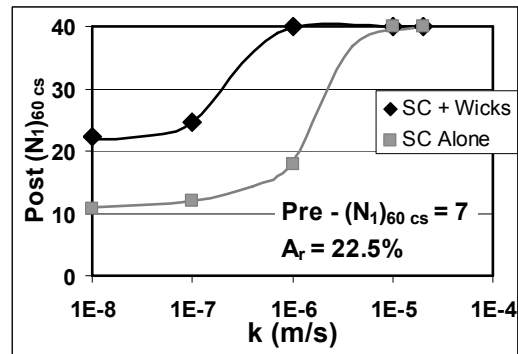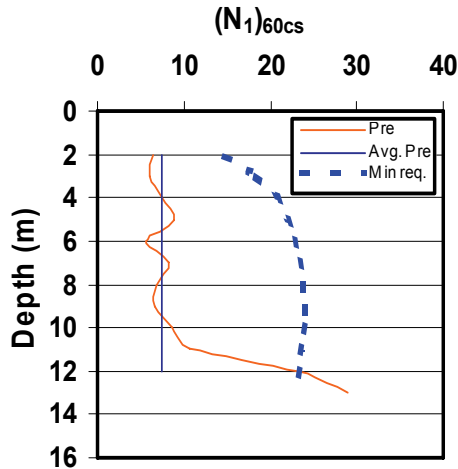
Figure 6-13. Pre- and Required $(N_1)_{60cs}$ Profile Figure 6-14. Post-improvement $(N_1)_{60cs}$ Chart

Based on the design flowchart shown in Figure 6-12, the design charts corresponding to a pre-improvement $(N_1)_{60cs}$= 7 were chosen from Section.4.5. Figure 6-13 indicates that the required minimum post-improvement $(N_1)_{60cs}$ varies from about 13 to 23 for depths from 2 to 6 m and remain at about 23 below the depth of 6 m. The design chart shown in Figure 6-14 indicates that a vibro-stone column at a replacement ratio of 22.5% would yield post-improvement $(N_1)_{60cs}$ of about 25. The recommended stone column diameter is 0.9 m at a center-to-center spacing of 1.8 m. Wick drain with dimensions of 100 mm x 5 mm should be preinstalled at centers between each stone column. Although the SC diameter can be reduced (lower replacement ratio) at shallower depths, such fine tuning is not applied in general practice.

6.3.2 Design Example 2

A nonuniform (layered) 9.0 m silty sand deposit is considered in this example with fines content and hydraulic conductivity of 25% and 10^{-7} m/s, respectively. The groundwater level is at 1.0 m. A 1.0 m thick compacted granular working pad was constructed over the site as previously shown in Figure 6-5 (generally it is not required to make a working pad for SC construction; however, it is used to be consistent with the DC design examples), making the ground water a depth of 2.0 m below the working surface. The pre-improvement equivalent clean sand normalized SPT profile $(N_1)_{60cs}$ is shown in Figure 6-15. The depth values shown in this figure refer to depth below the working surface.

Based on liquefaction potential analysis using SPT procedures (Youd et al. 2001), the minimum required $(N_1)_{60cs}$ profile to resist liquefaction at this site was estimated for a design earthquake of magnitude $M = 7.5$ and peak horizontal accleration $a_{max} = 0.25g$. This minimum required $(N_1)_{60cs}$ profile is also shown in Figure 6-15. Two layers located between depths of 2.0 m to 4.0 m and 6.0 m to 10.0 m were found to be susceptible to liquefaction. The combined average $(N_1)_{60cs}$ for these two layers is about 16.

The post-improvement charts corresponding to $(N_1)_{60cs} = 16$ and $k = 10^{-7}$ m/s were chosen from Section 4.5. Two SC configurations, with and without wick drains, can be selected for this site

64

based on the design charts shown in Figures 6-16a,b. For SC without wicks, an area replacement ratio of 22.5% would produce a post-improvement $(N_1)_{60cs}$ of about 21 (Figure 6-16a), which is satisfactory for shallower depths up to 4 m. However, for 6 to 10 m depth, the replacement ratio should be slightly increased to about 28.0% (using extrapolation). The recommended stone column diameter is 1.0 m at a center-to-center spacing of 1.8 m.
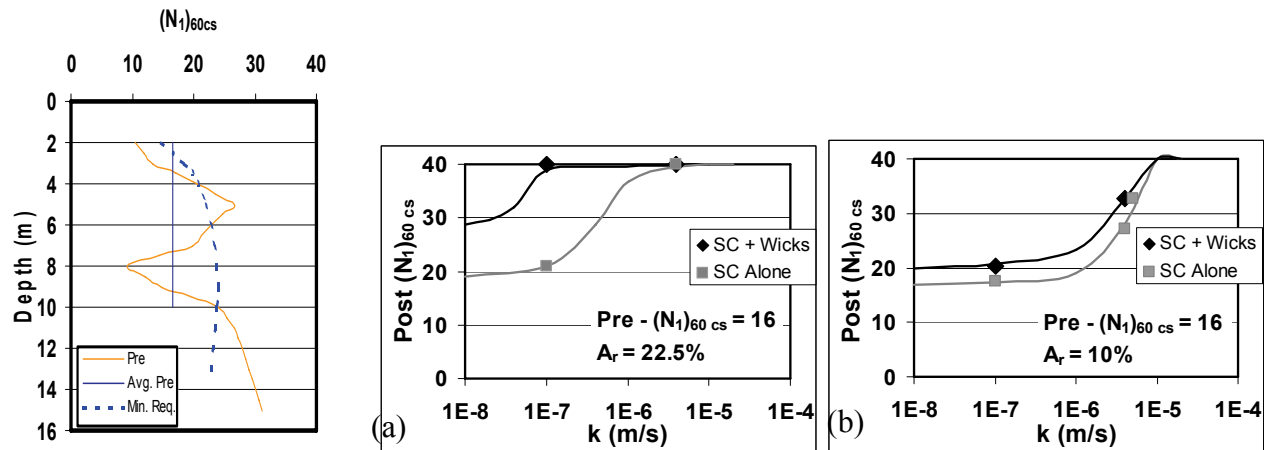
Figure 6-15. Pre- and Required $(N_1)_{60cs}$ Figure 6-16. Post-improvement $(N_1)_{60cs}$ Charts

For SC with wicks, an area replacement ratio of 10.0% would produce a post-improvement $(N_1)_{60cs}$ of about 21 (Figure 6-16b), which is satisfactory for shallower depths up to 4 m. However, for 6 to 10 m depth, the replacement ratio should be slightly increased to about 12.5% (using extrapolation). The recommended stone column diameter is 1.0 m at a center-to-center spacing of 2.7 m. Wick drains with dimensions of 100 mm x 5 mm should be preinstalled at centers between each stone column. Either system (SC with or without wicks) could be selected based on the cost and ease of construction considerations.

6.3.3 Design Example 3

In this example, the soil deposit is a dense silty sand deposit having a weak layer in the vicinity of 6 to 12 m depth as shown in Figure 6-17. The fines content and the hydraulic conductivity for the silty sand layer are estimated to be about 25% and 10^{-7} m/s, respectively. The groundwater level is at 2.0 m. The minimum required $(N_1)_{60cs}$ profile to resist liquefaction due to a design earthquake of magnitude $M = 7.5$ and peak horizontal acceleration $a_{max} = 0.25g$ is also shown in Figure 6-17. Soil layer between depths 6.0 and 12.0 m is liquefiable for the design earthquake. The average $(N_1)_{60cs}$ for this liquefiable layer is 16.

The post-improvement charts relevant for this case are shown in Figures 6-18a and b. For SC without wick drains, 1.0 m diameter stone columns should be installed at 1.8 m spacing. However, improvement is needed only for depths from 6 to 12 m. Therefore, the SC diameter at shallower depths up to 6 m could be about 0.45 m (or equal to that of the hole created by the vibratory probe) for the purpose of extending the drainage path to the surface and for filling the cavity created by the probe.

Similarly, for SC with wick drains, SC diameter should be 1.0 m for depths ranging from 6 to 12 m, and the spacing should be 2.7 m. Wick drains with dimensions of 100 mm x 5 mm should be preinstalled at centers between each stone column. Either system (SC with or without wicks) could be selected based on the cost and ease of construction considerations.
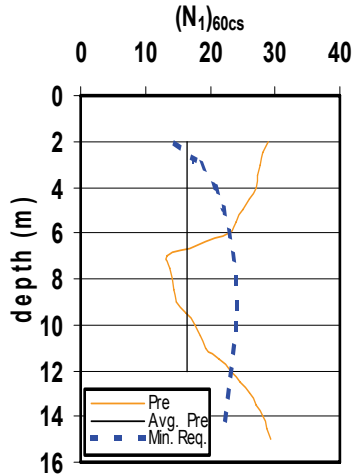
Figure 6-17. Pre- and Required $(N_1)_{60cs}$ **Figure 6-18. Post-improvement** $(N_1)_{60cs}$ **Charts**
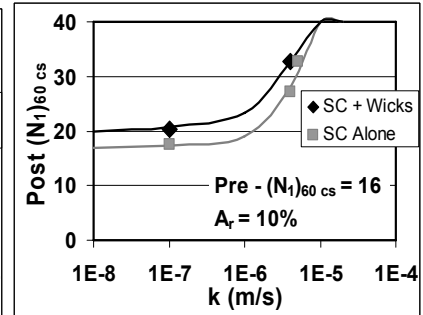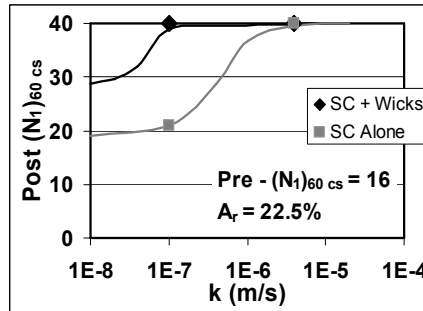
CHAPTER 7
CONCLUSIONS

The geotechnical literature on soil densification techniques using dynamic compaction and vibro-stone columns to mitigate liquefaction hazards mainly depends on design guidelines based on previous case histories. Furthermore, these techniques and guidelines are primarily applicable to relatively clean sand deposits. The use of pre-installed wick drains during dynamic compaction and vibro-stone columns have been found to be beneficial in densifying non-plastic silty soil deposits using these techniques. However, no analytical technique has been available to study these techniques, and design dynamic compaction and vibro-stone column techniques to mitigate liquefaction at a site for a design earthquake, for both sands and non-plastic silty soils. The focus of this report was to develop a numerical simulation model to simulate dynamic compaction and vibro-stone column processes and quantify the changes in soil density during installation projects, and develop improved design guidelines for dynamic compaction or vibro-stone column parameters to remediate liquefaction at a given site containing sands and non-plastic silty soils.

In this report, an analytical model for simulation of the performance of soil deposits during ground improvement projects, using energy principles governing soil liquefaction and soil densification by consolidation during dynamic compaction and stone column installation, has been developed. Simple attenuation relationships were used to estimate the energy dissipated in the soil. Experimental data based on energy principles was used to estimate the pore pressures generated as a function of the energy dissipated in the soil. Coupled consolidation equations were used to simulate soil consolidation. Based on this analytical model, a rational design procedure was developed to determine the densification achievable using each technique, with or without supplemental wick drains, for liquefaction mitigation of loose sand and non-plastic silty soils. The design charts developed using this simulation model have been compared with data from instrumented field test and available case histories through collaboration with ground improvement industry partners. Stepwise design procedures and design examples are presented.

The simulation models for soil densification using both dynamic compaction and vibro-stone column have been verified for both saturated loose sand deposits and non-plastic silty sand deposits using either case history records or instrumented field studies, in collaboration with ground improvement industry partners. The effects of site-specific soil conditions (soil density, penetration resistance, permeability, fines content) as well as dynamic compaction of vibro-stone column operational parameters on post-improvement density and penetration resistances, depths of improvements, etc. have been studied. Design charts and design guidelines for choosing dynamic compaction and vibro-stone column parameters for liquefaction mitigation have been developed, based on the simulation models. Design procedural flowcharts and design examples have been developed. These developments are hoped to advance the use of dynamic compaction and vibro stone columns to mitigate liquefaction potential in sand and non-plastic silty sand site in a more rational way. A summary of publications resulting from this work that contains details of the work presented herein are presented in Appendix A.

CHAPTER 8
REFERENCES

Andrews, D.C.A. (1998), "Liquefaction of silty soils: susceptibility, deformation, and remediation," *PhD Dissertation*, Dept. of Civil Eng., USC, CA.

Andrus, R.D., and Chung, R.M. (1995), "Ground improvement techniques for liquefaction remediation near existing lifelines," *NISTIR report # 5714*, Building and fire research laboratory, National Institute of Standards and Technology, Gaithersburg, MD.

Atukorala, U.D., Wijewickreme, D., and Butler, R.C. (1992), "Ground improvement and testing of random fills and alluvial soils," Transportation research record 1369, pp 98-107.

Baez, J.I. (1995), "A design model for the reduction of soil liquefaction by vibro-stone columns" Ph.D. Dissertation, USC, Los Angeles, CA. 207 p.

Baez, J.I. (2004), "Liquefaction mitigation at Marina Del Rey, CA," Personal communications.

Baez, J.I., and Martin, G. (1992), "Quantitative evaluation of stone column techniques for earthquake liquefaction mitigation," Proc. 10th World Conf. Earthq. Eng., Balkema, Rotterdam. pp.1477-83.

Baez, J.I., and Martin, G.R. (1993), "Advances in the design of vibro systems for the improvement of liquefaction resistance," Proceeding of the symposium on ground improvement, Vancouver Geotech. Society, Vancouver, B.C., Canada.

Barksdale, R.D. and Bachus, R.C. (1983), "Design and Construction of Stone Columns," Volume 1, Report No. 1, FHWA/RD 83/026, Federal Highway Administration, 210P.

Chow, Y.K., Yong, D.M., Yong, K.Y., and Lee, S.L. (1992), "Dynamic compaction analysis," ASCE, Journal of Geotechnical Engineering, Vol. 118(8), p 1141-1157.

Chow, Y. K., Yong, D. M., Yong, K. Y., and Lee, S. L. (1994), "Dynamic compaction of loose granular soils: effect of print spacing," ASCE, Journal of Geotechnical Engineering, Vol. 120(7), p 1115-1133.

Davis, R. O., and Berrill, J. B. (1982), "Energy dissipation and seismic liquefaction in sands," Earthquake Engineering and Structural Dynamics, Vol. 10, p59–68.

Desai, C. S. (2000), "Evaluation of liquefaction using disturbed state and energy approaches," ASCE, J. of Geotech. And Geoenv. Eng., Vol. 126, No. 7, pp 618-631.

Dise, K., Stevens, M.G., and Von Thun, J.L. (1994), "Dynamic compaction to remediate liquefiable embankment foundation soils," ASCE, *Geotech. sp. pub.*, No. 45, pp.1-25.

Dobson, T. (1987), "Case histories of the vibro systems to minimize the risk of liquefaction," Soil improvement - a ten year update. Proc., ASCE Convention, GSP. 12, J.P.Welsh, edr., ASCE, Atlantic city, NJ, pp.167-183.

Dowding, C.H. (1996), "Construction vibrations," Prentice Hall, Upper Saddle River, NJ.

Drumheller et al. (1997), "Ground improvement," Ground improvement, ground reinforcement, ground treatment - Developments 1987-1997, V.R.Schaefer, edr., Geot. Sp. Publ. No. 69, ASCE, Logan, Utah. pp. 1-71.

Elias, V., Welsh, J., Warren, J. and Lukas, R. (1999), "Ground improvement technical summaries," Demonstration project 116, Publication No. FHWA-SA-98-086R, Federal Highway Administration, Washington D.C.

Fahoum, K. (2001), "Soil improvement and liquefaction mitigation by deep dynamic compaction," Foundations and Ground Improvement, ASCE, GSP No. 113, pp. 311-324.

Figueroa, J. L., Saada, A. S., Liang, L., and Dahisaria, N. M. (1994), "Evaluation of soil liquefaction by energy principles," ASCE, J. of Geotech. Eng., Vol. 120, No. 9, pp 1554-1569.

FHWA (2001), "Stone columns," Ground Improvement Technical Summaries, II, Publication No. FHWA-SA-98-086R: 7-1 to 7-84.

Green, R. and Mitchell, J. K., (2004), Energy-based evaluation and remediation of liquefiable soils, Geotrans 2004, *ASCE, Proc. Geotech. Eng. for transportation projects*, 1961-1970.

Han, J. (1998), "Ground modification by a combination of dynamic compaction, consolidation, and replacement," Proc. of the 4th Int. Conf. on case hist. in geotech. Engrg., St. Louis, Missouri, pp.341-346.

Kanagalingam, T. and Thevanayagam, S. (2006), "Contribution of fines to the compressive strength of mixedsoils," Discussion, Geotechnique Geotechnique.

Kramer, S.L. and Holtz, R.D. (1991), "Soil improvement and foundation remediation with emphasis on seismic hazards," NSF workshop on Soil improvement and foundation remediation, University of Washington, Seattle, Washington.

Law, K.T., Cao, Y.L., and He, G.N. (1990), "An energy approach for assessing seismic liquefaction potential," Canadian Geotechnical Journal, Vol. 27, p320–329.

Luehring, R., Snorteland, N., Mejia, L., and Stevens, M. (2001), "Liquefaction mitigation of a silty dam foundation using vibro-stone columns and drainage wicks: a case history at salmon lake dam," Proc. 21st USSD annual meeting and lecture, Denver, CO.

Lukas, R.G. (1986), "Dynamic compaction for highway construction, design and construction guidelines," Report# FHWA/RD-86/133, Federal Highway Administration, Washington D.C.

Lukas, R.G. (1995), "Dynamic compaction," Report No. FHWA/SA/95/037, Federal Highway Administration, Washington, DC.

Mayne, P.W. (1985), "Ground vibrations during dynamic compaction," Vibration Problems in geotechnical engineering, Gazetas and Selig, editors, ASCE, p 247–265.

Meek J.W., and Wolf, J.P. (1993), "Cone models for nearly incompressible soil," Earthquake Engineering and Structural Dynamics, Vol. 22, p 649-663.

Meyerhof, G.G. (1957), "Discussion on research on determining the density of sands by spoon penetration testing," Proceedings of the Fourth International Conference on Soil Mechanics and Foundation Engineering, London, UK, p 110.

Meyerhof, G.G. (1976), "Bearing capacity and settlement of pile foundations," ASCE, Journal of Geotechnical Engineering, Vol. 102(1), p 197-259.

Meyer, M.E., Tan, C.K., and Drumheller, J.C. (2001), "Liquefaction mitigation at JFK Airport using dynamic compaction," Foundations and Ground Improvement, ASCE, GSP No. 113, pp. 685-700.

Miller, G.F., and Pursey, H. (1955), "On the partition of energy between elastic waves in a semi-infinite soild," Proceedings of the Royal Society of London, Series A, Vol. 233, p 55-69.

Mitchell, J.K. (1981), "Soil improvement state-of-the art report," Proceedings of the Tenth International Conference of Soil Mechanics and Foundation Engineering, Stockholm, Sweden, p 509–565.

Mitchell, J.K., Baxter, C.D.P., and Munson, T.C. (1995), "Performance of improved ground during earthquakes," Soil Improvement for Earthquake Hazard Mitigation, ASCE, GSP No. 49, pp 1-36.

Nashed, R., Thevanayagam, S., Martin, G. R., and Shenthan, T. (2004), "Liquefaction mitigation in silty soils using dynamic compaction and wick drains," Proc. 13th World Conference on Earthq. Eng., Vancouver, Canada, Paper no. 1951.

Nashed, R. (2005), "Liquefaction mitigation of silty soils using dynamic compaction," *Ph.D. Dissertation*, University at Buffalo, Buffalo, NY.

NCEER (1997), Proceedings of the NCEER Workshop on Evaluation of Liquefaction Resistance of Soils, Technical Report NCEER-97-0022, p1-40.

Nemat-Nasser, S., and Shokooh A. (1979), "A unified approach to densification and liquefaction of cohesionless sand in cyclic shearing," Canadian Geotechnical Journal, Vol. 16, p 659-678.

Onoue, A. (1988), "Diagrams considering well resistance for designing spacing ratio of gravel drains," Soils and foundations, Vol.28, No.3, Sept.1988. pp.160-168.

Richart, F. E., Hall, J.R., and Woods, R. D. (1970), "Vibrations of soils and foundations," Prentice-Hall, Englewood Cliffs, NJ.

Robertson, P.K. and Wride, C.E. (1998), "Evaluating cyclic liquefaction potential using the cone penetration test," Canadian Geotechnical Journal, Vol. 35, p 442-459.

Seed, H.B, P.P. Martin and J. Lysmer. (1976), "Pore water pressure change during soil liquefaction," J. Geotech. Eng. Div., ASCE, Vol.102(4), pp.323-346.

Seed, H.B., and J.R. Booker. (1977), "Stabilization of potentially liquefiable sand deposits using gravel drains," J. Geotech. Eng. Div., ASCE, Vol.103(7), pp.757-68.

Shenthan, T., Nashed, R., Thevanayagam, S., and Martin, G. R. (2004a), "Liquefaction mitigation in silty soils using composite stone columns and dynamic compaction," MCEER Research Progress and Accomplishments 2003-2004: *http://mceer.buffalo.edu/publications/resaccom/0304,* pp. 205-220.

Shenthan, T., Nashed, R., Thevanayagam, S., and Martin, G. R. (2004b), "Liquefaction mitigation in silty soils using composite stone columns and dynamic compaction," J. Earthquake Engineering and Engineering vibrations, Vol.3, No. 1.

Shenthan, T., Thevanayagam, S., and Martin, G.R. (2004c), "Densification of saturated silty soils using composite stone columns for liquefaction mitigation," Proc., 13th World Conference on Earthquake Engineering, Vancouver, BC, Canada.

Shenthan, T., Thevanayagam, S., and Martin, G.R. (2004d), "Ground remediation for silty soils using composite stone columns," *Annual Report for Research Year 4*, MCEER Report, FHWA Contract # DTFH61-98-C-00094.

Shenthan, T. (2001), "Factors affecting liquefaction mitigation in silty soils using stone columns," MS Thesis, University at Buffalo, NY, 220p.

Shenthan, T. (2005), "Liquefaction mitigation in silty soils using composite stone column," *Ph.D. Dissertation*, University at Buffalo, Buffalo, NY.

Slocombe, B.C. (1993), "Dynamic compaction," Chapter 2 in Ground improvement, Moseley, M. P., Editor, CRC Press, Florida.

Thevanayagam S., and Martin G.R. (2001), "Liquefaction and post-liquefaction dissipation / densification characteristics of silty soils" MCEER, Annual Report for Research Year 1, FHWA Contract # DTFH61-98-C-00094: II85-98, Buffalo, NY.

Thevanayagam, S., Martin, G.R., Shenthan, T., and Liang, J. (2001), "Post-liquefaction pore pressure dissipation and densification in silty soils," Proc. 4th Int. Conf. on Recent Adv. in Geot. Earthq. Eng. and Soil Dyn., San Diego, CA, Paper 4.28.

Thevanayagam, S., and Martin, G.R. (2002), "Liquefaction in silty soil: screening and remediation issues," Soil Dynamics and earthquake Engineering, October 2002.

Thevanayagam, S., Kanagalingam, T., and Shenthan, T. (2002), "Contact density – confining stress – energy to liquefaction," *Proc. 15th ASCE Eng. Mech. Conf.*, Columbia Univ., NY.

Thevanayagam, S., Kanagalingam, T., and Shenthan, T. (2003), "Intergrain friction, contact density, and cyclic resistance of sands," Proceedings 2003 Pacific Conference on Earthquake Engineering, University of Canterbury, Christchurch, New Zealand.

Thevanayagam, S., Nashed, R., Shenthan, T., and Martin, G. R. (2005), "Liquefaction and remediation in silty soils," California Dept. of Trans., Caltrans research workshop.

Tokimatsu, K., and Seed, H. B. (1984), "Simplified procedures for the evaluation of settlements in clean sands," Report No. UCB/EERC-84/16, Earthquake Engineering Research Center, University of California, Berkeley, California.

Welsh, J.P. (1986), "In situ testing for ground modification techniques," Use of in situ tests in geotechnical engineering, ASCE, Geotechnical special publication No. 6, p 322-335.

Youd et al. (2001), Liquefaction resistance of soils: Summary report from the 1996 NCEER and 1998 NCEER/NSF workshops on evaluation of liquefaction resistance of soils, *ASCE, J. Geotech. & Geoenv. Eng.,* 127(10), 817-833.

APPENDIX A
PUBLICATIONS RESULTING FROM THIS WORK

Nashed, R., Thevanayagam, S., Martin, G. R., and Shenthan, T. (2004), "Liquefaction mitigation in silty soils using dynamic compaction and wick drains," Proc. 13th World Conference on Earthq. Eng., Vancouver, Canada, Paper no. 1951.

Nashed, R. (2005), "Liquefaction mitigation of silty soils using dynamic compaction," Ph.D. Dissertation, University at Buffalo, Buffalo, NY.

Nashed, R., Thevanayagam, S., and Martin, G. R. (2006a), "Simulation of dynamic compaction processes in saturated silty soils," Geo Congress 2006, ASCE, Atlanta, GA.

Nashed, R., Thevanayagam, S., and Martin, G. R. (2006b), "A Design Procedure for Liquefaction Mitigation of Silty Soils Using Dynamic Compaction," 8th National Conf. of Earthqu. Eng., Paper No. 1408, San Francisco, CA.

Nashed, R., Thevanayagam, S., and Martin, G. R. (2006c), "Densification of saturated silty soils using dynamic compaction: I," ASCE, J. of Geotech. and Geoenviron. Eng. (In preparation).

Nashed, R., Thevanayagam, S., and Martin, G. R. (2006d), "Densification of saturated silty soils using dynamic compaction: II," ASCE, J. of Geotech. and Geoenviron. Eng. (In preparation),

Shenthan, T. (2001), "Factors affecting liquefaction mitigation in silty soils using stone columns," MS Thesis, University at Buffalo, NY, 220p.

Shenthan, T., Jia, W., and Thevanayagam, S. (2002a), "Recent advances in liquefaction mitigation in sands and silty soils," Proc., KEERC-MCEER joint seminar on Retrofit Strategies for Critical Facilities, Buffalo, NY.

Shenthan, T., and Thevanayagam, S. (2002b), "Liquefaction mitigation techniques for silty soils," Proc., 18th US-Japan Bridge Eng. Workshop, St. Louis, Missouri.

Shenthan, T., Thevanayagam, S., and Martin, G.R. (2003), "Analysis of densification during composite stone column installation in silty soils," Proc., 12th Panamerican Conference on Soil Mechanics and Geotechnical Engineering/39th U.S. Rock Mechanics Symposium, MIT, Cambridge, MA.

Shenthan, T., Nashed, R., Thevanayagam, S., and Martin, G. R. (2004a), "Liquefaction mitigation in silty soils using composite stone columns and dynamic compaction," MCEER Research Progress and Accomplishments 2003-2004: *http://mceer.buffalo.edu/publications /resaccom/0304,* pp. 205-220.

Shenthan, T., Nashed, R., Thevanayagam, S., and Martin, G. R. (2004b), "Liquefaction mitigation in silty soils using composite stone columns and dynamic compaction," J. Earthquake Engineering and Engineering vibrations, Vol.3, No. 1.

Shenthan, T., Thevanayagam, S., and Martin, G.R. (2004c), "Densification of saturated silty soils using composite stone columns for liquefaction mitigation," Proc., 13th World Conference on Earthquake Engineering, Vancouver, BC, Canada.

Shenthan, T., Thevanayagam, S., and Martin, G.R. (2004d), "Ground remediation for silty soils using composite stone columns," Annual Report for Research Year 4, MCEER Report, FHWA Contract # DTFH61-98-C-00094.

Shenthan, T. (2005), "Liquefaction mitigation in silty soils using composite stone column," Ph.D. Dissertation, University at Buffalo, Buffalo, NY.

Shenthan, T. (2006), "Soil densification using vibro-stone columns supplemented with wick drains," Student Research Accomplishments 2005-2006, MCEER, Buffalo, NY.

Shenthan, T., Thevanayagam, S., and Martin, G. R. (2006a), "Numerical Simulation of soil densification using vibro-stone columns," Geo Congress 2006, Atlanta, GA.

Shenthan, T., Thevanayagam, S., and Martin, G.R. (2006b), "Soil densification using vibro-stone columns supplemented with wick drains," Proc., EERI's 8th U.S. National Conference on Earthquake Engineering (8NCEE), San Francisco, CA.

Thevanayagam S., and Martin GR. (2001), "Liquefaction and post-liquefaction dissipation / densification characteristics of silty soils" MCEER, Annual Report for Research Year 1, FHWA Contract # DTFH61-98-C-00094: II85-98, Buffalo, NY.

Thevanayagam, S., Martin, G.R., Shenthan, T., and Liang, J. (2001), "Post-liquefaction pore pressure dissipation and densification in silty soils," Proc. 4th Int. Conf. on Recent Adv. in Geot. Earthq. Eng. and Soil Dyn., San Diego, CA, Paper 4.28.

Thevanayagam, S., Kanagalingam, T., and Shenthan, T. (2002a), "Contact density – confining stress – energy to liquefaction," Proc. 15th ASCE Eng. Mech Conf. Columbia Univ., Paper 428.

Thevanayagam, S., Martin, G. R., and Shenthan, T. (2002b), "Ground remediation for silty soils using composite stone columns," Annual Report for Research Year 2, MCEER Highway Project, FHWA Contract DTFH61-98-C-00094, p II109-118.

Thevanayagam, S., Shenthan, T., Mohan, S. and Liang, J. (2002c), "Undrained fragility of sands, silty sands and silt," ASCE, J. Geotech. & Geoenv. Eng. 128 (10): 849-859.

Thevanayagam, S., Kanagalingam, T., and Shenthan, T. (2003a), "Intergrain friction, Contact density, and cyclic resistance of sands," Proc., 2003 Pacific Conf. on Earthq. Eng., Univ. of Canterbury, Christchurch, New Zealand: Paper# 115.

Thevanayagam, S., Kanagalingam, T., and Shenthan, T. (2003b), "Intergrain friction, Contact density, and cyclic resistance of silty sands," Proc., 12th Panamerican Conference on Soil Mechanics and Geotechnical Engineering/39th U.S. Rock Mechanics Symposium, MIT, Cambridge, MA: June 22-26, 2003.

Thevanayagam, S., Martin, G. R., and Shenthan, T. (2003c), "Ground remediation for silty soils using composite stone columns," Annual Report for Research Year 3, MCEER Highway Project, FHWA Contract DTFH61-98-C-00094.

Thevanayagam, S., Nashed, R., Martin, G. R., and Shenthan, T. (2004), "Ground remediation for silty soils using composite dynamic compaction," Annual Report for Research Year 4, MCEER Highway Project, FHWA Contract DTFH61-98-C-00094.

Thevanayagam, S., Nashed, R., Shenthan, T., and Martin, G. R. (2005a), "Liquefaction mitigation for silty soils using dynamic compaction and stone columns: Design methods," Annual Report for Research Year 5, MCEER Highway Project, FHWA Contract DTFH61-98-C-00094. Thevanayagam, S., Nashed, R., Shenthan, T., and Martin, G. R. (2005b), "Liquefaction and remediation in silty soils," California Dept. of Trans., Caltrans research workshop.

Thevanayagam, S., Nashed, R., Shenthan, T., and Martin, G. R. (2005c), "Soil Densification Based on Vibratory and Earthquake Energy Considerations," In "New Applications & Challenging Soils for Ground Improvement Technologies," US-Japan Workshop, September 8-10, 2005, Kyoto, Japan.

Multidisciplinary Center for Earthquake Engineering Research
List of Technical Reports

The Multidisciplinary Center for Earthquake Engineering Research (MCEER) publishes technical reports on a variety of subjects related to earthquake engineering written by authors funded through MCEER. These reports are available from both MCEER Publications and the National Technical Information Service (NTIS). Requests for reports should be directed to MCEER Publications, Multidisciplinary Center for Earthquake Engineering Research, State University of New York at Buffalo, Red Jacket Quadrangle, Buffalo, New York 14261. Reports can also be requested through NTIS, 5285 Port Royal Road, Springfield, Virginia 22161. NTIS accession numbers are shown in parenthesis, if available.

NCEER-87-0001 "First-Year Program in Research, Education and Technology Transfer," 3/5/87, (PB88-134275, A04, MF-A01).

NCEER-87-0002 "Experimental Evaluation of Instantaneous Optimal Algorithms for Structural Control," by R.C. Lin, T.T. Soong and A.M. Reinhorn, 4/20/87, (PB88-134341, A04, MF-A01).

NCEER-87-0003 "Experimentation Using the Earthquake Simulation Facilities at University at Buffalo," by A.M. Reinhorn and R.L. Ketter, to be published.

NCEER-87-0004 "The System Characteristics and Performance of a Shaking Table," by J.S. Hwang, K.C. Chang and G.C. Lee, 6/1/87, (PB88-134259, A03, MF-A01). This report is available only through NTIS (see address given above).

NCEER-87-0005 "A Finite Element Formulation for Nonlinear Viscoplastic Material Using a Q Model," by O. Gyebi and G. Dasgupta, 11/2/87, (PB88-213764, A08, MF-A01).

NCEER-87-0006 "Symbolic Manipulation Program (SMP) - Algebraic Codes for Two and Three Dimensional Finite Element Formulations," by X. Lee and G. Dasgupta, 11/9/87, (PB88-218522, A05, MF-A01).

NCEER-87-0007 "Instantaneous Optimal Control Laws for Tall Buildings Under Seismic Excitations," by J.N. Yang, A. Akbarpour and P. Ghaemmaghami, 6/10/87, (PB88-134333, A06, MF-A01). This report is only available through NTIS (see address given above).

NCEER-87-0008 "IDARC: Inelastic Damage Analysis of Reinforced Concrete Frame - Shear-Wall Structures," by Y.J. Park, A.M. Reinhorn and S.K. Kunnath, 7/20/87, (PB88-134325, A09, MF-A01). This report is only available through NTIS (see address given above).

NCEER-87-0009 "Liquefaction Potential for New York State: A Preliminary Report on Sites in Manhattan and Buffalo," by M. Budhu, V. Vijayakumar, R.F. Giese and L. Baumgras, 8/31/87, (PB88-163704, A03, MF-A01). This report is available only through NTIS (see address given above).

NCEER-87-0010 "Vertical and Torsional Vibration of Foundations in Inhomogeneous Media," by A.S. Veletsos and K.W. Dotson, 6/1/87, (PB88-134291, A03, MF-A01). This report is only available through NTIS (see address given above).

NCEER-87-0011 "Seismic Probabilistic Risk Assessment and Seismic Margins Studies for Nuclear Power Plants," by Howard H.M. Hwang, 6/15/87, (PB88-134267, A03, MF-A01). This report is only available through NTIS (see address given above).

NCEER-87-0012 "Parametric Studies of Frequency Response of Secondary Systems Under Ground-Acceleration Excitations," by Y. Yong and Y.K. Lin, 6/10/87, (PB88-134309, A03, MF-A01). This report is only available through NTIS (see address given above).

NCEER-87-0013 "Frequency Response of Secondary Systems Under Seismic Excitation," by J.A. HoLung, J. Cai and Y.K. Lin, 7/31/87, (PB88-134317, A05, MF-A01). This report is only available through NTIS (see address given above).

NCEER-87-0014 "Modelling Earthquake Ground Motions in Seismically Active Regions Using Parametric Time Series Methods," by G.W. Ellis and A.S. Cakmak, 8/25/87, (PB88-134283, A08, MF-A01). This report is only available through NTIS (see address given above).

NCEER-87-0015   "Detection and Assessment of Seismic Structural Damage," by E. DiPasquale and A.S. Cakmak, 8/25/87, (PB88-163712, A05, MF-A01). This report is only available through NTIS (see address given above).

NCEER-87-0016   "Pipeline Experiment at Parkfield, California," by J. Isenberg and E. Richardson, 9/15/87, (PB88-163720, A03, MF-A01). This report is available only through NTIS (see address given above).

NCEER-87-0017   "Digital Simulation of Seismic Ground Motion," by M. Shinozuka, G. Deodatis and T. Harada, 8/31/87, (PB88-155197, A04, MF-A01). This report is available only through NTIS (see address given above).

NCEER-87-0018   "Practical Considerations for Structural Control: System Uncertainty, System Time Delay and Truncation of Small Control Forces," J.N. Yang and A. Akbarpour, 8/10/87, (PB88-163738, A08, MF-A01). This report is only available through NTIS (see address given above).

NCEER-87-0019   "Modal Analysis of Nonclassically Damped Structural Systems Using Canonical Transformation," by J.N. Yang, S. Sarkani and F.X. Long, 9/27/87, (PB88-187851, A04, MF-A01).

NCEER-87-0020   "A Nonstationary Solution in Random Vibration Theory," by J.R. Red-Horse and P.D. Spanos, 11/3/87, (PB88-163746, A03, MF-A01).

NCEER-87-0021   "Horizontal Impedances for Radially Inhomogeneous Viscoelastic Soil Layers," by A.S. Veletsos and K.W. Dotson, 10/15/87, (PB88-150859, A04, MF-A01).

NCEER-87-0022   "Seismic Damage Assessment of Reinforced Concrete Members," by Y.S. Chung, C. Meyer and M. Shinozuka, 10/9/87, (PB88-150867, A05, MF-A01). This report is available only through NTIS (see address given above).

NCEER-87-0023   "Active Structural Control in Civil Engineering," by T.T. Soong, 11/11/87, (PB88-187778, A03, MF-A01).

NCEER-87-0024   "Vertical and Torsional Impedances for Radially Inhomogeneous Viscoelastic Soil Layers," by K.W. Dotson and A.S. Veletsos, 12/87, (PB88-187786, A03, MF-A01).

NCEER-87-0025   "Proceedings from the Symposium on Seismic Hazards, Ground Motions, Soil-Liquefaction and Engineering Practice in Eastern North America," October 20-22, 1987, edited by K.H. Jacob, 12/87, (PB88-188115, A23, MF-A01). This report is available only through NTIS (see address given above).

NCEER-87-0026   "Report on the Whittier-Narrows, California, Earthquake of October 1, 1987," by J. Pantelic and A. Reinhorn, 11/87, (PB88-187752, A03, MF-A01). This report is available only through NTIS (see address given above).

NCEER-87-0027   "Design of a Modular Program for Transient Nonlinear Analysis of Large 3-D Building Structures," by S. Srivastav and J.F. Abel, 12/30/87, (PB88-187950, A05, MF-A01). This report is only available through NTIS (see address given above).

NCEER-87-0028   "Second-Year Program in Research, Education and Technology Transfer," 3/8/88, (PB88-219480, A04, MF-A01).

NCEER-88-0001   "Workshop on Seismic Computer Analysis and Design of Buildings With Interactive Graphics," by W. McGuire, J.F. Abel and C.H. Conley, 1/18/88, (PB88-187760, A03, MF-A01). This report is only available through NTIS (see address given above).

NCEER-88-0002   "Optimal Control of Nonlinear Flexible Structures," by J.N. Yang, F.X. Long and D. Wong, 1/22/88, (PB88-213772, A06, MF-A01).

NCEER-88-0003   "Substructuring Techniques in the Time Domain for Primary-Secondary Structural Systems," by G.D. Manolis and G. Juhn, 2/10/88, (PB88-213780, A04, MF-A01).

NCEER-88-0004   "Iterative Seismic Analysis of Primary-Secondary Systems," by A. Singhal, L.D. Lutes and P.D. Spanos, 2/23/88, (PB88-213798, A04, MF-A01).

NCEER-88-0005   "Stochastic Finite Element Expansion for Random Media," by P.D. Spanos and R. Ghanem, 3/14/88, (PB88-213806, A03, MF-A01).

NCEER-88-0006   "Combining Structural Optimization and Structural Control," by F.Y. Cheng and C.P. Pantelides, 1/10/88, (PB88-213814, A05, MF-A01).

NCEER-88-0007   "Seismic Performance Assessment of Code-Designed Structures," by H.H-M. Hwang, J-W. Jaw and H-J. Shau, 3/20/88, (PB88-219423, A04, MF-A01). This report is only available through NTIS (see address given above).

NCEER-88-0008   "Reliability Analysis of Code-Designed Structures Under Natural Hazards," by H.H-M. Hwang, H. Ushiba and M. Shinozuka, 2/29/88, (PB88-229471, A07, MF-A01). This report is only available through NTIS (see address given above).

NCEER-88-0009   "Seismic Fragility Analysis of Shear Wall Structures," by J-W Jaw and H.H-M. Hwang, 4/30/88, (PB89-102867, A04, MF-A01).

NCEER-88-0010   "Base Isolation of a Multi-Story Building Under a Harmonic Ground Motion - A Comparison of Performances of Various Systems," by F-G Fan, G. Ahmadi and I.G. Tadjbakhsh, 5/18/88, (PB89-122238, A06, MF-A01). This report is only available through NTIS (see address given above).

NCEER-88-0011   "Seismic Floor Response Spectra for a Combined System by Green's Functions," by F.M. Lavelle, L.A. Bergman and P.D. Spanos, 5/1/88, (PB89-102875, A03, MF-A01).

NCEER-88-0012   "A New Solution Technique for Randomly Excited Hysteretic Structures," by G.Q. Cai and Y.K. Lin, 5/16/88, (PB89-102883, A03, MF-A01).

NCEER-88-0013   "A Study of Radiation Damping and Soil-Structure Interaction Effects in the Centrifuge," by K. Weissman, supervised by J.H. Prevost, 5/24/88, (PB89-144703, A06, MF-A01).

NCEER-88-0014   "Parameter Identification and Implementation of a Kinematic Plasticity Model for Frictional Soils," by J.H. Prevost and D.V. Griffiths, to be published.

NCEER-88-0015   "Two- and Three- Dimensional Dynamic Finite Element Analyses of the Long Valley Dam," by D.V. Griffiths and J.H. Prevost, 6/17/88, (PB89-144711, A04, MF-A01).

NCEER-88-0016   "Damage Assessment of Reinforced Concrete Structures in Eastern United States," by A.M. Reinhorn, M.J. Seidel, S.K. Kunnath and Y.J. Park, 6/15/88, (PB89-122220, A04, MF-A01). This report is only available through NTIS (see address given above).

NCEER-88-0017   "Dynamic Compliance of Vertically Loaded Strip Foundations in Multilayered Viscoelastic Soils," by S. Ahmad and A.S.M. Israil, 6/17/88, (PB89-102891, A04, MF-A01).

NCEER-88-0018   "An Experimental Study of Seismic Structural Response With Added Viscoelastic Dampers," by R.C. Lin, Z. Liang, T.T. Soong and R.H. Zhang, 6/30/88, (PB89-122212, A05, MF-A01). This report is available only through NTIS (see address given above).

NCEER-88-0019   "Experimental Investigation of Primary - Secondary System Interaction," by G.D. Manolis, G. Juhn and A.M. Reinhorn, 5/27/88, (PB89-122204, A04, MF-A01).

NCEER-88-0020   "A Response Spectrum Approach For Analysis of Nonclassically Damped Structures," by J.N. Yang, S. Sarkani and F.X. Long, 4/22/88, (PB89-102909, A04, MF-A01).

NCEER-88-0021   "Seismic Interaction of Structures and Soils: Stochastic Approach," by A.S. Veletsos and A.M. Prasad, 7/21/88, (PB89-122196, A04, MF-A01). This report is only available through NTIS (see address given above).

NCEER-88-0022   "Identification of the Serviceability Limit State and Detection of Seismic Structural Damage," by E. DiPasquale and A.S. Cakmak, 6/15/88, (PB89-122188, A05, MF-A01). This report is available only through NTIS (see address given above).

NCEER-88-0023   "Multi-Hazard Risk Analysis: Case of a Simple Offshore Structure," by B.K. Bhartia and E.H. Vanmarcke, 7/21/88, (PB89-145213, A05, MF-A01).

NCEER-88-0024   "Automated Seismic Design of Reinforced Concrete Buildings," by Y.S. Chung, C. Meyer and M. Shinozuka, 7/5/88, (PB89-122170, A06, MF-A01). This report is available only through NTIS (see address given above).

NCEER-88-0025   "Experimental Study of Active Control of MDOF Structures Under Seismic Excitations," by L.L. Chung, R.C. Lin, T.T. Soong and A.M. Reinhorn, 7/10/88, (PB89-122600, A04, MF-A01).

NCEER-88-0026   "Earthquake Simulation Tests of a Low-Rise Metal Structure," by J.S. Hwang, K.C. Chang, G.C. Lee and R.L. Ketter, 8/1/88, (PB89-102917, A04, MF-A01).

NCEER-88-0027   "Systems Study of Urban Response and Reconstruction Due to Catastrophic Earthquakes," by F. Kozin and H.K. Zhou, 9/22/88, (PB90-162348, A04, MF-A01).

NCEER-88-0028   "Seismic Fragility Analysis of Plane Frame Structures," by H.H-M. Hwang and Y.K. Low, 7/31/88, (PB89-131445, A06, MF-A01).

NCEER-88-0029   "Response Analysis of Stochastic Structures," by A. Kardara, C. Bucher and M. Shinozuka, 9/22/88, (PB89-174429, A04, MF-A01).

NCEER-88-0030   "Nonnormal Accelerations Due to Yielding in a Primary Structure," by D.C.K. Chen and L.D. Lutes, 9/19/88, (PB89-131437, A04, MF-A01).

NCEER-88-0031   "Design Approaches for Soil-Structure Interaction," by A.S. Veletsos, A.M. Prasad and Y. Tang, 12/30/88, (PB89-174437, A03, MF-A01). This report is available only through NTIS (see address given above).

NCEER-88-0032   "A Re-evaluation of Design Spectra for Seismic Damage Control," by C.J. Turkstra and A.G. Tallin, 11/7/88, (PB89-145221, A05, MF-A01).

NCEER-88-0033   "The Behavior and Design of Noncontact Lap Splices Subjected to Repeated Inelastic Tensile Loading," by V.E. Sagan, P. Gergely and R.N. White, 12/8/88, (PB89-163737, A08, MF-A01).

NCEER-88-0034   "Seismic Response of Pile Foundations," by S.M. Mamoon, P.K. Banerjee and S. Ahmad, 11/1/88, (PB89-145239, A04, MF-A01).

NCEER-88-0035   "Modeling of R/C Building Structures With Flexible Floor Diaphragms (IDARC2)," by A.M. Reinhorn, S.K. Kunnath and N. Panahshahi, 9/7/88, (PB89-207153, A07, MF-A01).

NCEER-88-0036   "Solution of the Dam-Reservoir Interaction Problem Using a Combination of FEM, BEM with Particular Integrals, Modal Analysis, and Substructuring," by C-S. Tsai, G.C. Lee and R.L. Ketter, 12/31/88, (PB89-207146, A04, MF-A01).

NCEER-88-0037   "Optimal Placement of Actuators for Structural Control," by F.Y. Cheng and C.P. Pantelides, 8/15/88, (PB89-162846, A05, MF-A01).

NCEER-88-0038   "Teflon Bearings in Aseismic Base Isolation: Experimental Studies and Mathematical Modeling," by A. Mokha, M.C. Constantinou and A.M. Reinhorn, 12/5/88, (PB89-218457, A10, MF-A01). This report is available only through NTIS (see address given above).

NCEER-88-0039   "Seismic Behavior of Flat Slab High-Rise Buildings in the New York City Area," by P. Weidlinger and M. Ettouney, 10/15/88, (PB90-145681, A04, MF-A01).

NCEER-88-0040   "Evaluation of the Earthquake Resistance of Existing Buildings in New York City," by P. Weidlinger and M. Ettouney, 10/15/88, to be published.

NCEER-88-0041   "Small-Scale Modeling Techniques for Reinforced Concrete Structures Subjected to Seismic Loads," by W. Kim, A. El-Attar and R.N. White, 11/22/88, (PB89-189625, A05, MF-A01).

NCEER-88-0042   "Modeling Strong Ground Motion from Multiple Event Earthquakes," by G.W. Ellis and A.S. Cakmak, 10/15/88, (PB89-174445, A03, MF-A01).

NCEER-88-0043   "Nonstationary Models of Seismic Ground Acceleration," by M. Grigoriu, S.E. Ruiz and E. Rosenblueth, 7/15/88, (PB89-189617, A04, MF-A01).

NCEER-88-0044   "SARCF User's Guide: Seismic Analysis of Reinforced Concrete Frames," by Y.S. Chung, C. Meyer and M. Shinozuka, 11/9/88, (PB89-174452, A08, MF-A01).

NCEER-88-0045   "First Expert Panel Meeting on Disaster Research and Planning," edited by J. Pantelic and J. Stoyle, 9/15/88, (PB89-174460, A05, MF-A01).

NCEER-88-0046   "Preliminary Studies of the Effect of Degrading Infill Walls on the Nonlinear Seismic Response of Steel Frames," by C.Z. Chrysostomou, P. Gergely and J.F. Abel, 12/19/88, (PB89-208383, A05, MF-A01).

NCEER-88-0047   "Reinforced Concrete Frame Component Testing Facility - Design, Construction, Instrumentation and Operation," by S.P. Pessiki, C. Conley, T. Bond, P. Gergely and R.N. White, 12/16/88, (PB89-174478, A04, MF-A01).

NCEER-89-0001   "Effects of Protective Cushion and Soil Compliancy on the Response of Equipment Within a Seismically Excited Building," by J.A. HoLung, 2/16/89, (PB89-207179, A04, MF-A01).

NCEER-89-0002   "Statistical Evaluation of Response Modification Factors for Reinforced Concrete Structures," by H.H-M. Hwang and J-W. Jaw, 2/17/89, (PB89-207187, A05, MF-A01).

NCEER-89-0003   "Hysteretic Columns Under Random Excitation," by G-Q. Cai and Y.K. Lin, 1/9/89, (PB89-196513, A03, MF-A01).

NCEER-89-0004   "Experimental Study of `Elephant Foot Bulge' Instability of Thin-Walled Metal Tanks," by Z-H. Jia and R.L. Ketter, 2/22/89, (PB89-207195, A03, MF-A01).

NCEER-89-0005   "Experiment on Performance of Buried Pipelines Across San Andreas Fault," by J. Isenberg, E. Richardson and T.D. O'Rourke, 3/10/89, (PB89-218440, A04, MF-A01). This report is available only through NTIS (see address given above).

NCEER-89-0006   "A Knowledge-Based Approach to Structural Design of Earthquake-Resistant Buildings," by M. Subramani, P. Gergely, C.H. Conley, J.F. Abel and A.H. Zaghw, 1/15/89, (PB89-218465, A06, MF-A01).

NCEER-89-0007   "Liquefaction Hazards and Their Effects on Buried Pipelines," by T.D. O'Rourke and P.A. Lane, 2/1/89, (PB89-218481, A09, MF-A01).

NCEER-89-0008   "Fundamentals of System Identification in Structural Dynamics," by H. Imai, C-B. Yun, O. Maruyama and M. Shinozuka, 1/26/89, (PB89-207211, A04, MF-A01).

NCEER-89-0009   "Effects of the 1985 Michoacan Earthquake on Water Systems and Other Buried Lifelines in Mexico," by A.G. Ayala and M.J. O'Rourke, 3/8/89, (PB89-207229, A06, MF-A01).

NCEER-89-R010   "NCEER Bibliography of Earthquake Education Materials," by K.E.K. Ross, Second Revision, 9/1/89, (PB90-125352, A05, MF-A01). This report is replaced by NCEER-92-0018.

NCEER-89-0011   "Inelastic Three-Dimensional Response Analysis of Reinforced Concrete Building Structures (IDARC-3D), Part I - Modeling," by S.K. Kunnath and A.M. Reinhorn, 4/17/89, (PB90-114612, A07, MF-A01). This report is available only through NTIS (see address given above).

NCEER-89-0012   "Recommended Modifications to ATC-14," by C.D. Poland and J.O. Malley, 4/12/89, (PB90-108648, A15, MF-A01).

NCEER-89-0013   "Repair and Strengthening of Beam-to-Column Connections Subjected to Earthquake Loading," by M. Corazao and A.J. Durrani, 2/28/89, (PB90-109885, A06, MF-A01).

NCEER-89-0014   "Program EXKAL2 for Identification of Structural Dynamic Systems," by O. Maruyama, C-B. Yun, M. Hoshiya and M. Shinozuka, 5/19/89, (PB90-109877, A09, MF-A01).

NCEER-89-0015   "Response of Frames With Bolted Semi-Rigid Connections, Part I - Experimental Study and Analytical Predictions," by P.J. DiCorso, A.M. Reinhorn, J.R. Dickerson, J.B. Radziminski and W.L. Harper, 6/1/89, to be published.

NCEER-89-0016   "ARMA Monte Carlo Simulation in Probabilistic Structural Analysis," by P.D. Spanos and M.P. Mignolet, 7/10/89, (PB90-109893, A03, MF-A01).

NCEER-89-P017   "Preliminary Proceedings from the Conference on Disaster Preparedness - The Place of Earthquake Education in Our Schools," Edited by K.E.K. Ross, 6/23/89, (PB90-108606, A03, MF-A01).

NCEER-89-0017   "Proceedings from the Conference on Disaster Preparedness - The Place of Earthquake Education in Our Schools," Edited by K.E.K. Ross, 12/31/89, (PB90-207895, A012, MF-A02). This report is available only through NTIS (see address given above).

NCEER-89-0018   "Multidimensional Models of Hysteretic Material Behavior for Vibration Analysis of Shape Memory Energy Absorbing Devices, by E.J. Graesser and F.A. Cozzarelli, 6/7/89, (PB90-164146, A04, MF-A01).

NCEER-89-0019   "Nonlinear Dynamic Analysis of Three-Dimensional Base Isolated Structures (3D-BASIS)," by S. Nagarajaiah, A.M. Reinhorn and M.C. Constantinou, 8/3/89, (PB90-161936, A06, MF-A01). This report has been replaced by NCEER-93-0011.

NCEER-89-0020   "Structural Control Considering Time-Rate of Control Forces and Control Rate Constraints," by F.Y. Cheng and C.P. Pantelides, 8/3/89, (PB90-120445, A04, MF-A01).

NCEER-89-0021   "Subsurface Conditions of Memphis and Shelby County," by K.W. Ng, T-S. Chang and H-H.M. Hwang, 7/26/89, (PB90-120437, A03, MF-A01).

NCEER-89-0022   "Seismic Wave Propagation Effects on Straight Jointed Buried Pipelines," by K. Elhmadi and M.J. O'Rourke, 8/24/89, (PB90-162322, A10, MF-A02).

NCEER-89-0023   "Workshop on Serviceability Analysis of Water Delivery Systems," edited by M. Grigoriu, 3/6/89, (PB90-127424, A03, MF-A01).

NCEER-89-0024   "Shaking Table Study of a 1/5 Scale Steel Frame Composed of Tapered Members," by K.C. Chang, J.S. Hwang and G.C. Lee, 9/18/89, (PB90-160169, A04, MF-A01).

NCEER-89-0025   "DYNA1D: A Computer Program for Nonlinear Seismic Site Response Analysis - Technical Documentation," by Jean H. Prevost, 9/14/89, (PB90-161944, A07, MF-A01). This report is available only through NTIS (see address given above).

NCEER-89-0026   "1:4 Scale Model Studies of Active Tendon Systems and Active Mass Dampers for Aseismic Protection," by A.M. Reinhorn, T.T. Soong, R.C. Lin, Y.P. Yang, Y. Fukao, H. Abe and M. Nakai, 9/15/89, (PB90-173246, A10, MF-A02). This report is available only through NTIS (see address given above).

NCEER-89-0027   "Scattering of Waves by Inclusions in a Nonhomogeneous Elastic Half Space Solved by Boundary Element Methods," by P.K. Hadley, A. Askar and A.S. Cakmak, 6/15/89, (PB90-145699, A07, MF-A01).

NCEER-89-0028   "Statistical Evaluation of Deflection Amplification Factors for Reinforced Concrete Structures," by H.H.M. Hwang, J-W. Jaw and A.L. Ch'ng, 8/31/89, (PB90-164633, A05, MF-A01).

NCEER-89-0029   "Bedrock Accelerations in Memphis Area Due to Large New Madrid Earthquakes," by H.H.M. Hwang, C.H.S. Chen and G. Yu, 11/7/89, (PB90-162330, A04, MF-A01).

NCEER-89-0030   "Seismic Behavior and Response Sensitivity of Secondary Structural Systems," by Y.Q. Chen and T.T. Soong, 10/23/89, (PB90-164658, A08, MF-A01).

NCEER-89-0031   "Random Vibration and Reliability Analysis of Primary-Secondary Structural Systems," by Y. Ibrahim, M. Grigoriu and T.T. Soong, 11/10/89, (PB90-161951, A04, MF-A01).

NCEER-89-0032   "Proceedings from the Second U.S. - Japan Workshop on Liquefaction, Large Ground Deformation and Their Effects on Lifelines, September 26-29, 1989," Edited by T.D. O'Rourke and M. Hamada, 12/1/89, (PB90-209388, A22, MF-A03).

NCEER-89-0033   "Deterministic Model for Seismic Damage Evaluation of Reinforced Concrete Structures," by J.M. Bracci, A.M. Reinhorn, J.B. Mander and S.K. Kunnath, 9/27/89, (PB91-108803, A06, MF-A01).

NCEER-89-0034   "On the Relation Between Local and Global Damage Indices," by E. DiPasquale and A.S. Cakmak, 8/15/89, (PB90-173865, A05, MF-A01).

NCEER-89-0035   "Cyclic Undrained Behavior of Nonplastic and Low Plasticity Silts," by A.J. Walker and H.E. Stewart, 7/26/89, (PB90-183518, A10, MF-A01).

NCEER-89-0036   "Liquefaction Potential of Surficial Deposits in the City of Buffalo, New York," by M. Budhu, R. Giese and L. Baumgrass, 1/17/89, (PB90-208455, A04, MF-A01).

NCEER-89-0037   "A Deterministic Assessment of Effects of Ground Motion Incoherence," by A.S. Veletsos and Y. Tang, 7/15/89, (PB90-164294, A03, MF-A01).

NCEER-89-0038   "Workshop on Ground Motion Parameters for Seismic Hazard Mapping," July 17-18, 1989, edited by R.V. Whitman, 12/1/89, (PB90-173923, A04, MF-A01).

NCEER-89-0039   "Seismic Effects on Elevated Transit Lines of the New York City Transit Authority," by C.J. Costantino, C.A. Miller and E. Heymsfield, 12/26/89, (PB90-207887, A06, MF-A01).

NCEER-89-0040   "Centrifugal Modeling of Dynamic Soil-Structure Interaction," by K. Weissman, Supervised by J.H. Prevost, 5/10/89, (PB90-207879, A07, MF-A01).

NCEER-89-0041   "Linearized Identification of Buildings With Cores for Seismic Vulnerability Assessment," by I-K. Ho and A.E. Aktan, 11/1/89, (PB90-251943, A07, MF-A01).

NCEER-90-0001   "Geotechnical and Lifeline Aspects of the October 17, 1989 Loma Prieta Earthquake in San Francisco," by T.D. O'Rourke, H.E. Stewart, F.T. Blackburn and T.S. Dickerman, 1/90, (PB90-208596, A05, MF-A01).

NCEER-90-0002   "Nonnormal Secondary Response Due to Yielding in a Primary Structure," by D.C.K. Chen and L.D. Lutes, 2/28/90, (PB90-251976, A07, MF-A01).

NCEER-90-0003   "Earthquake Education Materials for Grades K-12," by K.E.K. Ross, 4/16/90, (PB91-251984, A05, MF-A05). This report has been replaced by NCEER-92-0018.

NCEER-90-0004   "Catalog of Strong Motion Stations in Eastern North America," by R.W. Busby, 4/3/90, (PB90-251984, A05, MF-A01).

NCEER-90-0005   "NCEER Strong-Motion Data Base: A User Manual for the GeoBase Release (Version 1.0 for the Sun3)," by P. Friberg and K. Jacob, 3/31/90 (PB90-258062, A04, MF-A01).

NCEER-90-0006   "Seismic Hazard Along a Crude Oil Pipeline in the Event of an 1811-1812 Type New Madrid Earthquake," by H.H.M. Hwang and C-H.S. Chen, 4/16/90, (PB90-258054, A04, MF-A01).

NCEER-90-0007   "Site-Specific Response Spectra for Memphis Sheahan Pumping Station," by H.H.M. Hwang and C.S. Lee, 5/15/90, (PB91-108811, A05, MF-A01).

NCEER-90-0008   "Pilot Study on Seismic Vulnerability of Crude Oil Transmission Systems," by T. Ariman, R. Dobry, M. Grigoriu, F. Kozin, M. O'Rourke, T. O'Rourke and M. Shinozuka, 5/25/90, (PB91-108837, A06, MF-A01).

NCEER-90-0009   "A Program to Generate Site Dependent Time Histories: EQGEN," by G.W. Ellis, M. Srinivasan and A.S. Cakmak, 1/30/90, (PB91-108829, A04, MF-A01).

NCEER-90-0010   "Active Isolation for Seismic Protection of Operating Rooms," by M.E. Talbott, Supervised by M. Shinozuka, 6/8/9, (PB91-110205, A05, MF-A01).

NCEER-90-0011   "Program LINEARID for Identification of Linear Structural Dynamic Systems," by C-B. Yun and M. Shinozuka, 6/25/90, (PB91-110312, A08, MF-A01).

NCEER-90-0012   "Two-Dimensional Two-Phase Elasto-Plastic Seismic Response of Earth Dams," by A.N. Yiagos, Supervised by J.H. Prevost, 6/20/90, (PB91-110197, A13, MF-A02).

NCEER-90-0013   "Secondary Systems in Base-Isolated Structures: Experimental Investigation, Stochastic Response and Stochastic Sensitivity," by G.D. Manolis, G. Juhn, M.C. Constantinou and A.M. Reinhorn, 7/1/90, (PB91-110320, A08, MF-A01).

NCEER-90-0014   "Seismic Behavior of Lightly-Reinforced Concrete Column and Beam-Column Joint Details," by S.P. Pessiki, C.H. Conley, P. Gergely and R.N. White, 8/22/90, (PB91-108795, A11, MF-A02).

NCEER-90-0015   "Two Hybrid Control Systems for Building Structures Under Strong Earthquakes," by J.N. Yang and A. Danielians, 6/29/90, (PB91-125393, A04, MF-A01).

NCEER-90-0016   "Instantaneous Optimal Control with Acceleration and Velocity Feedback," by J.N. Yang and Z. Li, 6/29/90, (PB91-125401, A03, MF-A01).

NCEER-90-0017   "Reconnaissance Report on the Northern Iran Earthquake of June 21, 1990," by M. Mehrain, 10/4/90, (PB91-125377, A03, MF-A01).

NCEER-90-0018   "Evaluation of Liquefaction Potential in Memphis and Shelby County," by T.S. Chang, P.S. Tang, C.S. Lee and H. Hwang, 8/10/90, (PB91-125427, A09, MF-A01).

NCEER-90-0019   "Experimental and Analytical Study of a Combined Sliding Disc Bearing and Helical Steel Spring Isolation System," by M.C. Constantinou, A.S. Mokha and A.M. Reinhorn, 10/4/90, (PB91-125385, A06, MF-A01). This report is available only through NTIS (see address given above).

NCEER-90-0020   "Experimental Study and Analytical Prediction of Earthquake Response of a Sliding Isolation System with a Spherical Surface," by A.S. Mokha, M.C. Constantinou and A.M. Reinhorn, 10/11/90, (PB91-125419, A05, MF-A01).

NCEER-90-0021   "Dynamic Interaction Factors for Floating Pile Groups," by G. Gazetas, K. Fan, A. Kaynia and E. Kausel, 9/10/90, (PB91-170381, A05, MF-A01).

NCEER-90-0022   "Evaluation of Seismic Damage Indices for Reinforced Concrete Structures," by S. Rodriguez-Gomez and A.S. Cakmak, 9/30/90, PB91-171322, A06, MF-A01).

NCEER-90-0023   "Study of Site Response at a Selected Memphis Site," by H. Desai, S. Ahmad, E.S. Gazetas and M.R. Oh, 10/11/90, (PB91-196857, A03, MF-A01).

NCEER-90-0024   "A User's Guide to Strongmo: Version 1.0 of NCEER's Strong-Motion Data Access Tool for PCs and Terminals," by P.A. Friberg and C.A.T. Susch, 11/15/90, (PB91-171272, A03, MF-A01).

NCEER-90-0025   "A Three-Dimensional Analytical Study of Spatial Variability of Seismic Ground Motions," by L-L. Hong and A.H.-S. Ang, 10/30/90, (PB91-170399, A09, MF-A01).

NCEER-90-0026   "MUMOID User's Guide - A Program for the Identification of Modal Parameters," by S. Rodriguez-Gomez and E. DiPasquale, 9/30/90, (PB91-171298, A04, MF-A01).

NCEER-90-0027   "SARCF-II User's Guide - Seismic Analysis of Reinforced Concrete Frames," by S. Rodriguez-Gomez, Y.S. Chung and C. Meyer, 9/30/90, (PB91-171280, A05, MF-A01).

NCEER-90-0028   "Viscous Dampers: Testing, Modeling and Application in Vibration and Seismic Isolation," by N. Makris and M.C. Constantinou, 12/20/90 (PB91-190561, A06, MF-A01).

NCEER-90-0029   "Soil Effects on Earthquake Ground Motions in the Memphis Area," by H. Hwang, C.S. Lee, K.W. Ng and T.S. Chang, 8/2/90, (PB91-190751, A05, MF-A01).

NCEER-91-0001 "Proceedings from the Third Japan-U.S. Workshop on Earthquake Resistant Design of Lifeline Facilities and Countermeasures for Soil Liquefaction, December 17-19, 1990," edited by T.D. O'Rourke and M. Hamada, 2/1/91, (PB91-179259, A99, MF-A04).

NCEER-91-0002 "Physical Space Solutions of Non-Proportionally Damped Systems," by M. Tong, Z. Liang and G.C. Lee, 1/15/91, (PB91-179242, A04, MF-A01).

NCEER-91-0003 "Seismic Response of Single Piles and Pile Groups," by K. Fan and G. Gazetas, 1/10/91, (PB92-174994, A04, MF-A01).

NCEER-91-0004 "Damping of Structures: Part 1 - Theory of Complex Damping," by Z. Liang and G. Lee, 10/10/91, (PB92-197235, A12, MF-A03).

NCEER-91-0005 "3D-BASIS - Nonlinear Dynamic Analysis of Three Dimensional Base Isolated Structures: Part II," by S. Nagarajaiah, A.M. Reinhorn and M.C. Constantinou, 2/28/91, (PB91-190553, A07, MF-A01). This report has been replaced by NCEER-93-0011.

NCEER-91-0006 "A Multidimensional Hysteretic Model for Plasticity Deforming Metals in Energy Absorbing Devices," by E.J. Graesser and F.A. Cozzarelli, 4/9/91, (PB92-108364, A04, MF-A01).

NCEER-91-0007 "A Framework for Customizable Knowledge-Based Expert Systems with an Application to a KBES for Evaluating the Seismic Resistance of Existing Buildings," by E.G. Ibarra-Anaya and S.J. Fenves, 4/9/91, (PB91-210930, A08, MF-A01).

NCEER-91-0008 "Nonlinear Analysis of Steel Frames with Semi-Rigid Connections Using the Capacity Spectrum Method," by G.G. Deierlein, S-H. Hsieh, Y-J. Shen and J.F. Abel, 7/2/91, (PB92-113828, A05, MF-A01).

NCEER-91-0009 "Earthquake Education Materials for Grades K-12," by K.E.K. Ross, 4/30/91, (PB91-212142, A06, MF-A01). This report has been replaced by NCEER-92-0018.

NCEER-91-0010 "Phase Wave Velocities and Displacement Phase Differences in a Harmonically Oscillating Pile," by N. Makris and G. Gazetas, 7/8/91, (PB92-108356, A04, MF-A01).

NCEER-91-0011 "Dynamic Characteristics of a Full-Size Five-Story Steel Structure and a 2/5 Scale Model," by K.C. Chang, G.C. Yao, G.C. Lee, D.S. Hao and Y.C. Yeh," 7/2/91, (PB93-116648, A06, MF-A02).

NCEER-91-0012 "Seismic Response of a 2/5 Scale Steel Structure with Added Viscoelastic Dampers," by K.C. Chang, T.T. Soong, S-T. Oh and M.L. Lai, 5/17/91, (PB92-110816, A05, MF-A01).

NCEER-91-0013 "Earthquake Response of Retaining Walls; Full-Scale Testing and Computational Modeling," by S. Alampalli and A-W.M. Elgamal, 6/20/91, to be published.

NCEER-91-0014 "3D-BASIS-M: Nonlinear Dynamic Analysis of Multiple Building Base Isolated Structures," by P.C. Tsopelas, S. Nagarajaiah, M.C. Constantinou and A.M. Reinhorn, 5/28/91, (PB92-113885, A09, MF-A02).

NCEER-91-0015 "Evaluation of SEAOC Design Requirements for Sliding Isolated Structures," by D. Theodossiou and M.C. Constantinou, 6/10/91, (PB92-114602, A11, MF-A03).

NCEER-91-0016 "Closed-Loop Modal Testing of a 27-Story Reinforced Concrete Flat Plate-Core Building," by H.R. Somaprasad, T. Toksoy, H. Yoshiyuki and A.E. Aktan, 7/15/91, (PB92-129980, A07, MF-A02).

NCEER-91-0017 "Shake Table Test of a 1/6 Scale Two-Story Lightly Reinforced Concrete Building," by A.G. El-Attar, R.N. White and P. Gergely, 2/28/91, (PB92-222447, A06, MF-A02).

NCEER-91-0018 "Shake Table Test of a 1/8 Scale Three-Story Lightly Reinforced Concrete Building," by A.G. El-Attar, R.N. White and P. Gergely, 2/28/91, (PB93-116630, A08, MF-A02).

NCEER-91-0019 "Transfer Functions for Rigid Rectangular Foundations," by A.S. Veletsos, A.M. Prasad and W.H. Wu, 7/31/91, to be published.

NCEER-91-0020   "Hybrid Control of Seismic-Excited Nonlinear and Inelastic Structural Systems," by J.N. Yang, Z. Li and A. Danielians, 8/1/91, (PB92-143171, A06, MF-A02).

NCEER-91-0021   "The NCEER-91 Earthquake Catalog: Improved Intensity-Based Magnitudes and Recurrence Relations for U.S. Earthquakes East of New Madrid," by L. Seeber and J.G. Armbruster, 8/28/91, (PB92-176742, A06, MF-A02).

NCEER-91-0022   "Proceedings from the Implementation of Earthquake Planning and Education in Schools: The Need for Change - The Roles of the Changemakers," by K.E.K. Ross and F. Winslow, 7/23/91, (PB92-129998, A12, MF-A03).

NCEER-91-0023   "A Study of Reliability-Based Criteria for Seismic Design of Reinforced Concrete Frame Buildings," by H.H.M. Hwang and H-M. Hsu, 8/10/91, (PB92-140235, A09, MF-A02).

NCEER-91-0024   "Experimental Verification of a Number of Structural System Identification Algorithms," by R.G. Ghanem, H. Gavin and M. Shinozuka, 9/18/91, (PB92-176577, A18, MF-A04).

NCEER-91-0025   "Probabilistic Evaluation of Liquefaction Potential," by H.H.M. Hwang and C.S. Lee," 11/25/91, (PB92-143429, A05, MF-A01).

NCEER-91-0026   "Instantaneous Optimal Control for Linear, Nonlinear and Hysteretic Structures - Stable Controllers," by J.N. Yang and Z. Li, 11/15/91, (PB92-163807, A04, MF-A01).

NCEER-91-0027   "Experimental and Theoretical Study of a Sliding Isolation System for Bridges," by M.C. Constantinou, A. Kartoum, A.M. Reinhorn and P. Bradford, 11/15/91, (PB92-176973, A10, MF-A03).

NCEER-92-0001   "Case Studies of Liquefaction and Lifeline Performance During Past Earthquakes, Volume 1: Japanese Case Studies," Edited by M. Hamada and T. O'Rourke, 2/17/92, (PB92-197243, A18, MF-A04).

NCEER-92-0002   "Case Studies of Liquefaction and Lifeline Performance During Past Earthquakes, Volume 2: United States Case Studies," Edited by T. O'Rourke and M. Hamada, 2/17/92, (PB92-197250, A20, MF-A04).

NCEER-92-0003   "Issues in Earthquake Education," Edited by K. Ross, 2/3/92, (PB92-222389, A07, MF-A02).

NCEER-92-0004   "Proceedings from the First U.S. - Japan Workshop on Earthquake Protective Systems for Bridges," Edited by I.G. Buckle, 2/4/92, (PB94-142239, A99, MF-A06).

NCEER-92-0005   "Seismic Ground Motion from a Haskell-Type Source in a Multiple-Layered Half-Space," A.P. Theoharis, G. Deodatis and M. Shinozuka, 1/2/92, to be published.

NCEER-92-0006   "Proceedings from the Site Effects Workshop," Edited by R. Whitman, 2/29/92, (PB92-197201, A04, MF-A01).

NCEER-92-0007   "Engineering Evaluation of Permanent Ground Deformations Due to Seismically-Induced Liquefaction," by M.H. Baziar, R. Dobry and A-W.M. Elgamal, 3/24/92, (PB92-222421, A13, MF-A03).

NCEER-92-0008   "A Procedure for the Seismic Evaluation of Buildings in the Central and Eastern United States," by C.D. Poland and J.O. Malley, 4/2/92, (PB92-222439, A20, MF-A04).

NCEER-92-0009   "Experimental and Analytical Study of a Hybrid Isolation System Using Friction Controllable Sliding Bearings," by M.Q. Feng, S. Fujii and M. Shinozuka, 5/15/92, (PB93-150282, A06, MF-A02).

NCEER-92-0010   "Seismic Resistance of Slab-Column Connections in Existing Non-Ductile Flat-Plate Buildings," by A.J. Durrani and Y. Du, 5/18/92, (PB93-116812, A06, MF-A02).

NCEER-92-0011   "The Hysteretic and Dynamic Behavior of Brick Masonry Walls Upgraded by Ferrocement Coatings Under Cyclic Loading and Strong Simulated Ground Motion," by H. Lee and S.P. Prawel, 5/11/92, to be published.

NCEER-92-0012   "Study of Wire Rope Systems for Seismic Protection of Equipment in Buildings," by G.F. Demetriades, M.C. Constantinou and A.M. Reinhorn, 5/20/92, (PB93-116655, A08, MF-A02).

NCEER-92-0013   "Shape Memory Structural Dampers: Material Properties, Design and Seismic Testing," by P.R. Witting and F.A. Cozzarelli, 5/26/92, (PB93-116663, A05, MF-A01).

NCEER-92-0014   "Longitudinal Permanent Ground Deformation Effects on Buried Continuous Pipelines," by M.J. O'Rourke, and C. Nordberg, 6/15/92, (PB93-116671, A08, MF-A02).

NCEER-92-0015   "A Simulation Method for Stationary Gaussian Random Functions Based on the Sampling Theorem," by M. Grigoriu and S. Balopoulou, 6/11/92, (PB93-127496, A05, MF-A01).

NCEER-92-0016   "Gravity-Load-Designed Reinforced Concrete Buildings: Seismic Evaluation of Existing Construction and Detailing Strategies for Improved Seismic Resistance," by G.W. Hoffmann, S.K. Kunnath, A.M. Reinhorn and J.B. Mander, 7/15/92, (PB94-142007, A08, MF-A02).

NCEER-92-0017   "Observations on Water System and Pipeline Performance in the Limón Area of Costa Rica Due to the April 22, 1991 Earthquake," by M. O'Rourke and D. Ballantyne, 6/30/92, (PB93-126811, A06, MF-A02).

NCEER-92-0018   "Fourth Edition of Earthquake Education Materials for Grades K-12," Edited by K.E.K. Ross, 8/10/92, (PB93-114023, A07, MF-A02).

NCEER-92-0019   "Proceedings from the Fourth Japan-U.S. Workshop on Earthquake Resistant Design of Lifeline Facilities and Countermeasures for Soil Liquefaction," Edited by M. Hamada and T.D. O'Rourke, 8/12/92, (PB93-163939, A99, MF-E11).

NCEER-92-0020   "Active Bracing System: A Full Scale Implementation of Active Control," by A.M. Reinhorn, T.T. Soong, R.C. Lin, M.A. Riley, Y.P. Wang, S. Aizawa and M. Higashino, 8/14/92, (PB93-127512, A06, MF-A02).

NCEER-92-0021   "Empirical Analysis of Horizontal Ground Displacement Generated by Liquefaction-Induced Lateral Spreads," by S.F. Bartlett and T.L. Youd, 8/17/92, (PB93-188241, A06, MF-A02).

NCEER-92-0022   "IDARC Version 3.0: Inelastic Damage Analysis of Reinforced Concrete Structures," by S.K. Kunnath, A.M. Reinhorn and R.F. Lobo, 8/31/92, (PB93-227502, A07, MF-A02).

NCEER-92-0023   "A Semi-Empirical Analysis of Strong-Motion Peaks in Terms of Seismic Source, Propagation Path and Local Site Conditions, by M. Kamiyama, M.J. O'Rourke and R. Flores-Berrones, 9/9/92, (PB93-150266, A08, MF-A02).

NCEER-92-0024   "Seismic Behavior of Reinforced Concrete Frame Structures with Nonductile Details, Part I: Summary of Experimental Findings of Full Scale Beam-Column Joint Tests," by A. Beres, R.N. White and P. Gergely, 9/30/92, (PB93-227783, A05, MF-A01).

NCEER-92-0025   "Experimental Results of Repaired and Retrofitted Beam-Column Joint Tests in Lightly Reinforced Concrete Frame Buildings," by A. Beres, S. El-Borgi, R.N. White and P. Gergely, 10/29/92, (PB93-227791, A05, MF-A01).

NCEER-92-0026   "A Generalization of Optimal Control Theory: Linear and Nonlinear Structures," by J.N. Yang, Z. Li and S. Vongchavalitkul, 11/2/92, (PB93-188621, A05, MF-A01).

NCEER-92-0027   "Seismic Resistance of Reinforced Concrete Frame Structures Designed Only for Gravity Loads: Part I - Design and Properties of a One-Third Scale Model Structure," by J.M. Bracci, A.M. Reinhorn and J.B. Mander, 12/1/92, (PB94-104502, A08, MF-A02).

NCEER-92-0028   "Seismic Resistance of Reinforced Concrete Frame Structures Designed Only for Gravity Loads: Part II - Experimental Performance of Subassemblages," by L.E. Aycardi, J.B. Mander and A.M. Reinhorn, 12/1/92, (PB94-104510, A08, MF-A02).

NCEER-92-0029   "Seismic Resistance of Reinforced Concrete Frame Structures Designed Only for Gravity Loads: Part III - Experimental Performance and Analytical Study of a Structural Model," by J.M. Bracci, A.M. Reinhorn and J.B. Mander, 12/1/92, (PB93-227528, A09, MF-A01).

NCEER-92-0030 "Evaluation of Seismic Retrofit of Reinforced Concrete Frame Structures: Part I - Experimental Performance of Retrofitted Subassemblages," by D. Choudhuri, J.B. Mander and A.M. Reinhorn, 12/8/92, (PB93-198307, A07, MF-A02).

NCEER-92-0031 "Evaluation of Seismic Retrofit of Reinforced Concrete Frame Structures: Part II - Experimental Performance and Analytical Study of a Retrofitted Structural Model," by J.M. Bracci, A.M. Reinhorn and J.B. Mander, 12/8/92, (PB93-198315, A09, MF-A03).

NCEER-92-0032 "Experimental and Analytical Investigation of Seismic Response of Structures with Supplemental Fluid Viscous Dampers," by M.C. Constantinou and M.D. Symans, 12/21/92, (PB93-191435, A10, MF-A03). This report is available only through NTIS (see address given above).

NCEER-92-0033 "Reconnaissance Report on the Cairo, Egypt Earthquake of October 12, 1992," by M. Khater, 12/23/92, (PB93-188621, A03, MF-A01).

NCEER-92-0034 "Low-Level Dynamic Characteristics of Four Tall Flat-Plate Buildings in New York City," by H. Gavin, S. Yuan, J. Grossman, E. Pekelis and K. Jacob, 12/28/92, (PB93-188217, A07, MF-A02).

NCEER-93-0001 "An Experimental Study on the Seismic Performance of Brick-Infilled Steel Frames With and Without Retrofit," by J.B. Mander, B. Nair, K. Wojtkowski and J. Ma, 1/29/93, (PB93-227510, A07, MF-A02).

NCEER-93-0002 "Social Accounting for Disaster Preparedness and Recovery Planning," by S. Cole, E. Pantoja and V. Razak, 2/22/93, (PB94-142114, A12, MF-A03).

NCEER-93-0003 "Assessment of 1991 NEHRP Provisions for Nonstructural Components and Recommended Revisions," by T.T. Soong, G. Chen, Z. Wu, R-H. Zhang and M. Grigoriu, 3/1/93, (PB93-188639, A06, MF-A02).

NCEER-93-0004 "Evaluation of Static and Response Spectrum Analysis Procedures of SEAOC/UBC for Seismic Isolated Structures," by C.W. Winters and M.C. Constantinou, 3/23/93, (PB93-198299, A10, MF-A03).

NCEER-93-0005 "Earthquakes in the Northeast - Are We Ignoring the Hazard? A Workshop on Earthquake Science and Safety for Educators," edited by K.E.K. Ross, 4/2/93, (PB94-103066, A09, MF-A02).

NCEER-93-0006 "Inelastic Response of Reinforced Concrete Structures with Viscoelastic Braces," by R.F. Lobo, J.M. Bracci, K.L. Shen, A.M. Reinhorn and T.T. Soong, 4/5/93, (PB93-227486, A05, MF-A02).

NCEER-93-0007 "Seismic Testing of Installation Methods for Computers and Data Processing Equipment," by K. Kosar, T.T. Soong, K.L. Shen, J.A. HoLung and Y.K. Lin, 4/12/93, (PB93-198299, A07, MF-A02).

NCEER-93-0008 "Retrofit of Reinforced Concrete Frames Using Added Dampers," by A. Reinhorn, M. Constantinou and C. Li, to be published.

NCEER-93-0009 "Seismic Behavior and Design Guidelines for Steel Frame Structures with Added Viscoelastic Dampers," by K.C. Chang, M.L. Lai, T.T. Soong, D.S. Hao and Y.C. Yeh, 5/1/93, (PB94-141959, A07, MF-A02).

NCEER-93-0010 "Seismic Performance of Shear-Critical Reinforced Concrete Bridge Piers," by J.B. Mander, S.M. Waheed, M.T.A. Chaudhary and S.S. Chen, 5/12/93, (PB93-227494, A08, MF-A02).

NCEER-93-0011 "3D-BASIS-TABS: Computer Program for Nonlinear Dynamic Analysis of Three Dimensional Base Isolated Structures," by S. Nagarajaiah, C. Li, A.M. Reinhorn and M.C. Constantinou, 8/2/93, (PB94-141819, A09, MF-A02).

NCEER-93-0012 "Effects of Hydrocarbon Spills from an Oil Pipeline Break on Ground Water," by O.J. Helweg and H.H.M. Hwang, 8/3/93, (PB94-141942, A06, MF-A02).

NCEER-93-0013 "Simplified Procedures for Seismic Design of Nonstructural Components and Assessment of Current Code Provisions," by M.P. Singh, L.E. Suarez, E.E. Matheu and G.O. Maldonado, 8/4/93, (PB94-141827, A09, MF-A02).

NCEER-93-0014 "An Energy Approach to Seismic Analysis and Design of Secondary Systems," by G. Chen and T.T. Soong, 8/6/93, (PB94-142767, A11, MF-A03).

NCEER-93-0015   "Proceedings from School Sites: Becoming Prepared for Earthquakes - Commemorating the Third Anniversary of the Loma Prieta Earthquake," Edited by F.E. Winslow and K.E.K. Ross, 8/16/93, (PB94-154275, A16, MF-A02).

NCEER-93-0016   "Reconnaissance Report of Damage to Historic Monuments in Cairo, Egypt Following the October 12, 1992 Dahshur Earthquake," by D. Sykora, D. Look, G. Croci, E. Karaesmen and E. Karaesmen, 8/19/93, (PB94-142221, A08, MF-A02).

NCEER-93-0017   "The Island of Guam Earthquake of August 8, 1993," by S.W. Swan and S.K. Harris, 9/30/93, (PB94-141843, A04, MF-A01).

NCEER-93-0018   "Engineering Aspects of the October 12, 1992 Egyptian Earthquake," by A.W. Elgamal, M. Amer, K. Adalier and A. Abul-Fadl, 10/7/93, (PB94-141983, A05, MF-A01).

NCEER-93-0019   "Development of an Earthquake Motion Simulator and its Application in Dynamic Centrifuge Testing," by I. Krstelj, Supervised by J.H. Prevost, 10/23/93, (PB94-181773, A-10, MF-A03).

NCEER-93-0020   "NCEER-Taisei Corporation Research Program on Sliding Seismic Isolation Systems for Bridges: Experimental and Analytical Study of a Friction Pendulum System (FPS)," by M.C. Constantinou, P. Tsopelas, Y-S. Kim and S. Okamoto, 11/1/93, (PB94-142775, A08, MF-A02).

NCEER-93-0021   "Finite Element Modeling of Elastomeric Seismic Isolation Bearings," by L.J. Billings, Supervised by R. Shepherd, 11/8/93, to be published.

NCEER-93-0022   "Seismic Vulnerability of Equipment in Critical Facilities: Life-Safety and Operational Consequences," by K. Porter, G.S. Johnson, M.M. Zadeh, C. Scawthorn and S. Eder, 11/24/93, (PB94-181765, A16, MF-A03).

NCEER-93-0023   "Hokkaido Nansei-oki, Japan Earthquake of July 12, 1993, by P.I. Yanev and C.R. Scawthorn, 12/23/93, (PB94-181500, A07, MF-A01).

NCEER-94-0001   "An Evaluation of Seismic Serviceability of Water Supply Networks with Application to the San Francisco Auxiliary Water Supply System," by I. Markov, Supervised by M. Grigoriu and T. O'Rourke, 1/21/94, (PB94-204013, A07, MF-A02).

NCEER-94-0002   "NCEER-Taisei Corporation Research Program on Sliding Seismic Isolation Systems for Bridges: Experimental and Analytical Study of Systems Consisting of Sliding Bearings, Rubber Restoring Force Devices and Fluid Dampers," Volumes I and II, by P. Tsopelas, S. Okamoto, M.C. Constantinou, D. Ozaki and S. Fujii, 2/4/94, (PB94-181740, A09, MF-A02 and PB94-181757, A12, MF-A03).

NCEER-94-0003   "A Markov Model for Local and Global Damage Indices in Seismic Analysis," by S. Rahman and M. Grigoriu, 2/18/94, (PB94-206000, A12, MF-A03).

NCEER-94-0004   "Proceedings from the NCEER Workshop on Seismic Response of Masonry Infills," edited by D.P. Abrams, 3/1/94, (PB94-180783, A07, MF-A02).

NCEER-94-0005   "The Northridge, California Earthquake of January 17, 1994: General Reconnaissance Report," edited by J.D. Goltz, 3/11/94, (PB94-193943, A10, MF-A03).

NCEER-94-0006   "Seismic Energy Based Fatigue Damage Analysis of Bridge Columns: Part I - Evaluation of Seismic Capacity," by G.A. Chang and J.B. Mander, 3/14/94, (PB94-219185, A11, MF-A03).

NCEER-94-0007   "Seismic Isolation of Multi-Story Frame Structures Using Spherical Sliding Isolation Systems," by T.M. Al-Hussaini, V.A. Zayas and M.C. Constantinou, 3/17/94, (PB94-193745, A09, MF-A02).

NCEER-94-0008   "The Northridge, California Earthquake of January 17, 1994: Performance of Highway Bridges," edited by I.G. Buckle, 3/24/94, (PB94-193851, A06, MF-A02).

NCEER-94-0009   "Proceedings of the Third U.S.-Japan Workshop on Earthquake Protective Systems for Bridges," edited by I.G. Buckle and I. Friedland, 3/31/94, (PB94-195815, A99, MF-A06).

NCEER-94-0010 "3D-BASIS-ME: Computer Program for Nonlinear Dynamic Analysis of Seismically Isolated Single and Multiple Structures and Liquid Storage Tanks," by P.C. Tsopelas, M.C. Constantinou and A.M. Reinhorn, 4/12/94, (PB94-204922, A09, MF-A02).

NCEER-94-0011 "The Northridge, California Earthquake of January 17, 1994: Performance of Gas Transmission Pipelines," by T.D. O'Rourke and M.C. Palmer, 5/16/94, (PB94-204989, A05, MF-A01).

NCEER-94-0012 "Feasibility Study of Replacement Procedures and Earthquake Performance Related to Gas Transmission Pipelines," by T.D. O'Rourke and M.C. Palmer, 5/25/94, (PB94-206638, A09, MF-A02).

NCEER-94-0013 "Seismic Energy Based Fatigue Damage Analysis of Bridge Columns: Part II - Evaluation of Seismic Demand," by G.A. Chang and J.B. Mander, 6/1/94, (PB95-18106, A08, MF-A02).

NCEER-94-0014 "NCEER-Taisei Corporation Research Program on Sliding Seismic Isolation Systems for Bridges: Experimental and Analytical Study of a System Consisting of Sliding Bearings and Fluid Restoring Force/Damping Devices," by P. Tsopelas and M.C. Constantinou, 6/13/94, (PB94-219144, A10, MF-A03).

NCEER-94-0015 "Generation of Hazard-Consistent Fragility Curves for Seismic Loss Estimation Studies," by H. Hwang and J-R. Huo, 6/14/94, (PB95-181996, A09, MF-A02).

NCEER-94-0016 "Seismic Study of Building Frames with Added Energy-Absorbing Devices," by W.S. Pong, C.S. Tsai and G.C. Lee, 6/20/94, (PB94-219136, A10, A03).

NCEER-94-0017 "Sliding Mode Control for Seismic-Excited Linear and Nonlinear Civil Engineering Structures," by J. Yang, J. Wu, A. Agrawal and Z. Li, 6/21/94, (PB95-138483, A06, MF-A02).

NCEER-94-0018 "3D-BASIS-TABS Version 2.0: Computer Program for Nonlinear Dynamic Analysis of Three Dimensional Base Isolated Structures," by A.M. Reinhorn, S. Nagarajaiah, M.C. Constantinou, P. Tsopelas and R. Li, 6/22/94, (PB95-182176, A08, MF-A02).

NCEER-94-0019 "Proceedings of the International Workshop on Civil Infrastructure Systems: Application of Intelligent Systems and Advanced Materials on Bridge Systems," Edited by G.C. Lee and K.C. Chang, 7/18/94, (PB95-252474, A20, MF-A04).

NCEER-94-0020 "Study of Seismic Isolation Systems for Computer Floors," by V. Lambrou and M.C. Constantinou, 7/19/94, (PB95-138533, A10, MF-A03).

NCEER-94-0021 "Proceedings of the U.S.-Italian Workshop on Guidelines for Seismic Evaluation and Rehabilitation of Unreinforced Masonry Buildings," Edited by D.P. Abrams and G.M. Calvi, 7/20/94, (PB95-138749, A13, MF-A03).

NCEER-94-0022 "NCEER-Taisei Corporation Research Program on Sliding Seismic Isolation Systems for Bridges: Experimental and Analytical Study of a System Consisting of Lubricated PTFE Sliding Bearings and Mild Steel Dampers," by P. Tsopelas and M.C. Constantinou, 7/22/94, (PB95-182184, A08, MF-A02).

NCEER-94-0023 "Development of Reliability-Based Design Criteria for Buildings Under Seismic Load," by Y.K. Wen, H. Hwang and M. Shinozuka, 8/1/94, (PB95-211934, A08, MF-A02).

NCEER-94-0024 "Experimental Verification of Acceleration Feedback Control Strategies for an Active Tendon System," by S.J. Dyke, B.F. Spencer, Jr., P. Quast, M.K. Sain, D.C. Kaspari, Jr. and T.T. Soong, 8/29/94, (PB95-212320, A05, MF-A01).

NCEER-94-0025 "Seismic Retrofitting Manual for Highway Bridges," Edited by I.G. Buckle and I.F. Friedland, published by the Federal Highway Administration (PB95-212676, A15, MF-A03).

NCEER-94-0026 "Proceedings from the Fifth U.S.-Japan Workshop on Earthquake Resistant Design of Lifeline Facilities and Countermeasures Against Soil Liquefaction," Edited by T.D. O'Rourke and M. Hamada, 11/7/94, (PB95-220802, A99, MF-E08).

NCEER-95-0001 "Experimental and Analytical Investigation of Seismic Retrofit of Structures with Supplemental Damping: Part 1 - Fluid Viscous Damping Devices," by A.M. Reinhorn, C. Li and M.C. Constantinou, 1/3/95, (PB95-266599, A09, MF-A02).

NCEER-95-0002 "Experimental and Analytical Study of Low-Cycle Fatigue Behavior of Semi-Rigid Top-And-Seat Angle Connections," by G. Pekcan, J.B. Mander and S.S. Chen, 1/5/95, (PB95-220042, A07, MF-A02).

NCEER-95-0003 "NCEER-ATC Joint Study on Fragility of Buildings," by T. Anagnos, C. Rojahn and A.S. Kiremidjian, 1/20/95, (PB95-220026, A06, MF-A02).

NCEER-95-0004 "Nonlinear Control Algorithms for Peak Response Reduction," by Z. Wu, T.T. Soong, V. Gattulli and R.C. Lin, 2/16/95, (PB95-220349, A05, MF-A01).

NCEER-95-0005 "Pipeline Replacement Feasibility Study: A Methodology for Minimizing Seismic and Corrosion Risks to Underground Natural Gas Pipelines," by R.T. Eguchi, H.A. Seligson and D.G. Honegger, 3/2/95, (PB95-252326, A06, MF-A02).

NCEER-95-0006 "Evaluation of Seismic Performance of an 11-Story Frame Building During the 1994 Northridge Earthquake," by F. Naeim, R. DiSulio, K. Benuska, A. Reinhorn and C. Li, to be published.

NCEER-95-0007 "Prioritization of Bridges for Seismic Retrofitting," by N. Basöz and A.S. Kiremidjian, 4/24/95, (PB95-252300, A08, MF-A02).

NCEER-95-0008 "Method for Developing Motion Damage Relationships for Reinforced Concrete Frames," by A. Singhal and A.S. Kiremidjian, 5/11/95, (PB95-266607, A06, MF-A02).

NCEER-95-0009 "Experimental and Analytical Investigation of Seismic Retrofit of Structures with Supplemental Damping: Part II - Friction Devices," by C. Li and A.M. Reinhorn, 7/6/95, (PB96-128087, A11, MF-A03).

NCEER-95-0010 "Experimental Performance and Analytical Study of a Non-Ductile Reinforced Concrete Frame Structure Retrofitted with Elastomeric Spring Dampers," by G. Pekcan, J.B. Mander and S.S. Chen, 7/14/95, (PB96-137161, A08, MF-A02).

NCEER-95-0011 "Development and Experimental Study of Semi-Active Fluid Damping Devices for Seismic Protection of Structures," by M.D. Symans and M.C. Constantinou, 8/3/95, (PB96-136940, A23, MF-A04).

NCEER-95-0012 "Real-Time Structural Parameter Modification (RSPM): Development of Innervated Structures," by Z. Liang, M. Tong and G.C. Lee, 4/11/95, (PB96-137153, A06, MF-A01).

NCEER-95-0013 "Experimental and Analytical Investigation of Seismic Retrofit of Structures with Supplemental Damping: Part III - Viscous Damping Walls," by A.M. Reinhorn and C. Li, 10/1/95, (PB96-176409, A11, MF-A03).

NCEER-95-0014 "Seismic Fragility Analysis of Equipment and Structures in a Memphis Electric Substation," by J-R. Huo and H.H.M. Hwang, 8/10/95, (PB96-128087, A09, MF-A02).

NCEER-95-0015 "The Hanshin-Awaji Earthquake of January 17, 1995: Performance of Lifelines," Edited by M. Shinozuka, 11/3/95, (PB96-176383, A15, MF-A03).

NCEER-95-0016 "Highway Culvert Performance During Earthquakes," by T.L. Youd and C.J. Beckman, available as NCEER-96-0015.

NCEER-95-0017 "The Hanshin-Awaji Earthquake of January 17, 1995: Performance of Highway Bridges," Edited by I.G. Buckle, 12/1/95, to be published.

NCEER-95-0018 "Modeling of Masonry Infill Panels for Structural Analysis," by A.M. Reinhorn, A. Madan, R.E. Valles, Y. Reichmann and J.B. Mander, 12/8/95, (PB97-110886, MF-A01, A06).

NCEER-95-0019 "Optimal Polynomial Control for Linear and Nonlinear Structures," by A.K. Agrawal and J.N. Yang, 12/11/95, (PB96-168737, A07, MF-A02).

NCEER-95-0020   "Retrofit of Non-Ductile Reinforced Concrete Frames Using Friction Dampers," by R.S. Rao, P. Gergely and R.N. White, 12/22/95, (PB97-133508, A10, MF-A02).

NCEER-95-0021   "Parametric Results for Seismic Response of Pile-Supported Bridge Bents," by G. Mylonakis, A. Nikolaou and G. Gazetas, 12/22/95, (PB97-100242, A12, MF-A03).

NCEER-95-0022   "Kinematic Bending Moments in Seismically Stressed Piles," by A. Nikolaou, G. Mylonakis and G. Gazetas, 12/23/95, (PB97-113914, MF-A03, A13).

NCEER-96-0001   "Dynamic Response of Unreinforced Masonry Buildings with Flexible Diaphragms," by A.C. Costley and D.P. Abrams," 10/10/96, (PB97-133573, MF-A03, A15).

NCEER-96-0002   "State of the Art Review: Foundations and Retaining Structures," by I. Po Lam, to be published.

NCEER-96-0003   "Ductility of Rectangular Reinforced Concrete Bridge Columns with Moderate Confinement," by N. Wehbe, M. Saiidi, D. Sanders and B. Douglas, 11/7/96, (PB97-133557, A06, MF-A02).

NCEER-96-0004   "Proceedings of the Long-Span Bridge Seismic Research Workshop," edited by I.G. Buckle and I.M. Friedland, to be published.

NCEER-96-0005   "Establish Representative Pier Types for Comprehensive Study: Eastern United States," by J. Kulicki and Z. Prucz, 5/28/96, (PB98-119217, A07, MF-A02).

NCEER-96-0006   "Establish Representative Pier Types for Comprehensive Study: Western United States," by R. Imbsen, R.A. Schamber and T.A. Osterkamp, 5/28/96, (PB98-118607, A07, MF-A02).

NCEER-96-0007   "Nonlinear Control Techniques for Dynamical Systems with Uncertain Parameters," by R.G. Ghanem and M.I. Bujakov, 5/27/96, (PB97-100259, A17, MF-A03).

NCEER-96-0008   "Seismic Evaluation of a 30-Year Old Non-Ductile Highway Bridge Pier and Its Retrofit," by J.B. Mander, B. Mahmoodzadegan, S. Bhadra and S.S. Chen, 5/31/96, (PB97-110902, MF-A03, A10).

NCEER-96-0009   "Seismic Performance of a Model Reinforced Concrete Bridge Pier Before and After Retrofit," by J.B. Mander, J.H. Kim and C.A. Ligozio, 5/31/96, (PB97-110910, MF-A02, A10).

NCEER-96-0010   "IDARC2D Version 4.0: A Computer Program for the Inelastic Damage Analysis of Buildings," by R.E. Valles, A.M. Reinhorn, S.K. Kunnath, C. Li and A. Madan, 6/3/96, (PB97-100234, A17, MF-A03).

NCEER-96-0011   "Estimation of the Economic Impact of Multiple Lifeline Disruption: Memphis Light, Gas and Water Division Case Study," by S.E. Chang, H.A. Seligson and R.T. Eguchi, 8/16/96, (PB97-133490, A11, MF-A03).

NCEER-96-0012   "Proceedings from the Sixth Japan-U.S. Workshop on Earthquake Resistant Design of Lifeline Facilities and Countermeasures Against Soil Liquefaction, Edited by M. Hamada and T. O'Rourke, 9/11/96, (PB97-133581, A99, MF-A06).

NCEER-96-0013   "Chemical Hazards, Mitigation and Preparedness in Areas of High Seismic Risk: A Methodology for Estimating the Risk of Post-Earthquake Hazardous Materials Release," by H.A. Seligson, R.T. Eguchi, K.J. Tierney and K. Richmond, 11/7/96, (PB97-133565, MF-A02, A08).

NCEER-96-0014   "Response of Steel Bridge Bearings to Reversed Cyclic Loading," by J.B. Mander, D-K. Kim, S.S. Chen and G.J. Premus, 11/13/96, (PB97-140735, A12, MF-A03).

NCEER-96-0015   "Highway Culvert Performance During Past Earthquakes," by T.L. Youd and C.J. Beckman, 11/25/96, (PB97-133532, A06, MF-A01).

NCEER-97-0001   "Evaluation, Prevention and Mitigation of Pounding Effects in Building Structures," by R.E. Valles and A.M. Reinhorn, 2/20/97, (PB97-159552, A14, MF-A03).

NCEER-97-0002   "Seismic Design Criteria for Bridges and Other Highway Structures," by C. Rojahn, R. Mayes, D.G. Anderson, J. Clark, J.H. Hom, R.V. Nutt and M.J. O'Rourke, 4/30/97, (PB97-194658, A06, MF-A03).

NCEER-97-0003   "Proceedings of the U.S.-Italian Workshop on Seismic Evaluation and Retrofit," Edited by D.P. Abrams and G.M. Calvi, 3/19/97, (PB97-194666, A13, MF-A03).

NCEER-97-0004   "Investigation of Seismic Response of Buildings with Linear and Nonlinear Fluid Viscous Dampers," by A.A. Seleemah and M.C. Constantinou, 5/21/97, (PB98-109002, A15, MF-A03).

NCEER-97-0005   "Proceedings of the Workshop on Earthquake Engineering Frontiers in Transportation Facilities," edited by G.C. Lee and I.M. Friedland, 8/29/97, (PB98-128911, A25, MR-A04).

NCEER-97-0006   "Cumulative Seismic Damage of Reinforced Concrete Bridge Piers," by S.K. Kunnath, A. El-Bahy, A. Taylor and W. Stone, 9/2/97, (PB98-108814, A11, MF-A03).

NCEER-97-0007   "Structural Details to Accommodate Seismic Movements of Highway Bridges and Retaining Walls," by R.A. Imbsen, R.A. Schamber, E. Thorkildsen, A. Kartoum, B.T. Martin, T.N. Rosser and J.M. Kulicki, 9/3/97, (PB98-108996, A09, MF-A02).

NCEER-97-0008   "A Method for Earthquake Motion-Damage Relationships with Application to Reinforced Concrete Frames," by A. Singhal and A.S. Kiremidjian, 9/10/97, (PB98-108988, A13, MF-A03).

NCEER-97-0009   "Seismic Analysis and Design of Bridge Abutments Considering Sliding and Rotation," by K. Fishman and R. Richards, Jr., 9/15/97, (PB98-108897, A06, MF-A02).

NCEER-97-0010   "Proceedings of the FHWA/NCEER Workshop on the National Representation of Seismic Ground Motion for New and Existing Highway Facilities," edited by I.M. Friedland, M.S. Power and R.L. Mayes, 9/22/97, (PB98-128903, A21, MF-A04).

NCEER-97-0011   "Seismic Analysis for Design or Retrofit of Gravity Bridge Abutments," by K.L. Fishman, R. Richards, Jr. and R.C. Divito, 10/2/97, (PB98-128937, A08, MF-A02).

NCEER-97-0012   "Evaluation of Simplified Methods of Analysis for Yielding Structures," by P. Tsopelas, M.C. Constantinou, C.A. Kircher and A.S. Whittaker, 10/31/97, (PB98-128929, A10, MF-A03).

NCEER-97-0013   "Seismic Design of Bridge Columns Based on Control and Repairability of Damage," by C-T. Cheng and J.B. Mander, 12/8/97, (PB98-144249, A11, MF-A03).

NCEER-97-0014   "Seismic Resistance of Bridge Piers Based on Damage Avoidance Design," by J.B. Mander and C-T. Cheng, 12/10/97, (PB98-144223, A09, MF-A02).

NCEER-97-0015   "Seismic Response of Nominally Symmetric Systems with Strength Uncertainty," by S. Balopoulou and M. Grigoriu, 12/23/97, (PB98-153422, A11, MF-A03).

NCEER-97-0016   "Evaluation of Seismic Retrofit Methods for Reinforced Concrete Bridge Columns," by T.J. Wipf, F.W. Klaiber and F.M. Russo, 12/28/97, (PB98-144215, A12, MF-A03).

NCEER-97-0017   "Seismic Fragility of Existing Conventional Reinforced Concrete Highway Bridges," by C.L. Mullen and A.S. Cakmak, 12/30/97, (PB98-153406, A08, MF-A02).

NCEER-97-0018   "Loss Asssessment of Memphis Buildings," edited by D.P. Abrams and M. Shinozuka, 12/31/97, (PB98-144231, A13, MF-A03).

NCEER-97-0019   "Seismic Evaluation of Frames with Infill Walls Using Quasi-static Experiments," by K.M. Mosalam, R.N. White and P. Gergely, 12/31/97, (PB98-153455, A07, MF-A02).

NCEER-97-0020   "Seismic Evaluation of Frames with Infill Walls Using Pseudo-dynamic Experiments," by K.M. Mosalam, R.N. White and P. Gergely, 12/31/97, (PB98-153430, A07, MF-A02).

NCEER-97-0021   "Computational Strategies for Frames with Infill Walls: Discrete and Smeared Crack Analyses and Seismic Fragility," by K.M. Mosalam, R.N. White and P. Gergely, 12/31/97, (PB98-153414, A10, MF-A02).

NCEER-97-0022 "Proceedings of the NCEER Workshop on Evaluation of Liquefaction Resistance of Soils," edited by T.L. Youd and I.M. Idriss, 12/31/97, (PB98-155617, A15, MF-A03).

MCEER-98-0001 "Extraction of Nonlinear Hysteretic Properties of Seismically Isolated Bridges from Quick-Release Field Tests," by Q. Chen, B.M. Douglas, E.M. Maragakis and I.G. Buckle, 5/26/98, (PB99-118838, A06, MF-A01).

MCEER-98-0002 "Methodologies for Evaluating the Importance of Highway Bridges," by A. Thomas, S. Eshenaur and J. Kulicki, 5/29/98, (PB99-118846, A10, MF-A02).

MCEER-98-0003 "Capacity Design of Bridge Piers and the Analysis of Overstrength," by J.B. Mander, A. Dutta and P. Goel, 6/1/98, (PB99-118853, A09, MF-A02).

MCEER-98-0004 "Evaluation of Bridge Damage Data from the Loma Prieta and Northridge, California Earthquakes," by N. Basoz and A. Kiremidjian, 6/2/98, (PB99-118861, A15, MF-A03).

MCEER-98-0005 "Screening Guide for Rapid Assessment of Liquefaction Hazard at Highway Bridge Sites," by T. L. Youd, 6/16/98, (PB99-118879, A06, not available on microfiche).

MCEER-98-0006 "Structural Steel and Steel/Concrete Interface Details for Bridges," by P. Ritchie, N. Kauhl and J. Kulicki, 7/13/98, (PB99-118945, A06, MF-A01).

MCEER-98-0007 "Capacity Design and Fatigue Analysis of Confined Concrete Columns," by A. Dutta and J.B. Mander, 7/14/98, (PB99-118960, A14, MF-A03).

MCEER-98-0008 "Proceedings of the Workshop on Performance Criteria for Telecommunication Services Under Earthquake Conditions," edited by A.J. Schiff, 7/15/98, (PB99-118952, A08, MF-A02).

MCEER-98-0009 "Fatigue Analysis of Unconfined Concrete Columns," by J.B. Mander, A. Dutta and J.H. Kim, 9/12/98, (PB99-123655, A10, MF-A02).

MCEER-98-0010 "Centrifuge Modeling of Cyclic Lateral Response of Pile-Cap Systems and Seat-Type Abutments in Dry Sands," by A.D. Gadre and R. Dobry, 10/2/98, (PB99-123606, A13, MF-A03).

MCEER-98-0011 "IDARC-BRIDGE: A Computational Platform for Seismic Damage Assessment of Bridge Structures," by A.M. Reinhorn, V. Simeonov, G. Mylonakis and Y. Reichman, 10/2/98, (PB99-162919, A15, MF-A03).

MCEER-98-0012 "Experimental Investigation of the Dynamic Response of Two Bridges Before and After Retrofitting with Elastomeric Bearings," by D.A. Wendichansky, S.S. Chen and J.B. Mander, 10/2/98, (PB99-162927, A15, MF-A03).

MCEER-98-0013 "Design Procedures for Hinge Restrainers and Hinge Sear Width for Multiple-Frame Bridges," by R. Des Roches and G.L. Fenves, 11/3/98, (PB99-140477, A13, MF-A03).

MCEER-98-0014 "Response Modification Factors for Seismically Isolated Bridges," by M.C. Constantinou and J.K. Quarshie, 11/3/98, (PB99-140485, A14, MF-A03).

MCEER-98-0015 "Proceedings of the U.S.-Italy Workshop on Seismic Protective Systems for Bridges," edited by I.M. Friedland and M.C. Constantinou, 11/3/98, (PB2000-101711, A22, MF-A04).

MCEER-98-0016 "Appropriate Seismic Reliability for Critical Equipment Systems: Recommendations Based on Regional Analysis of Financial and Life Loss," by K. Porter, C. Scawthorn, C. Taylor and N. Blais, 11/10/98, (PB99-157265, A08, MF-A02).

MCEER-98-0017 "Proceedings of the U.S. Japan Joint Seminar on Civil Infrastructure Systems Research," edited by M. Shinozuka and A. Rose, 11/12/98, (PB99-156713, A16, MF-A03).

MCEER-98-0018 "Modeling of Pile Footings and Drilled Shafts for Seismic Design," by I. PoLam, M. Kapuskar and D. Chaudhuri, 12/21/98, (PB99-157257, A09, MF-A02).

MCEER-99-0001   "Seismic Evaluation of a Masonry Infilled Reinforced Concrete Frame by Pseudodynamic Testing," by S.G. Buonopane and R.N. White, 2/16/99, (PB99-162851, A09, MF-A02).

MCEER-99-0002   "Response History Analysis of Structures with Seismic Isolation and Energy Dissipation Systems: Verification Examples for Program SAP2000," by J. Scheller and M.C. Constantinou, 2/22/99, (PB99-162869, A08, MF-A02).

MCEER-99-0003   "Experimental Study on the Seismic Design and Retrofit of Bridge Columns Including Axial Load Effects," by A. Dutta, T. Kokorina and J.B. Mander, 2/22/99, (PB99-162877, A09, MF-A02).

MCEER-99-0004   "Experimental Study of Bridge Elastomeric and Other Isolation and Energy Dissipation Systems with Emphasis on Uplift Prevention and High Velocity Near-source Seismic Excitation," by A. Kasalanati and M. C. Constantinou, 2/26/99, (PB99-162885, A12, MF-A03).

MCEER-99-0005   "Truss Modeling of Reinforced Concrete Shear-flexure Behavior," by J.H. Kim and J.B. Mander, 3/8/99, (PB99-163693, A12, MF-A03).

MCEER-99-0006   "Experimental Investigation and Computational Modeling of Seismic Response of a 1:4 Scale Model Steel Structure with a Load Balancing Supplemental Damping System," by G. Pekcan, J.B. Mander and S.S. Chen, 4/2/99, (PB99-162893, A11, MF-A03).

MCEER-99-0007   "Effect of Vertical Ground Motions on the Structural Response of Highway Bridges," by M.R. Button, C.J. Cronin and R.L. Mayes, 4/10/99, (PB2000-101411, A10, MF-A03).

MCEER-99-0008   "Seismic Reliability Assessment of Critical Facilities: A Handbook, Supporting Documentation, and Model Code Provisions," by G.S. Johnson, R.E. Sheppard, M.D. Quilici, S.J. Eder and C.R. Scawthorn, 4/12/99, (PB2000-101701, A18, MF-A04).

MCEER-99-0009   "Impact Assessment of Selected MCEER Highway Project Research on the Seismic Design of Highway Structures," by C. Rojahn, R. Mayes, D.G. Anderson, J.H. Clark, D'Appolonia Engineering, S. Gloyd and R.V. Nutt, 4/14/99, (PB99-162901, A10, MF-A02).

MCEER-99-0010   "Site Factors and Site Categories in Seismic Codes," by R. Dobry, R. Ramos and M.S. Power, 7/19/99, (PB2000-101705, A08, MF-A02).

MCEER-99-0011   "Restrainer Design Procedures for Multi-Span Simply-Supported Bridges," by M.J. Randall, M. Saiidi, E. Maragakis and T. Isakovic, 7/20/99, (PB2000-101702, A10, MF-A02).

MCEER-99-0012   "Property Modification Factors for Seismic Isolation Bearings," by M.C. Constantinou, P. Tsopelas, A. Kasalanati and E. Wolff, 7/20/99, (PB2000-103387, A11, MF-A03).

MCEER-99-0013   "Critical Seismic Issues for Existing Steel Bridges," by P. Ritchie, N. Kauhl and J. Kulicki, 7/20/99, (PB2000-101697, A09, MF-A02).

MCEER-99-0014   "Nonstructural Damage Database," by A. Kao, T.T. Soong and A. Vender, 7/24/99, (PB2000-101407, A06, MF-A01).

MCEER-99-0015   "Guide to Remedial Measures for Liquefaction Mitigation at Existing Highway Bridge Sites," by H.G. Cooke and J. K. Mitchell, 7/26/99, (PB2000-101703, A11, MF-A03).

MCEER-99-0016   "Proceedings of the MCEER Workshop on Ground Motion Methodologies for the Eastern United States," edited by N. Abrahamson and A. Becker, 8/11/99, (PB2000-103385, A07, MF-A02).

MCEER-99-0017   "Quindío, Colombia Earthquake of January 25, 1999: Reconnaissance Report," by A.P. Asfura and P.J. Flores, 10/4/99, (PB2000-106893, A06, MF-A01).

MCEER-99-0018   "Hysteretic Models for Cyclic Behavior of Deteriorating Inelastic Structures," by M.V. Sivaselvan and A.M. Reinhorn, 11/5/99, (PB2000-103386, A08, MF-A02).

MCEER-99-0019　"Proceedings of the 7th U.S.- Japan Workshop on Earthquake Resistant Design of Lifeline Facilities and Countermeasures Against Soil Liquefaction," edited by T.D. O'Rourke, J.P. Bardet and M. Hamada, 11/19/99, (PB2000-103354, A99, MF-A06).

MCEER-99-0020　"Development of Measurement Capability for Micro-Vibration Evaluations with Application to Chip Fabrication Facilities," by G.C. Lee, Z. Liang, J.W. Song, J.D. Shen and W.C. Liu, 12/1/99, (PB2000-105993, A08, MF-A02).

MCEER-99-0021　"Design and Retrofit Methodology for Building Structures with Supplemental Energy Dissipating Systems," by G. Pekcan, J.B. Mander and S.S. Chen, 12/31/99, (PB2000-105994, A11, MF-A03).

MCEER-00-0001　"The Marmara, Turkey Earthquake of August 17, 1999: Reconnaissance Report," edited by C. Scawthorn; with major contributions by M. Bruneau, R. Eguchi, T. Holzer, G. Johnson, J. Mander, J. Mitchell, W. Mitchell, A. Papageorgiou, C. Scaethorn, and G. Webb, 3/23/00, (PB2000-106200, A11, MF-A03).

MCEER-00-0002　"Proceedings of the MCEER Workshop for Seismic Hazard Mitigation of Health Care Facilities," edited by G.C. Lee, M. Ettouney, M. Grigoriu, J. Hauer and J. Nigg, 3/29/00, (PB2000-106892, A08, MF-A02).

MCEER-00-0003　"The Chi-Chi, Taiwan Earthquake of September 21, 1999: Reconnaissance Report," edited by G.C. Lee and C.H. Loh, with major contributions by G.C. Lee, M. Bruneau, I.G. Buckle, S.E. Chang, P.J. Flores, T.D. O'Rourke, M. Shinozuka, T.T. Soong, C-H. Loh, K-C. Chang, Z-J. Chen, J-S. Hwang, M-L. Lin, G-Y. Liu, K-C. Tsai, G.C. Yao and C-L. Yen, 4/30/00, (PB2001-100980, A10, MF-A02).

MCEER-00-0004　"Seismic Retrofit of End-Sway Frames of Steel Deck-Truss Bridges with a Supplemental Tendon System: Experimental and Analytical Investigation," by G. Pekcan, J.B. Mander and S.S. Chen, 7/1/00, (PB2001-100982, A10, MF-A02).

MCEER-00-0005　"Sliding Fragility of Unrestrained Equipment in Critical Facilities," by W.H. Chong and T.T. Soong, 7/5/00, (PB2001-100983, A08, MF-A02).

MCEER-00-0006　"Seismic Response of Reinforced Concrete Bridge Pier Walls in the Weak Direction," by N. Abo-Shadi, M. Saiidi and D. Sanders, 7/17/00, (PB2001-100981, A17, MF-A03).

MCEER-00-0007　"Low-Cycle Fatigue Behavior of Longitudinal Reinforcement in Reinforced Concrete Bridge Columns," by J. Brown and S.K. Kunnath, 7/23/00, (PB2001-104392, A08, MF-A02).

MCEER-00-0008　"Soil Structure Interaction of Bridges for Seismic Analysis," I. PoLam and H. Law, 9/25/00, (PB2001-105397, A08, MF-A02).

MCEER-00-0009　"Proceedings of the First MCEER Workshop on Mitigation of Earthquake Disaster by Advanced Technologies (MEDAT-1), edited by M. Shinozuka, D.J. Inman and T.D. O'Rourke, 11/10/00, (PB2001-105399, A14, MF-A03).

MCEER-00-0010　"Development and Evaluation of Simplified Procedures for Analysis and Design of Buildings with Passive Energy Dissipation Systems," by O.M. Ramirez, M.C. Constantinou, C.A. Kircher, A.S. Whittaker, M.W. Johnson, J.D. Gomez and C. Chrysostomou, 11/16/01, (PB2001-105523, A23, MF-A04).

MCEER-00-0011　"Dynamic Soil-Foundation-Structure Interaction Analyses of Large Caissons," by C-Y. Chang, C-M. Mok, Z-L. Wang, R. Settgast, F. Waggoner, M.A. Ketchum, H.M. Gonnermann and C-C. Chin, 12/30/00, (PB2001-104373, A07, MF-A02).

MCEER-00-0012　"Experimental Evaluation of Seismic Performance of Bridge Restrainers," by A.G. Vlassis, E.M. Maragakis and M. Saiid Saiidi, 12/30/00, (PB2001-104354, A09, MF-A02).

MCEER-00-0013　"Effect of Spatial Variation of Ground Motion on Highway Structures," by M. Shinozuka, V. Saxena and G. Deodatis, 12/31/00, (PB2001-108755, A13, MF-A03).

MCEER-00-0014　"A Risk-Based Methodology for Assessing the Seismic Performance of Highway Systems," by S.D. Werner, C.E. Taylor, J.E. Moore, II, J.S. Walton and S. Cho, 12/31/00, (PB2001-108756, A14, MF-A03).

MCEER-01-0001 "Experimental Investigation of P-Delta Effects to Collapse During Earthquakes," by D. Vian and M. Bruneau, 6/25/01, (PB2002-100534, A17, MF-A03).

MCEER-01-0002 "Proceedings of the Second MCEER Workshop on Mitigation of Earthquake Disaster by Advanced Technologies (MEDAT-2)," edited by M. Bruneau and D.J. Inman, 7/23/01, (PB2002-100434, A16, MF-A03).

MCEER-01-0003 "Sensitivity Analysis of Dynamic Systems Subjected to Seismic Loads," by C. Roth and M. Grigoriu, 9/18/01, (PB2003-100884, A12, MF-A03).

MCEER-01-0004 "Overcoming Obstacles to Implementing Earthquake Hazard Mitigation Policies: Stage 1 Report," by D.J. Alesch and W.J. Petak, 12/17/01, (PB2002-107949, A07, MF-A02).

MCEER-01-0005 "Updating Real-Time Earthquake Loss Estimates: Methods, Problems and Insights," by C.E. Taylor, S.E. Chang and R.T. Eguchi, 12/17/01, (PB2002-107948, A05, MF-A01).

MCEER-01-0006 "Experimental Investigation and Retrofit of Steel Pile Foundations and Pile Bents Under Cyclic Lateral Loadings," by A. Shama, J. Mander, B. Blabac and S. Chen, 12/31/01, (PB2002-107950, A13, MF-A03).

MCEER-02-0001 "Assessment of Performance of Bolu Viaduct in the 1999 Duzce Earthquake in Turkey" by P.C. Roussis, M.C. Constantinou, M. Erdik, E. Durukal and M. Dicleli, 5/8/02, (PB2003-100883, A08, MF-A02).

MCEER-02-0002 "Seismic Behavior of Rail Counterweight Systems of Elevators in Buildings," by M.P. Singh, Rildova and L.E. Suarez, 5/27/02. (PB2003-100882, A11, MF-A03).

MCEER-02-0003 "Development of Analysis and Design Procedures for Spread Footings," by G. Mylonakis, G. Gazetas, S. Nikolaou and A. Chauncey, 10/02/02, (PB2004-101636, A13, MF-A03, CD-A13).

MCEER-02-0004 "Bare-Earth Algorithms for Use with SAR and LIDAR Digital Elevation Models," by C.K. Huyck, R.T. Eguchi and B. Houshmand, 10/16/02, (PB2004-101637, A07, CD-A07).

MCEER-02-0005 "Review of Energy Dissipation of Compression Members in Concentrically Braced Frames," by K.Lee and M. Bruneau, 10/18/02, (PB2004-101638, A10, CD-A10).

MCEER-03-0001 "Experimental Investigation of Light-Gauge Steel Plate Shear Walls for the Seismic Retrofit of Buildings" by J. Berman and M. Bruneau, 5/2/03, (PB2004-101622, A10, MF-A03, CD-A10).

MCEER-03-0002 "Statistical Analysis of Fragility Curves," by M. Shinozuka, M.Q. Feng, H. Kim, T. Uzawa and T. Ueda, 6/16/03, (PB2004-101849, A09, CD-A09).

MCEER-03-0003 "Proceedings of the Eighth U.S.-Japan Workshop on Earthquake Resistant Design f Lifeline Facilities and Countermeasures Against Liquefaction," edited by M. Hamada, J.P. Bardet and T.D. O'Rourke, 6/30/03, (PB2004-104386, A99, CD-A99).

MCEER-03-0004 "Proceedings of the PRC-US Workshop on Seismic Analysis and Design of Special Bridges," edited by L.C. Fan and G.C. Lee, 7/15/03, (PB2004-104387, A14, CD-A14).

MCEER-03-0005 "Urban Disaster Recovery: A Framework and Simulation Model," by S.B. Miles and S.E. Chang, 7/25/03, (PB2004-104388, A07, CD-A07).

MCEER-03-0006 "Behavior of Underground Piping Joints Due to Static and Dynamic Loading," by R.D. Meis, M. Maragakis and R. Siddharthan, 11/17/03, (PB2005-102194, A13, MF-A03, CD-A00).

MCEER-03-0007 "Seismic Vulnerability of Timber Bridges and Timber Substructures," by A.A. Shama, J.B. Mander, I.M. Friedland and D.R. Allicock, 12/15/03.

MCEER-04-0001 "Experimental Study of Seismic Isolation Systems with Emphasis on Secondary System Response and Verification of Accuracy of Dynamic Response History Analysis Methods," by E. Wolff and M. Constantinou, 1/16/04 (PB2005-102195, A99, MF-E08, CD-A00).

MCEER-04-0002   "Tension, Compression and Cyclic Testing of Engineered Cementitious Composite Materials," by K. Kesner and S.L. Billington, 3/1/04, (PB2005-102196, A08, CD-A08).

MCEER-04-0003   "Cyclic Testing of Braces Laterally Restrained by Steel Studs to Enhance Performance During Earthquakes," by O.C. Celik, J.W. Berman and M. Bruneau, 3/16/04, (PB2005-102197, A13, MF-A03, CD-A00).

MCEER-04-0004   "Methodologies for Post Earthquake Building Damage Detection Using SAR and Optical Remote Sensing: Application to the August 17, 1999 Marmara, Turkey Earthquake," by C.K. Huyck, B.J. Adams, S. Cho, R.T. Eguchi, B. Mansouri and B. Houshmand, 6/15/04, (PB2005-104888, A10, CD-A00).

MCEER-04-0005   "Nonlinear Structural Analysis Towards Collapse Simulation: A Dynamical Systems Approach," by M.V. Sivaselvan and A.M. Reinhorn, 6/16/04, (PB2005-104889, A11, MF-A03, CD-A00).

MCEER-04-0006   "Proceedings of the Second PRC-US Workshop on Seismic Analysis and Design of Special Bridges," edited by G.C. Lee and L.C. Fan, 6/25/04, (PB2005-104890, A16, CD-A00).

MCEER-04-0007   "Seismic Vulnerability Evaluation of Axially Loaded Steel Built-up Laced Members," by K. Lee and M. Bruneau, 6/30/04, (PB2005-104891, A16, CD-A00).

MCEER-04-0008   "Evaluation of Accuracy of Simplified Methods of Analysis and Design of Buildings with Damping Systems for Near-Fault and for Soft-Soil Seismic Motions," by E.A. Pavlou and M.C. Constantinou, 8/16/04, (PB2005-104892, A08, MF-A02, CD-A00).

MCEER-04-0009   "Assessment of Geotechnical Issues in Acute Care Facilities in California," by M. Lew, T.D. O'Rourke, R. Dobry and M. Koch, 9/15/04, (PB2005-104893, A08, CD-A00).

MCEER-04-0010   "Scissor-Jack-Damper Energy Dissipation System," by A.N. Sigaher-Boyle and M.C. Constantinou, 12/1/04 (PB2005-108221).

MCEER-04-0011   "Seismic Retrofit of Bridge Steel Truss Piers Using a Controlled Rocking Approach," by M. Pollino and M. Bruneau, 12/20/04 (PB2006-105795).

MCEER-05-0001   "Experimental and Analytical Studies of Structures Seismically Isolated with an Uplift-Restraint Isolation System," by P.C. Roussis and M.C. Constantinou, 1/10/05 (PB2005-108222).

MCEER-05-0002   "A Versatile Experimentation Model for Study of Structures Near Collapse Applied to Seismic Evaluation of Irregular Structures," by D. Kusumastuti, A.M. Reinhorn and A. Rutenberg, 3/31/05 (PB2006-101523).

MCEER-05-0003   "Proceedings of the Third PRC-US Workshop on Seismic Analysis and Design of Special Bridges," edited by L.C. Fan and G.C. Lee, 4/20/05, (PB2006-105796).

MCEER-05-0004   "Approaches for the Seismic Retrofit of Braced Steel Bridge Piers and Proof-of-Concept Testing of an Eccentrically Braced Frame with Tubular Link," by J.W. Berman and M. Bruneau, 4/21/05 (PB2006-101524).

MCEER-05-0005   "Simulation of Strong Ground Motions for Seismic Fragility Evaluation of Nonstructural Components in Hospitals," by A. Wanitkorkul and A. Filiatrault, 5/26/05 (PB2006-500027).

MCEER-05-0006   "Seismic Safety in California Hospitals: Assessing an Attempt to Accelerate the Replacement or Seismic Retrofit of Older Hospital Facilities," by D.J. Alesch, L.A. Arendt and W.J. Petak, 6/6/05 (PB2006-105794).

MCEER-05-0007   "Development of Seismic Strengthening and Retrofit Strategies for Critical Facilities Using Engineered Cementitious Composite Materials," by K. Kesner and S.L. Billington, 8/29/05.

MCEER-05-0008   "Experimental and Analytical Studies of Base Isolation Systems for Seismic Protection of Power Transformers," by N. Murota, M.Q. Feng and G-Y. Liu, 9/30/05.

MCEER-05-0009   "3D-BASIS-ME-MB: Computer Program for Nonlinear Dynamic Analysis of Seismically Isolated Structures," by P.C. Tsopelas, P.C. Roussis, M.C. Constantinou, R. Buchanan and A.M. Reinhorn, 10/3/05.

MCEER-05-0010   "Steel Plate Shear Walls for Seismic Design and Retrofit of Building Structures," by D. Vian and M. Bruneau, 12/15/05.

MCEER-05-0011   "The Performance-Based Design Paradigm," by M.J. Astrella and A. Whittaker, 12/15/05.

MCEER-06-0001   "Seismic Fragility of Suspended Ceiling Systems," H. Badillo-Almaraz, A.S. Whittaker, A.M. Reinhorn and G.P. Cimellaro, 2/4/06.

MCEER-06-00002 "Multi-Dimensional Fragility of Structures," by G.P. Cimellaro, A.M. Reinhorn and M. Bruneau, 3/1/06.

MCEER-06-0003   "Built-Up Shear Links as Energy Dissipators for Seismic Protection of Bridges," by P. Dusicka, A.M. Itani and I.G. Buckle, 3/15/06.

MCEER-06-0004   "Analytical Investigation of the Structural Fuse Concept," by R.E. Vargas and M. Bruneau, 3/16/06.

MCEER-06-0005   "Experimental Investigation of the Structural Fuse Concept," by R.E. Vargas and M. Bruneau, 3/17/06.

MCEER-06-0006   "Further Development of Tubular Eccentrically Braced Frame Links for the Seismic Retrofit of Braced Steel Truss Bridge Piers," by J.W. Berman and M. Bruneau, 3/27/06.

MCEER-06-0007   "REDARS Validation Report," by S. Cho, C.K. Huyck, S. Ghosh and R.T. Eguchi, 8/7/06.

MCEER-06-0008   "Review of Current NDE Technologies for Post-Earthquake Assessment of Retrofitted Bridge Columns," by J.W. Song, Z. Liang and G.C. Lee, 8/21/06.

MCEER-06-0009   "Liquefaction Remediation in Silty Soils Using Dynamic Compaction and Stone Columns," by S. Thevanayagam, G.R. Martin, R. Nashed, T. Shenthan, T. Kanagalingam and N. Ecemis, 8/28/06.